IMPROVED STEAM TURBINE DESIGN FOR OPTIMUM EFFICIENCY AND REDUCED COST

KME-707







CONSORTIUM MATERIALS TECHNOLOGY for thermal energy processes





Improved Steam Turbine Design for Optimum Efficiency and Reduced Cost

KME-707

MARCUS THERN, MAGNUS GENRUP AND SRIKANTH DESHPANDE

Preface

The project has been performed within the framework of the materials technology research programme KME, Consortium materials technology for thermal energy processes, period 2014-2018. The consortium is at the forefront of developing material technology to create maximum efficiency for energy conversion of renewable fuels and waste. KME has its sights firmly set on continuing to raise the efficiency of long-term sustainable energy as well as ensuring international industrial competitiveness.

KME was established 1997 and is a multi-cliental group of companies over the entire value chain, including stakeholders from the material producers, manufacturers of systems and components for energy conversion and energy industry (utilities), that are interested in materials technology research. In the current programme stage, eight industrial companies and 14 energy companies participate in the consortium. The consortium is managed by Energiforsk.

The programme shall contribute to increasing knowledge within materials technology and process technology development to forward the development of thermal energy processes for efficient utilisation of renewable fuels and waste in power and heat production. The KME goals are to bring about cost-effective materials solutions for improved fuel flexibility, improved operating flexibility, increased availability and power production with low environmental impact.

KME's activities are characterised by long term industry and demand driven research and constitutes an important part of the effort to promote the development of new energy technology with the aim to create value and an economic, environmentally friendly and long term sustainable energy society.

The industry has participated in the project through own investment (60 %) and the Swedish Energy Agency has financed the academic partners (40 %).

Bertil Wahlund, Energiforsk



Abstract

The rationale for pursuing KME-707 is to lower the cost of ownership for the users but as natural result increasing the generation of climate-neutral electricity by increased efficiency. The results show that there is potential for improvement and that the amount of renewable electricity can be increased. The work has been focused on stage #11 and #16 in a SST-900 turbine and stage #2 in a SST-700 module. The former is an IP/LP module with tall stages whilst the latter is a HP module with short stages. For the tall stage, the work has been directed towards the profile- and end-wall losses and for the short stage mainly the end-wall loss.

The results show, for example, that the stage #16 profile loss can be reduced by 0.74 percent and that the secondary losses is reduced by the suggested means. The analysis shows that the reduction in secondary losses are high - on the order of 30 percent (expressed as secondary kinetic energy - SKE).



Sammanfattning

Sverige har ett ambitiöst mål att ställa om energisystemet till ett helt förnybart innan 2040. Detta kommer att, ur ett el genereringsperspektiv, innefatta en stor andel ny produktion. Samtidigt kommer under denna tidsperiod fram to 2040 sannolikt alla kärnkraftsblock att fasas ut. Detta kommer att innebära att man måste installera annan kontrollerbar "icke tidpunkts och väderberoende" produktion. En del kommer med stor sannolikhet vara biobränsleeldade ånganläggningar. Man kan också anta att dessa kommer att bygga på antingen bubbel- eller cirkulerande bäddas, dvs. att elda flis. Kostnaden för bränsle som levererats på bränslegården ligger idag på cirka 20 öre/kWh men man kan anta att detta kommer att stiga allt eftersom konkurrensen från andra typer av energibärare (tex biogas för fordon) ökar.

Enda sättet att minska bränsle-förbrukningen (för en viss given produktion) är att öka verkningsgraden på anläggningen. Detta kan ske på i huvudsak två sätt nämligen; processverkningsgraden och turbinens verkningsgrad. Det förstnämnda innebär i princip att man höjer ångdata med högre temperatur och tryck i pannan. I tillägg till detta kommer man sannolikt behöva införa reheat, där man återvärmer ångan efter expansionen i högtrycksturbinen. Detta är dock inte helt enkelt eftersom de tänkta bränsletyperna är korrosiva och materialvalen behöver studeras och utvecklas för att kunna nå höga verkningsgrader. Man måste ha mycket avancerade ångdata om man ska nå 50 procent elverkningsgrad och man kan förvänta sig intervallet 600...650°C och 300 bar. De nämnda nivåerna avser kondensturbiner exempelvis kraftvärmeturbin med kondenssvans. Även elutbytet i kraftvärmesammanhang, för ett visst givet värmeunderlag, ökar med högre cykel-verkningsgrad. Man brukar tala om kvoten mellan el- och värmeproduktion som normalt benämns som α -talet. Ångcykelns admissionsdata och kondensortryck kommer att ge det totala tillgängliga värmefallet som är tillgängligt för turbinen. Turbinens isentropa verkningsgrad är ett mått på hur väl som vi förvaltar detta – dvs. mycket förenklat beskriver hur bra turbinen är. Syftet med KME-707 är att öka verkningsgraden som, oavsett tillgängligt, värmefall kommer att öka elproduktionen.

Kostanden för att fräsa med femaxlig (flank) har sjunkit och det är idag möjligt att tillverka geometrier som var utopiska bara för några år sedan – till samma kostnad som för prismatiska (tvåaxlig fräsning). Detta innebär att man kan höja verkningsgraden utan att öka kostnaden, alternativt belasta stegen hårdare och på så sätt minska antalet med bibehållen prestanda.

Syftet med KME-707 är således att minska kostnaderna för användarna genom större elproduktion – dvs. potentiellt lägre "cost of ownership".

Forskningsprojektet har utförts tillsammans med Siemens och projektet har haft tillgång till riktiga referensgeometrier. Dessa steg kommer från SST-700 och -900 (fd. VAX II et al.) och har valts med omsorg. De steg som har undersökts är #11 och #16 i mellan- och lågtrycksmodulen och steg #2 i högtrycksmodulen. Siemens utvecklade själva steg #17 tidigare i projektet. Syftet med urvalet är att få med både steg som har högt "aspect ratio - AR" dvs. skovelhöjd/kordan och även lågt dito. Ett steg med högt AR har låga sekundär- och läckageförluster och förlusterna domineras av profilförlusterna. Situationen i steg #2 i högtrycksmodulen har lågt AR och därmed höga sekundär-



förluster och samtidigt höga Reynoldstal som gör att man måste ha låg ytråhet för låga profilförluster. För att vara möjligt att implementera resultaten i Siemens produktportfölj, bibehölls originalarean för minsta sektionerna¹. Detta innebär att både reaktionsgraderna och stegbelastningarna behölls på sitt ursprungliga värde. En av anledningarna var att inte öka turbinernas axialkrafter eftersom detta skulle påverka både axiallager och växlar.

Den ursprungliga projektplanen byggde på beräkningar med tvådimensionella lösare för "plan" skovelströmning och CFD - men inga prov. Under projektets gång visade sig nödvändigt att prova några geometrier eftersom CFD inte alltid kunde kvantifiera vinsterna trots förbättrade egenskaper i strömningsfälten. Dessa prov utfördes i Indien på ITT under hösten 2016. Detta är ett känt problem och generellt kan man säga att CFD inte är lika exakt som FEM för strukturmekanik. Detta beror på att det finns modeller som bygger på empiri och dessa är inte optimala under alla förutsättningar. Ett sådant exempel från projektet är C-formad ledskena (namnet kommer från att denna från sidan liknar ett "C"), där CFD (Ansys CFXTM) missade den förväntade responsen. Designfilosofin bakom C-formen är att motverka det högre tycket som uppstår lokalt vid ändväggarna och på så sätt motverka migration inåt i kanalen. Dessa effekter diskuteras utförligt i rapporten och läsaren hänvisas dit för vidare bakgrunder. Proven visar en avsevärd reduktion av sekundärförlusten och virvlarna "trycks" mot ändväggarna vilket är helt enligt intentionen. Ansys CFX™ missar de beskrivna effekterna kvalitativt, mer eller mindre, helt och CFD resultatet ger fel information vid handen. Istället har alternativa metoder använts för att kvalitativt utvärdera förbättringar i strömningsfältet vid införande av exempelvis "compound lean". I detta projekt har minskning av "sekundärkinetisk" energi och helicitet används som ett mått på förbättringar av strömningsfältet. Läsaren hänvisas till de relevanta sektionerna i rapporten för en utförlig beskrivning.

I projektet har följande delar ingått:

Förbättring	MT Steg #16	MT Steg #11	HT Steg #2
Förbättrad profil	Ja	Ja	Ja
Vridning	Ja	Ja	Ja
Stacking	Ja	Ja	-
Avancerad stacking	-	-	Ja

Profilförbärringar är dels avlägsnande av "incidence" (felanströmning) men primärt förbättrade belastningsfördelningar. Detta innebär att man optimerar exempelvis sugsidorna för minsta möjliga förlust. Profiler som har högst belastning närmast den trängsta sektionen brukar anses ge lägst profilförlust eftersom gränsskiktet är tunnast möjliga. Detta måste emellertid balanseras mot andra aerodynamiska fenomen son diffusionshastighet etc. Resultaten visar att det finns potential att höja stegverkningsgraden med 0.8 procent, endast genom profilförbättringar.

-



¹ Eng. "throat"

De korta stegen i högtrycksmodulen användes för att studera effekter av avancerad stackning för både statorn och rotorn i steg #2. Principen här är att införa avancerade geometrier även för rotorn där man utnyttjar en komponent av lyftkraften i riktning mot ändväggen. Detta infördes tillsammans med C-formen för att optimera hela steget. Den sistnämnda ändringen provades på ITT i Indien och uppvisar avsevärd sänkning av förlusterna.

Sammanfattningsvis så visar projektet att det finns möjlighet att förbättra turbinerna och på detta sätt kan mer förnybar el produceras. Arbetet har fokuserats steg med högt "aspect ratio" i MT/LT-modulen (dvs. långa profiler). Förbättringarna här är väsentligen bättre profiler och införande av vridning samt "lean/compound lean". I HT-modulen har arbetet fokuserats på att minska sekundärförlusterna.

Resultaten visar att, exempelvis, steg #16 profilförlust kan minskas så att stegverkningsgraden ökar med 0,74 procent. Vidare visar resultaten att den energi som är bunden i sekundärvirvlarna kan minskas med 30 procent.

$$\Delta \eta = 0.74 + f(\Delta SKE)$$

Under projektets gång avvecklade Siemens i Tyskland SST-700 och -900 på grund av överlapp i produktportföljen. Detta innebär att resultaten från KME-707 istället kan bli en serviceprodukt för befintligt turbinflotta. Siemens har köpt ett mycket stort amerikanskt bolag som heter Dresser-Rand som har en omfattande produktportfölj med turbiner som har låg reaktionsgrad och möjligtvis kan förbättringarna implementeras där. Detta är emellertid inte känt för författarna av denna rapport.

Nyckelord: Ångturbin, Prestanda, Aerodynamik, CFD, Mätning



Summary

The Swedish decision to have a fully renewable energy system by 2040 is ambitious and this will call for a plethora of new production means. In addition, the nuclear units will, by then, have reached the end of their economic- and technical lifespan. This means that a significant dispatchable generating capacity has to be installed in Sweden during the next 20 years. It is safe to assume that a large portion will be based on steam cycles with circulating- and bubbling beds (i.e. CFB and BFB). The cost of biomass is already today approximately 0.2 SEK/kWh (delivered at the fuel yard) and it is likely that it will be even higher in the future because of increased competition.

The only way of reducing fuel burn, for a certain power production, is to increase the efficiency. There are several means at the hand, but it may be summarized as either increase the average temperature of added heat (admission data) or/and increase the turbine efficiency. The former is chiefly to increase the steam temperature and the pressure, but will most likely also include reheat². This is by no means a simple task and will certainly call for significant wide TRL-range material research - because of the corrosive nature of some fuel-borne impurities (e.g. chlorides). The cycle electric net efficiency can be increased beyond 50 percent only if the steam data exceeds 300 bar and 600...650°C. It should be noted that the mentioned figures assumes cold-condensing operation (i.e. a condensing tail). In any case, an increased efficiency will increase the produced power for a certain heat load. Another means is to improve the components per se and one such example is the turbine efficiency. The thermodynamic cycle will result in an available isentropic heat drop that is set by the admission- and condenser data. The turbine isentropic efficiency is the ratio between the actual heat drop and the ideal ditto. Hence, a higher turbine efficiency will therefore increase the generation regardless of the cycle. The sole purpose of KME-707 is to increase the efficiency – hence more power for a certain heat input.

The motivation for pursuing the work in KME-707 is mainly modern manufacturing capacity where the prohibitive costs associated with five-axis flank milling has leveled with two-axis milling. This means that one can have advanced three-dimensional blades for, more or less, the same cost as for simpler two-dimensional (i.e. prismatic) blades. This means that one can improve the performance of a steam turbine without a significant additional cost. It should, however, be mentioned that other flowpath issues such as leakage- and seal flows will have a profound impact on the efficiency.

In summary, the work in KME-707 is aimed at reducing the cost of ownership by increasing the power production.

The vehicles for the research have been three stages in the Siemens SST-700 and -900 turbine series. The stages were selected for their geometrical features (i.e. high- and low aspect ratios) and that Siemens worked on one of the neighboring stages. For a high aspect ratio stage³ the relative influence from end-wall and leakage flows is lower than for a low aspect ratio stage – and vice versa. The stages were selected with this in mind and this gives a wide coverage of potential improvements. All research activities were carried out with the same throat areas for both the stators and rotors – hence the same



² Where the steam is heated a second time in the boiler – hence the name.

³ I.e. a high value of height/chord

level of loading and reaction. The rationale behind this was to maintain the same level of shaft thrust in order not to change the fundamental turbine design.

The original research plan was solely based on CFD-work and contained no test campaign. During the course of the project, however, it was deemed necessary to verify some of the analytical and numerical work by a test campaign. The reason for this was that the CFD-tools did not show the expected quantitative response for certain qualitative results. This problem is an established fact when working with CFD and reflects imperfections is the embedded models (i.e. transition, turbulence, etc.). One such example is the C-shaped vane where the leading edge sweep is used to mitigate the migration of low-momentum fluid towards the mid-passage. In this case the measurements fully supported the analytical reasoning, whilst the CFD-program failed to capture the trend. Most organizations (i.e. industry and academia) reverts to more physical approaches for evaluating complicated three-dimensional flow structures (such as secondary flows). Such examples are secondary kinetic energy (SKE) and helicity (cf. Figure 3-7) and both were extensively used as a gauge for assessing improvements. The drawback, however, is that it is not possible to assess in firm efficiency numbers. This is discussed further in detail in relevant sections in the report.

The research can be summarized as:

Feature	IP Stage #16	IP Stage #11	HP Stage #2
Improved profile	Yes	Yes	Yes
Twisting	Yes	Yes	Yes
Stacking	Yes	Yes	-
Advanced stacking	-	-	Yes

Improving a profile means typically that local incidence effects are mitigated or even removed and that the profile velocity distribution is optimized for minimum profile loss. This research showed that the stage efficiency for e.g. stages #11 and # 16could be increased by 0.8 percent. Stages #11 and #16 were the prime vehicles for research related to blade twisting and variants of lean.

The short stage in the HP-module was used for analyzing the effects due to advanced stacking for both the stator and the rotor. In addition to the stacking, a variant of sweep⁴ was introduced. The selected sweep resembles the letter "C" and is therefore referred to as C-shaping for clarity in the text (e.g. Figure 4-29). The C-shape was successfully tested during the test campaign in ITT in India and demonstrated a significantly lower secondary loss level (Figure 5-9). The C-shape must be introduced in concert with conventional compound lean and it could be seen as a way to mitigate one of the drawbacks with compound lean.

In summary, the results show that there is potential for improvement and that the amount of renewable electricity can be increased. The work has been focused on stage #11 and #16 in a SST-900 turbine and stage #2 in a SST-700 module. The former is an IP/LP module with tall stages whilst the latter is a HP module with short stages. For the tall

-



⁴ Axial stacking displacement

stage, the work has been directed towards the profile- and end-wall losses and for the short stage mainly the end-wall loss.

The results show that the stage #16 profile loss can be reduced by 0.74 percent and that the secondary losses is reduced by the suggested means. The analysis shows that the reduction in secondary losses are high - on the order of 30 percent (expressed as secondary kinetic energy - SKE).

$$\Delta \eta = 0.74 + f(\Delta SKE)$$

During the course of this project, Siemens AG (Germany) decided to discontinue the SST 700 and SST 900 units because of portfolio overlap. This means that the results potentially will be implemented as a service product for the Finspong range of units. Siemens has other low reaction products in the acquired Dresser-Rand in the US but it is unknown to the current authors if there will be a technology transfer.

Key words: Steam turbine, Performance, Aerodynamics, CFD, Measurements



List of content

1	Introduction				
	1.1	Backg	round	16	
	1.2	Descri	ption of the research field	17	
	1.3	Resea	rch task	17	
	1.4	Goal		18	
	1.5	Projec	t organisation	19	
2	Introd	luction ⁻	to the project KME-707	20	
	2.1	The pr	oject – an introduction	20	
	2.2	The cy	cle and the steam turbine	22	
	2.3		uction to flow path aerodynamics and design philosophy – a vade m for design	24	
3	Metho	odology	– turbine design	34	
	3.1	Bound	lary Conditions	35	
	3.2	Assum	ptions and simplifications	35	
	3.3	Mesh	details	35	
	3.4	Grid se	ensitivity study	37	
	3.5	Boundary conditions			
	3.6	Object	tive functions	38	
	3.7	Design	n limitations	40	
4	Result	ts		42	
	4.1	impro	vements in airfoil design – stage #16	42	
		4.1.1	Rotor improvements	44	
		4.1.2	Stator improvements	45	
	4.2	Perfor	mance with modified pitch-to-chord ratio	46	
		4.2.1	Pitch-to-chord ratio of stator	46	
		4.2.2	Pitch-to-chord ratio of rotor	48	
	4.3	Profili	ng summary	48	
	4.4	Profile	cloning	49	
	4.5	Design	n modifications to reduce secondary losses	50	
		4.5.1	Vortexing methods	51	
		4.5.2	Compound lean	52	
		4.5.3	Boundary layer fence	53	
	4.6	Merid	ional Flow path modifications	55	
		4.6.1	Flow path modifications	55	
		4.6.2	Tip shroud implementation	58	
	4.7	Short	stages – SST700 Stage #2	61	
		4.7.1	One-dimensional parameters of baseline geometry:	61	
		4.7.2	Three-dimensional features in baseline design	62	
		4.7.3	Three-dimensional rotor design	63	



5	Test	Test campaign			
	5.1	Methodology and instrumentation	68		
	5.2	Numerical approach	70		
	5.3	Results from measurements	71		
	5.4	The c-blade concept	73		
6	Conc	Conclusions			
7	Goal	Goal fulfilment			
8	Suggestions for future research work		78		
9	Literature references		80		
10	Publi	Publications			
11	Appe	Appendices			
	11.1	Secondary loss	85		
	11.2	Financial report	86		



List of Figures

Figure 1-1 Typical district heating plant	
Figure 2-1 SST-700 steam turbine	22
Figure 2-2 SST-900 steam turbine	22
Figure 2-3 Cascade aerodynamics	25
Figure 2-4 Cascade pressure distribution	25
Figure 2-5 Front- and aft-loaded profiles	26
Figure 2-6 Aft-loaded profile strategy	26
Figure 2-7 Secondary flow in a turbine cascade	28
Figure 2-8 Secondary flow and pressure gradient	28
Figure 2-9 Radial pressure gradient and radial equilibrium	
Figure 2-10 Meridional contouring (Russian kink)	30
Figure 2-11 Three-dimensional turbine view	
Figure 2-12 Relative Mach number levels	
Figure 2-13 Static pressure field	
Figure 2-14 Guide vane with compound lean	
Figure 3-1 CFD domain	
Figure 3-2 Smoot end-wall stage #11	
Figure 3-3 Extended geometry stage #11	
Figure 3-4 Grid independency study	
Figure 3-5 Inlet total pressure profile	
Figure 3-6 Secondary kinetic energy	
Figure 3-7 Helicity	
Figure 4-1 Cascade aerodynamics	
Figure 4-2 Modified rotor design	
Figure 4-3 Modified stator design	
Figure 4-4 Pitch-to-chord ratio	
Figure 4-5 Stator pitch-to-chord ratio	
Figure 4-6 Losses vs. the diffusion rate parameter	
Figure 4-7 Rotor pitch-to-chord ratio	
Figure 4-8 Efficiency gain with airfoil redesign	
Figure 4-9 Vortexing philosophies	
Figure 4-10 Vortexing designs	
Figure 4-11 Twisted vs. compound lean stator	
Figure 4-11 Twisted vs. Compound lean statol	
Figure 4-13 Reduction of vortex strength by boundary layer fence	
Figure 4-15 Blade loading comparison	
Figure 4-16 Vortexing designs	_
·	58
Figure 4-18 Tip shroud study	
Figure 4-19 Efficiency with tip shroud	
Figure 4-20 Streamwise vorticity – stator exit	
Figure 4-21 High pressure turbine stage - Flow path and stage parameters	
Figure 4-22 Velocity triangles – Stage #2	
Figure 4-23 Three-dimensional Analysis - Stage #2	
Figure 4-24 Datum stage #2	
Figure 4-25 Datum stator and 3D rotor	
Figure 4-26 Compound lean stator and datum rotor	
Figure 4-27 Compound lean stator and 3D rotor	
Figure 4-28 C-shaped compound lean stator and datum rotor	
Figure 4-29 C-shaped compound lean stator and 3D rotor	
Figure 5-1 HP-section of SST-700 and -900	
Figure 5-2 Schematic of test-section	69



Figure 5-3 Periodicity check	70
Figure 5-4 Blade-loading comparison	71
Figure 5-5 Secondary flow behavior	72
Figure 5-6 Overall loss behavior	72
Figure 5-7 Design configurations	73
Figure 5-8 Blade sweep and loading	74
Figure 5-9 Measured total pressure loss distributions	74
Figure 5-10 Calculated total pressure loss distributions	75
Figure 8-1 Turbine guide vane with non-axisymmetric end-wall contouring	78
Figure 11-1 Traupel secondary loss model	85



1 Introduction

1.1 BACKGROUND

Sweden has a large fleet of small and medium size turbines for district heating production and industrial backpressure. The produced electric power is today approximately five percent of the total production in Sweden. The steam cycle efficiency determines the fuel burn for a certain power output, hence having an, indeed, important impact on the direct operational cost. The steam cycle has the inherent advantage of being readily suitable for operation with renewable fuels. Operation with such fuels will introduce a plethora of issues related to the combustion system and heat transfer surfaces corrosion issues for the boilers. The latter will result in limitations for the available admission data and therefore limit the available average temperature of heat addition for the cycle. This pose a severe limitation for the attainable efficiency level and it can be argued that we are far from the full potential of the steam cycle. Unconstrained (in a sense) reheat utility plants have today capacity of 650°C and 300 bar admission data and are therefore approaching the 50 percent barrier. Rather than discussing in firm efficiency numbers, it is more relevant to discuss in terms of the Carnot potential – or more correctly - how we can increase it with the mentioned issues at the hand. The immediate remedy would otherwise be to increase the average temperature by utilizing more advanced admission data and thereby approach the maximum cycle temperature for reduced exergy loss. The second important parameter is the "cycle widening" which is the amount of irreversibility caused by the non-isentropic expansion in the turbine. It should, however, be noted that a complete and rigorous treatment would have to include other components such as pumps, preheaters, condensers, etc. and the reader is instead referred to the relevant literature.

The turbine efficiency has therefore an impact on the attainable cycle efficiency (i.e. the earlier discussed widening effect). It can be shown that the turbine efficiency is governed by the volumetric flow, heat drop (or pressure ratio) and the technology level. The first two have a clear coupling to the cycle data and cannot be discussed without bringing in the earlier reasoning related to thermodynamics and exergy. Both will, however, have a large impact on the attainable expansion efficiency. The turbine heat drop/pressure ratio will affect the amount of reheat-effect that governs the sum of all individual stages heat drops in relation to the total available heat drop. Loosely stated, a loss in a stage means more energy that is available for utilization the next. A larger volumetric flow means a physically larger turbine with taller blades. This means that effects because of clearances and secondary flows tends to be lower, hence more efficient. This is also the reason for having geared turbines when the volumetric flows are small. The discussion so far has mainly covered thermodynamics but there is a strong coupling to aerodynamics where dissipation (e.g. viscous shear in boundary layers and free shear layers) causes entropy generation. The objective of KME-707 is to increase the turbine by improving its aerodynamic performance and thereby improving the isentropic efficiency. The bulk of all other KME projects aim at improving materials, hence potentially increasing the average temperature of heat addition. Therefore, the KME-707 should be seen as the "other" part namely the turbine technology per se enhancer. It should, however, be mentioned that an increased isentropic turbine efficiency would render in less heat being rejected to the thermodynamic sink - simply by virtue of the first- and second laws of thermodynamics. This means that, for a certain heat input, less district heating will be produced. The current low electricity price has rendered in a situation where district



heating offers, in relative terms, higher value than electricity. This development has rendered in new Swedish heating plants being erected as heat only (HOP) with space left for future steam turbines. In any way a higher turbine efficiency, offer more electricity per unit of produced heat and once the electricity price increases will be a valuable feature.

The motivation for pursuing the work in KME-707 is mainly modern manufacturing capacity where the prohibitive costs associated with five-axis flank milling has leveled with two-axis milling. This means that one can have advanced three-dimensional blades for, more or less, the same cost as for simpler two-dimensional (i.e. prismatic) blades. This means that one can improve the performance of a steam turbine without a significant additional cost. It should, however, be mentioned that other flowpath issues such as leakage- and seal flows will have a profound impact on the efficiency.

In summary, the work in KME-707 is aimed at reducing the cost of ownership by increasing the power production.

During the course of this project, Siemens AG (Germany) decided to discontinue the SST 700 and SST 900 units because of portfolio overlap. This means that the results potentially will be implemented as a service product for the Finspong range of units. Siemens has other low reaction products in the acquired Dresser-Rand in the US but it is unknown to the current author if there will be a technology transfer.

1.2 DESCRIPTION OF THE RESEARCH FIELD

The research field in KME-707 is turbine aerodynamics, which is a discipline within fluid mechanics. All fluid mechanics originate from the Newton 2^{nd} law and therefore, in principle, is solving the $\mathbf{F}=\mathbf{m}\cdot\mathbf{a}$. The relation that is the very foundation of the Navier-Stokes (momentum) equations that is a set of non-linear hyperbolic-class equations covering the three principal directions. The set of governing equations cannot be solved analytically and practice is to use a dedicated finite-volume CFD-program.

1.3 RESEARCH TASK

The research in KME-707 is based on improving the aerodynamic performance of the turbine flow path. The expansion process in the turbine is, loosely stated, aimed at increasing the moment of momentum before the rotor and adding a reaction force to the rotor blade. The relation between them is the "degree of reaction" but in both cases, the velocity increases by turning the flow away from the axial direction. This turning requires, by virtue of the second the Newton 2nd law, a force in the desired turning direction. This lift force, in a confined channel, will manifest itself a pressure difference. This pressure difference (and how one distributes) it the absolute key to the performance of the expansion process. In the blade-to-blade plane, the pressure at the suction side is, for all practical cases, lower than the exit pressure. This means that there will be some deliberate aerodynamic diffusion where the pressure adopts to the exit pressure. This is controlled by carefully adjusting the radii of curvature of the blade from the throat (and sometimes upstream) to the trailing edge of the blade. From a pure fluid dynamic perspective, a thin boundary layer is desirable before any diffusion takes place. This means that one should try to accelerate for as long as possible and then have a rather short diffusion distance in the unconfined part of the blade. This can be shown when considering blades with higher exit Mach numbers, where the minimum loss exit ditto is when the velocity locally at the suction side is unity. It should, however, be noted that



some prominent organizations instead prefer rather front-loaded blades where the diffusion in minimized. The aim of research within this area is to find optimum blade loading strategies.

In addition to the blade-to-blade plane there is another level of freedom, namely the spanwise distributions of properties. In this work, several vortex distributions have been investigated. In laymen terms, vortexing is controlling the spanwise distributions of the velocity triangles – hence the static pressure gradient. In addition, the streamline curvature can be controlled between the rows. This offers another level of freedom in controlling e.g. the end-wall flows as well as the seals pressure drops. The research part is to find the optimum spanwise distributions for the given boundary conditions.

So far, the discussion has been related to optimized blade profiles and spanwise distribution of flow properties.

1.4 GOAL

The project goal is to increase the efficiency of SST-700 and -900 and thereby produce more power for a certain energy input. Most district heating plants today in Sweden utilizes renewable fuels already and an increased turbine efficiency will therefore increase the amount of renewable electricity. One could argue in a similar way for non-renewable fuels but it is safe to assume that the Swedish fleet of such plants will be phased out in all future scenarios.

The ambition of KME-707 is to increase the stage efficiency by two percent by reducing the losses. This is not to say that the cylinder efficiencies will increase by the same amount because of the reheat effect.

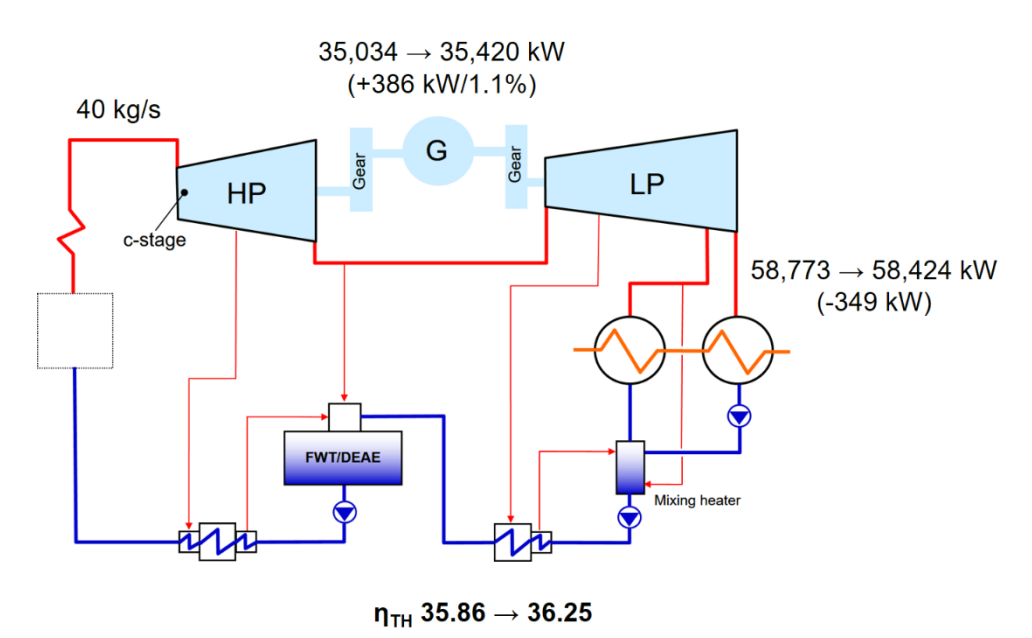


Figure 1-1 Typical district heating plant

Figure 1-1 is calculated by Siemens and shows the impact on the total plant from having two and one percent increased for the HP- and LP turbine, respectively. The reason for having two figures is simply short versus tall stages and the associated loss mechanisms.



The presented number in Figure 1-1 are for a certain heat input to the steam cycle of 97.7 MW, i.e. incorporates small effects because of the final feed water temperature. The power production should, with the present assumptions of improvement, be increased by 386 kW. The first- and second law of thermodynamics will then tell us that the rejected heat should reduce by the same amount. The difference is, however, minute and could be explained by other parasitic losses. An in-depth discussion is outside the present discussion.

At the time of writing, the electricity prices are significantly lower than the value of the district heating. It can therefore be argued that, from a pure economic perspective, that a lower turbine efficiency is better. However, electricity is, per definition, 100 percent exergy and this will certainly be appreciated in a future energy system.

1.5 PROJECT ORGANISATION

The bulk of the low-TRL research work was carried out at Lund University in close corporation with Siemens in Finspong.

Project manager: Professor Magnus Genrup

PhD-student: Dr Srikanth Deshpande

Supervisor: A/. Professor Marcus Thern

A part of the research was carried out at Indian Institute of Technology, Bombay. The funding for this research/testing campaign was provided by Erasmus+. The work at IIT in Bombay was supervised in-situ by Professor A. M. Pradeep.

Siemens has contributed throughout the project with the following staff:

Project manager: Oskar Mazur & Helena Oskarsson

Expertise: Senior specialist Åsa Nilsson, senior specialist Lars

Hedlund and specialist Åke Göransson

The project reference group is:

Helena Oskarsson (Siemens), Oskar Mazur (Siemens), Lars Hedlund (Siemens), Nicklas Simonsson (Vattenfall) and Per Rosén (E.ON).

Project budget:

The total project budget was 7,237,500 SEK, the total spending was, however, lower because of the PhD-student defended his thesis erlier and left for a position in the Swedish industry. The actual budget was 6,128,050 and all details are found in the financial statement in the appendix. It should, however, be noted that the full scope of the project was carried out (and reported here).



2 Introduction to the project KME-707

2.1 THE PROJECT – AN INTRODUCTION

A steam turbine is despite of being a mature technology, an indeed complicated machine to design because of the large number of involved disciplines. This work focuses on one of them, namely aerodynamics. The word "aerodynamics" is typically used in a rather loose sense and may cover many aspects. The prime purpose of this work, however, is to increase the efficiency of the machine by reducing the aerodynamic losses. The involved losses could be summarized as various means of producing entropy within the flow path.

The aim of the project is to increase the stage efficiency by two percent and thereby increasing the electricity production for the same fuel input – hence increasing the plant efficiency.

One cannot discuss the importance of the turbine efficiency without involving the steam cycle. The "other" possibility is to increase the cycle efficiency potential by increasing the average temperature of heat addition (\bar{T}). The latter is defined (in its simplest form without reheat) as:

$$\bar{T} = \frac{h_{adm} - h_{fw}}{s_{adm} - s_{fw}}$$

The involved parameters are enthalpy and entropy, which both are functions of the pressure and temperature. The resulting Carnot equivalent cycle efficiency is then written as:

$$\eta_{\mathit{C,CR}} = 1 - \frac{T_{\mathit{cond}}}{\bar{T}}$$

The difference between T_{adm} and \overline{T} ($T_{adm} > \overline{T}$) is a gauge of the exergy destruction (i.e. irreversibility) at cycle heat addition. One can show the same reasoning for the cycle heat reject. It has, however, no real practical impact on the steam cycle performance and will not be discussed further here. One should note that the turbine even is loss-free in this reasoning.

The most straightforward approach for increasing the efficiency is therefore simply to increase the steam pressure and temperature. This is by no means simple and there are several material limitations with respect to high temperature corrosion. These aspects are indeed well covered in other KME materials projects. However, as a rule of thumb, each 33 K increment in T_m results in one percent efficiency improvement.

In addition to the impact on the cycle performance, the process parameters have an effect on the turbine efficiency:

$$\eta_s = f(PR, \dot{V}, \dots) \text{ or } f(PR, C_T, \dots)$$

One can show that the performance of a turbine (for a certain technology level) is a function of the pressure ration (or heat drop) and the volumetric flow. The former is basically how "forgiving" the turbine is in terms of reheat, where a loss in a stage basically is more available energy for the next (except for the penultimate/final stage). This means that loss in early stages tends to have a relative less impact on the overall efficiency. The dependency from the volumetric flow is more straightforward simply because a larger volumetric flow results in a larger turbine. A larger turbine tends to



have higher Reynolds numbers, less impact from clearance- and secondary losses. A detailed discussion here is outside the scope of the current report and the reader is referred to relevant literature.

The effects on the cycle efficiency from having a non-isentropic turbine is introduced as "cycle widening". The ratio between the "real" cycle efficiency and the Carnot cycle equivalent efficiency is traditionally referred to as the "Carnot factor (CF)". This number is typically around 0.9 and takes into account effects from the steam turbine being non-isentropic and other irreversibility's (e.g. pump efficiency, heater grädigkeit, etc.). The Carnot factor impact on the steam cycle efficiency should be seen as the prime motivation for the KME-707 project.

So far, the discussion has omitted the boiler efficiency per se and the auxiliary consumption. It is instructive to add this for completeness and the resulting equation is:

$$\eta_{net} = \eta_{boiler} \cdot (CF \cdot \eta_{C,CR}) \cdot (1 - \alpha)$$

The boiler efficiency⁵ is typically approximately 0.90...0.95 and the parasitic (i.e. power house) consumption factor is around 0.05...0.10.



21

⁵ Cf. DIN for definition and reference conditions

2.2 THE CYCLE AND THE STEAM TURBINE

Steam turbines where introduced already in the late 19th century by de Laval and Parsons. Sweden has therefore one of the longest and proudest traditions within the field of steam turbines together with the UK. There was a significant difference between the two inventors, namely where to expand the steam in the stages. This is referred to as the "reaction level" and it is interesting to note that we still today, some 140 years later, debate whether high is better than low (or vice versa).

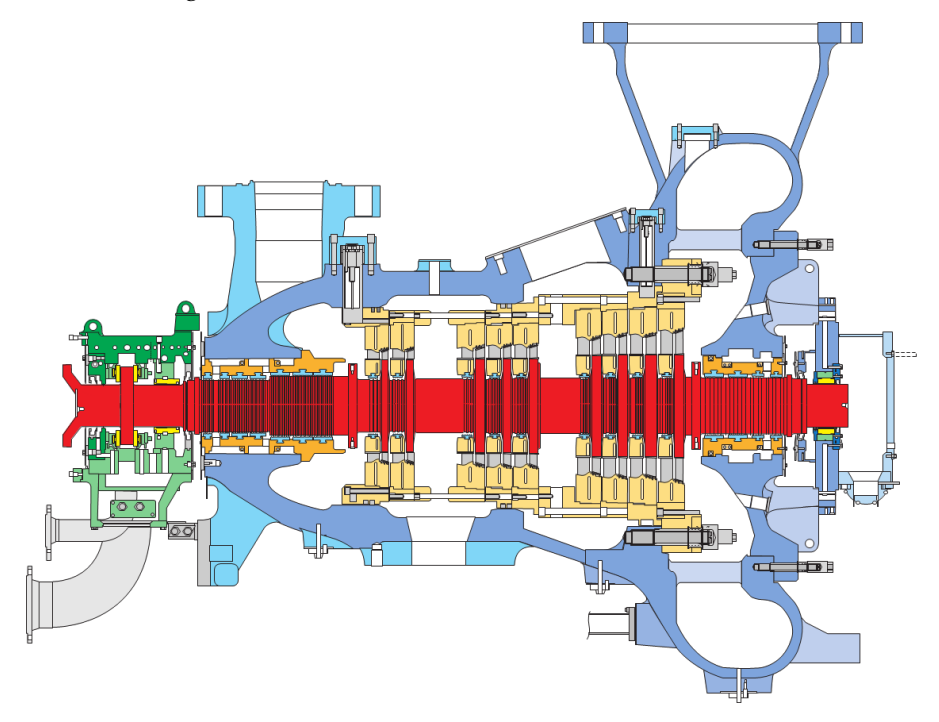


Figure 2-1 SST-700 steam turbine

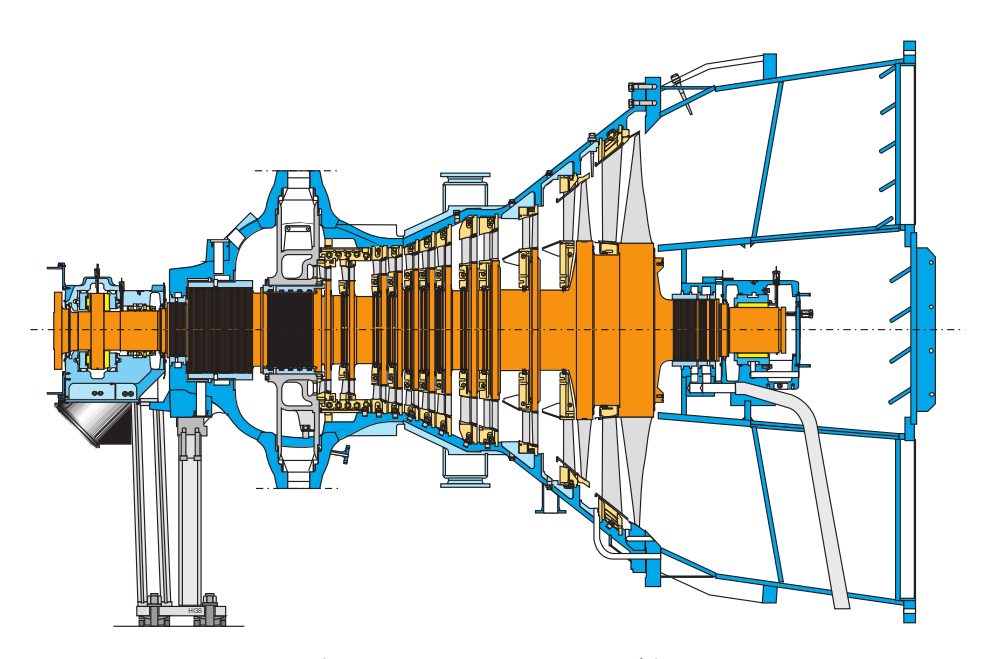


Figure 2-2 SST-900 steam turbine



The Siemens SST-700 and -900 are typical low-reaction designs where all short stages have approximately 20 percent reaction. It is common practice to design a steam turbine for low levels of intra-row swirl. The rationale behind this is the repeating stage concept and entry losses associated with the geometry and velocity before the guide vanes. It is possible to establish a relation that links the stage loading with the reaction as:

$$\psi = \frac{\Delta h_0}{u^2} = 2\left(1 - \Lambda - \underbrace{\varphi \tan \alpha_3}_{\approx 0}\right)$$

The preceding equation shows that the loading will be unity and two for 50 percent reaction and impulse, respectively. The Siemens units have some reaction (20 percent) in order to maintain root rotor and will therefore be somewhere in between. Both the reaction, the loading and the flow coefficient are important design parameters that controls many of the feature of the turbine. An in-depth discussion of all aspects of the mentioned parameters is outside the scope of the current report and the reader is referred to the relevant turbine literature (e.g. [1] and [2]).

One can show the stage loss impact on the previous discussed cycle widening reasoning by introducing stage entropy rise as:

$$\frac{\Delta s}{c_p} = \frac{\gamma - 1}{2} \cdot \left(\varsigma_{vane} \cdot M_2^2 + \varsigma_{rotor} \cdot M_{3,rel}^2 \right) \approx 0.15 \cdot \left(\varsigma_{vane} \cdot M_2^2 + \varsigma_{rotor} \cdot M_{3,rel}^2 \right)$$

The previous equation is important because it reveals to important fundamental turbine design considerations, namely:

- (i) For a 50 percent reaction turbine, the symmetrical velocity triangles offers the lowest maximum Mach number (M₂≈M₃,rel) hence potentially the lowest total loss if both loss coefficients are the same.
- (ii) For a lower reaction design where the vane exit Mach number is higher than ditto from the rotor (M₂>M_{3,rel}), then the importance of lowest possible vane loss is amplified.

It should, however, be mentioned that zero reaction would render in too low rotor hub acceleration (or even rotor recompression) and should be avoided. A too low value will increase both the secondary losses and the loss-sensitivity for the seal leakage flow mixing. In addition to the aerodynamics, the reaction effectively controls the rotor axial thrust load and therefore the axial bearing loading.

The total turbine efficiency can, in terms of entropy increment, be written as:

$$\begin{split} \eta_s &= \frac{h_{in} - h_{out}}{h_{in} - h_{out} + T_{out}(\sum_{i=1}^n \Delta s_i - s_{in})} \\ &\frac{1}{1+x} \approx 1 - x - x^2 + \cdots \end{split} \right\} :: \eta_s \approx 1 - \frac{T_{out}(\sum_{i=1}^n \Delta s_i - s_{in})}{h_{in} - h_{out}} \end{split}$$

One can apply the same reasoning on a stage-by-stage basis by, once again, applying the second Gibbs statement in order to demonstrate that a loss early in the expansion process is less detrimental for the turbine efficiency.



2.3 INTRODUCTION TO FLOW PATH AERODYNAMICS AND DESIGN PHILOSOPHY – A VADE MECUM FOR DESIGN

The involved fluid dynamics processes in a turbomachine are indeed complicated with several velocity - and length scales. The basic working principle is, on a fundamental level, quite simple – a combination of transferring the moment of momentum from the steam flow into the rotor and the reaction force from rotor acceleration. In any way, the velocity is formed by turning the flow away from the axial direction (thereby mimicking a simple schoolbook nozzle). Turning of a flow (actually any body with a mass - Cf. the second law by Newton) requires a lift force. This lift- or turning force is produced, by virtue of having a confined channel between the blades, by the pressure- and suction side. The rotor torque (force times radii) is then the reaction force associated with the mentioned turning processes.

The mentioned fundamental working principles will introduce losses through various sources and mechanisms. The associated losses can be summarized as:

- (i) Viscous dissipation in either boundary layers of free shear layers (e.g. mixing)
- (ii) Mixing of mass, momentum and energy
- (iii) Heat transfer across finite temperature differences
- (iv) Non-equilibrium (rapid expansion) and shock waves

In laymen terms, the duty of a turbomachinery blade is simply to turn the flow in order to accelerate (or diffuse for compressors). The turning will set up the suction- and pressure sides – with the associated higher- and lower velocities. It should, however, be noted that this velocity difference has absolutely nothing to do with the fact that the suction side of a blade is longer than the pressure side. Instead, the curvature is different on each side and this fundamentally creates the pressure difference across the passage. The Navier-Stokes equation is the "r"-direction in cylindrical coordinates is a convenient vehicle for the discussion:

$$\underbrace{\frac{\partial \mathcal{C}_r}{\partial t} + (\mathbf{V} \cdot \nabla) \mathcal{C}_r \underbrace{-\frac{\mathcal{C}_\theta^2}{r} = -\frac{1}{\rho} \frac{\partial p}{\partial r}}_{Euler-n} + g_r + \nu \left(\nabla^2 \mathcal{C}_r - \frac{\mathcal{C}_r}{r^2} - \frac{2}{r^2} \frac{\partial \mathcal{C}_\theta}{\partial \theta} \right)}_{Euler-n}$$

 $Navier-Stokes\ in\ cylindrical\ coordinates-r-direction$

The equation is written in short-form with the convective derivative and the LaPlacian operator:

$$(\mathbf{V} \cdot \nabla) = V_r \frac{\partial}{\partial r} + \frac{1}{r} V_\theta \frac{\partial}{\partial \theta} + V_z \frac{\partial}{\partial z}$$

$$\nabla^2 = \frac{1}{r} \frac{\partial}{\partial r} \left(r \frac{\partial}{\partial r} \right) + \frac{1}{r^2} \frac{\partial^2}{\partial \theta^2} + \frac{\partial^2}{\partial z^2}$$

By observation of the preceding N-S equation, the strong fundamental coupling between the tangential velocity C_{θ} (i.e. in the θ -direction) and the radius (1/r and 1/r²) is clearly visible (i.e. the last term of the left-hand side and the first term on the right-hand side). It may be convenient to assume a time- and spatial steady system to yield the simpler form:

$$\frac{1}{\rho}\frac{dp}{dr} = \frac{C_{\theta}^2}{r} + small\ viscous\ terms$$



If one neglects the viscous part on the RHS, then the "Euler-n" equation appears which is extremely useful when dealing with turbomachinery flows in simple terms. The Eulern equation tells us that there will be a pressure gradient if we turn a streamline (or vice versa).

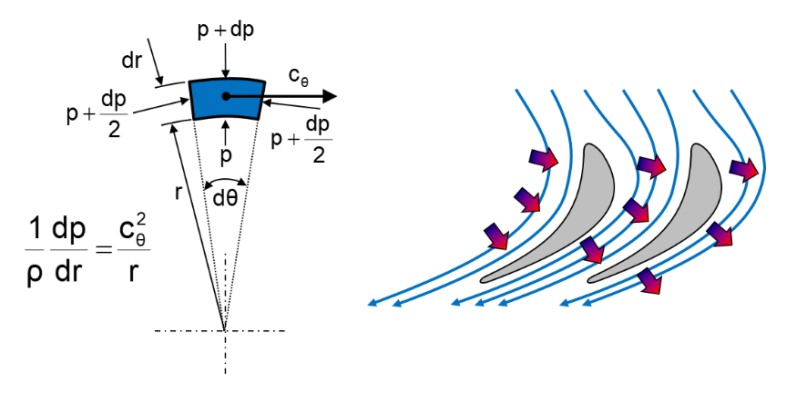


Figure 2-3 Cascade aerodynamics

As already mentioned the velocity on the suction side is higher than the ditto for the pressure side. There is a coupling between the velocity difference and the lift force for each blade in each row. It is normal practice to have rather high lift levels, which results in high local velocities within the cascade, which renders in locally lower pressures at the suction side than for the cascade backpressure.

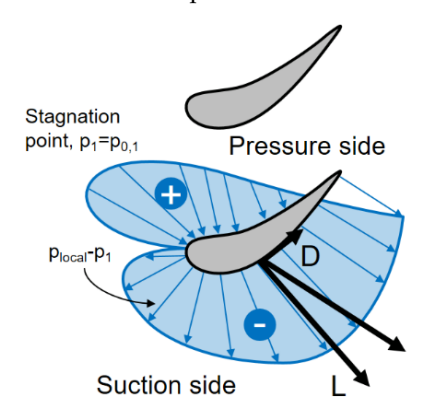


Figure 2-4 Cascade pressure distribution

This will result in a diffusion process that will have an impact on the losses in the boundary layer at the suction side of the blades. One can show that the bulk (typically 80 percent) of the boundary layer losses occurs within the zone of diffusion. Much of the aerodynamic optimization is, in a sense, heuristic and aims at optimizing the boundary layer before and the diffusion process per se.



Front loading – High Re Aft loading – Low Re W/W₂ 1.0 Turbulent B.L. X/B_x X/B_x

Figure 2-5 Front- and aft-loaded profiles

The figure above shows the velocity level at the edge of the boundary layer $(\delta_{99})^6$, i.e. what the boundary layer "experiences". The embedded area can be translated to static pressure, which integrated over the surface gives the blade lift force. According to Denton, the ideal suction side diffusion zone has a point of inflection in order to minimize the loss. The figure below show some typical features of how to create a profile with high performance.

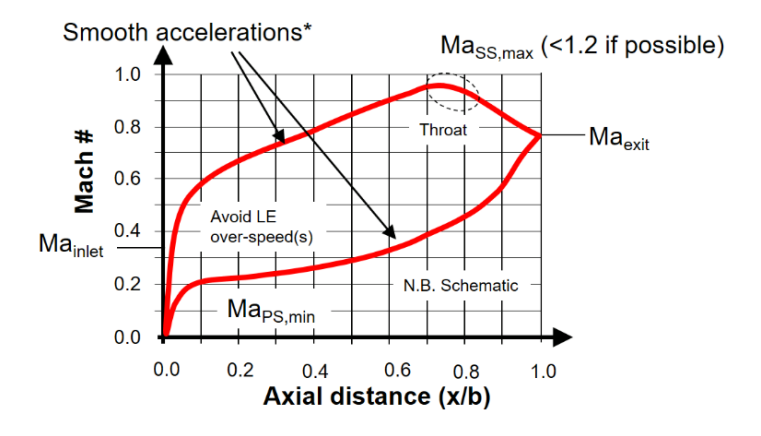


Figure 2-6 Aft-loaded profile strategy

It is in most cases optimum to have a continuous acceleration on the suction side and then a rather short diffusion zone. In any case, it is always desirable to have only one zone of diffusion along the profile, hence no local diffusion with subsequent acceleration. It is common practice to introduce the diffusion factor as gauge of the level:

$$D_{ss} = \frac{M_{max,ss}}{M_{exit}} - 1$$

The rate of diffusion is defined as:

$$Rate\ parameter = \frac{\left(M_{max,ss}/M_{exit}\right) - 1}{\Delta l_{diffusion}/l_{ss}} = \frac{D_{ss}}{\Delta l_{diffusion}/l_{ss}}$$

The former should be approximately 1.2...1.3 and the latter should be approximately 0.5...0.6 for optimum performance. It is frequently argued that CFD should have the capacity for replacing these "rule-of-thumbs" – but both have stood the test of time and are still used. Despite high level of sophistication, CFD is still today not capable of

KME

26

⁶ Defined as the point where the velocity reaches 99 percent of the free stream velocity

assessing the profile loss with high precision. It is still common practice to optimize the blade for a certain velocity profile rather than for a minimum loss value. This is one of the heuristic – or even grandma's secret recipes – type of empirical turbine technology features not described anywhere in the literature.

In addition to diffusion, the velocity level per se naturally also plays a role for loss (entropy) created from viscous shear (τ_{yx}) at the blade surface boundary layers:

$$\dot{S} = \frac{d}{dx} \int_0^{\delta_{99}} \rho \cdot C_x \cdot (s - s_{\delta_{99}}) \cdot dy = \int_0^{\delta_{99}} \frac{1}{T} \cdot \tau_{yx} \cdot dC_x$$

The preceding expression for entropy generation is from a rigorous point of view for a flat plat but can, after considerable algebra, be transformed into the useful form [3]:

$$\begin{split} \dot{S} &= \sum_{ss+ps} l \cdot h \cdot \int_0^1 \frac{C_D \cdot \rho \cdot C_{\delta_{99}}^3}{T} d \left(\frac{x}{l} \right) \\ \xi &= \frac{T \cdot \dot{S}}{\dot{m} \cdot C_2^2 / 2} \end{split} \} \xi = 2 \sum_{ss+ps} \frac{l}{s \cdot \cos \alpha_2} \int_0^1 \left(\frac{C_{\delta_{99}}}{C_2} \right)^3 d \left(\frac{x}{l} \right) \end{split}$$

This is the "U-cube" expression by Denton [3] and it gives at the hand that the accumulated loss along the surfaces (x/l) is a function of the velocity at the edge of the boundary layer cubed. It is now instructive to introduce the trade-off between the velocity level and the amount of wet surface. The Newton second-law tells us that the force is mass times acceleration and this fact gives at the hand that the mass flow per blade will control the required lift force. This means that an increased number of blades will reduce the size of the velocity- or pressure "bubble" – with potentially lower loss.

The preceding U-cube equation tells us that the loss production is proportional to the integral $\int C^3 dA$ – hence too much wet surface can also be detrimental to the performance.

In summary - a good aerodynamic design balances the velocity and diffusion levels with the amount of wet surface.

Out of the previous reasoning, one can establish as set of *rule of thumb* that has to be in place in order to maximize the efficiency.

- (i) The Reynolds number chiefly sets the optimum loading distribution (i.e. front- or aft loaded). The aft-loaded blade has several advantages over the front-loaded. One can show that a Mach number of unity at the suction side of the throat offers the lowest loss coefficient. This is because of the state of the boundary layer before the diffusion process. Most steam turbines have rather low exit Mach numbers and it is impractical to increase the amount of uncovered turning that is required in order to get a value of unity at the suction side. Instead, a more feasible practical approach is to design for approximately 20° uncovered turning.
- (ii) The suction side diffusion factor should be limited to approximately 1.2...1.3
- (iii) The rate of diffusion should be on the order of 0.5...0.6

⁷ Entropy production per row is the exit Mach number squared times the loss coefficient (\sim M²⁻ ζ). Hence, the lowest loss coefficient may not offer the lowest entropy production in a row.



27

- (iv) All local "over-speeds" and subsequent diffusion zones should be avoided (cf. below)
- (v) The profile inlet loading (i.e. at the front part of the blade) should be controlled in order to have sufficient and smooth suction side acceleration ($\leq 0.6 \cdot M_{max,ss}$). This parameter has a profound impact on the incidence sensitivity for a row.
- (vi) Optimized span-wise blade angle distribution for avoiding local incidence losses because of displayed stagnation points at the leading edge

So far, the discussion has been limited to the blade profile aerodynamics at the design point⁸. Another prominent source of loss is the flow field at the end-walls. There will be both new/fresh thin highly-skewed lossy (indeed) boundary layers and classic secondary flow. The latter is a prerequisite for the former (outside the scope of the discussion) because the horseshoe and the passage vortex introduces the required end-wall separation lines. The horseshoe vortex is formed when the approaching boundary layer stagnates at the leading edge of the blade (cf. Figure 2-7). The boundary layer then rollsup to a structure that assimilates a horseshoe and therefore the name.

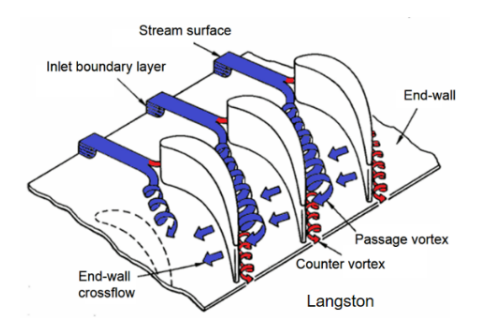


Figure 2-7 Secondary flow in a turbine cascade

The passage vortex is more direct and is, in simple terms, because of the slower-moving boundary layer and the earlier discussed blade-to-blade pressure gradient (see Figure 2-8). The boundary layer cannot withstand the pressure gradient (because of the shear work and dissipation in the viscous boundary layer) and rolls up into the large passage vortex.

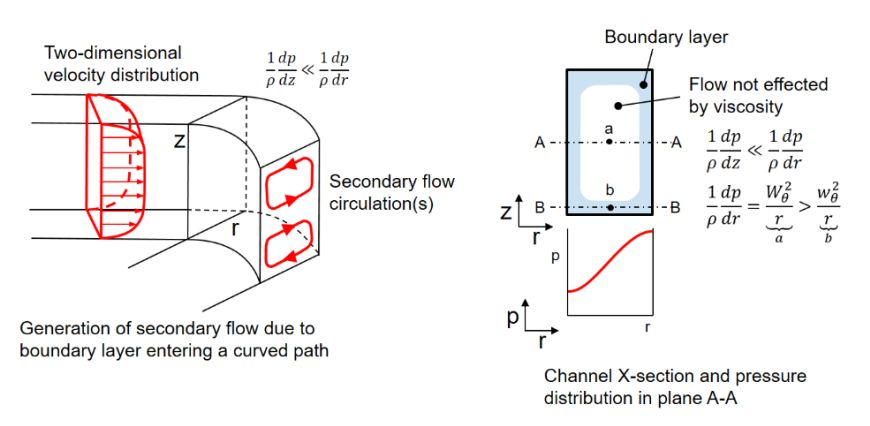


Figure 2-8 Secondary flow and pressure gradient



⁸ Off-design operation introduces a second class of profile loss related to incidence effects

Shorter stages will suffer more from this loss mechanism because of the increased relative importance. The loss is indeed complex and involves the *local* flow condition. The word local is highlighted because it involves several features as the span-wise variation of flow properties, leakage flows and blade loading. The latter introduces a strong link to the previous discussion with the blade loading, simply because it determines the blade-to-blade pressure gradient that creates the passage vortex.

The resulting secondary loss is a complicated function composed of:

Secondary loss = f(lift coefficient, aspect ratio, velocity ratio, ...)

The preceding equation shows the impact from some critical design parameters i.e. the blade-to-blade pressure difference, the ratio between height and chord and the row acceleration. The latter is not an issue for vanes but sets the minimum reaction for "low-reaction designs" – typically 5 percent.

During the course of the design, one sets the span-wise variation by twisting the blades as input data or similar. In the early days, especially for short stages with higher hub-tip-ratios of 0.75...0.80, the blades were prismatic (i.e. untwisted). In the past, this was solely driven by cost and design methodology limitations. Today, the situation is different and one can mill three-dimensional blades for the same cost as for two-dimensional. The state-of-the-art five-axis flank milling technology drives this development. There exists a handful of "typical" blade twisting philosophies namely: (i) constant blade angle, (ii) free vortex (iii) damped forced vortex and (iv) Brand-X type of parabolic vortexing. An in-depth discussion of all other possible variants is outside the scope of this text. As earlier mentioned, the constant section (or prismatic) blades for cost reasoning. It is not necessarily the same as compromising the efficiency but this is normally the case.

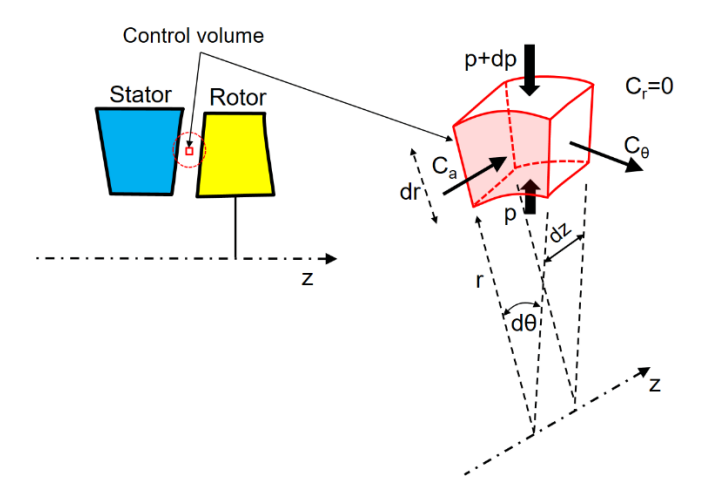


Figure 2-9 Radial pressure gradient and radial equilibrium

The earlier mentioned principle Euler-n equation applies here as well, by provision on applying it in the direction of the radial pressure gradient, namely in the hub- to tip direction. It is common practice to define an energy-momentum class of energy by combining the full Euler⁹ equations with the second Gibbs statement and the energy equation to yield:

⁹ I.e. N-S without the viscous terms





$$C_{m} \frac{dC_{m}}{dl} = \underbrace{\sin(\varphi - \gamma)C_{m} \frac{\partial C_{m}}{\partial m}}_{(a)} + \underbrace{\cos(\varphi - \gamma) \frac{C_{m}^{2}}{r_{c}}}_{(b)} - \underbrace{\frac{C_{\theta}}{r} \frac{d(r \cdot C_{\theta})}{dl}}_{(c)} + \underbrace{\frac{dh_{o}}{dl}}_{(d)} - \underbrace{\frac{ds}{dl}}_{(e)} - \underbrace{\sin(\varphi - \gamma)F_{m}}_{(F)}$$

Where:

- (a) Convective acceleration in the meridional direction
- (b) Streamline curvature
- (c) Angular momentum
- (d) Work gradient
- (e) Entropy (loss) gradient
- (f) Body force in the meridional direction
- (g) Body force in the normal direction (component of the blade lift force)

The preceding equation "couples" the meridional velocity (C_m) with the tangential velocity (C_θ) – hence the flow angle. Any serious designer well advised to, literally, memorize this equation because it will a clear guidance to many of the design decisions. Terms (b) and (g) could for example be used to explain the original blading in the SST-700 and -900. The cross section in Figure 2-1 of SST-700 turbine reveals that the turbine has "meridional profiling" or "Russian kinks" for reaction control. In addition to the flow path contour, the vanes have approximately 15° lean (pressure side down). These flow path features will affect the hub-tip plane though terms (b) and (g). The figures below show some of the design features together with Mach number- and static pressure levels [Figure 2-12 and Figure 2-13]. The mild static pressure radial gradient between the stators and rotors, that is shown in Figure 2-13, is achieved with the mentioned terms for contouring (b) and lean (g).

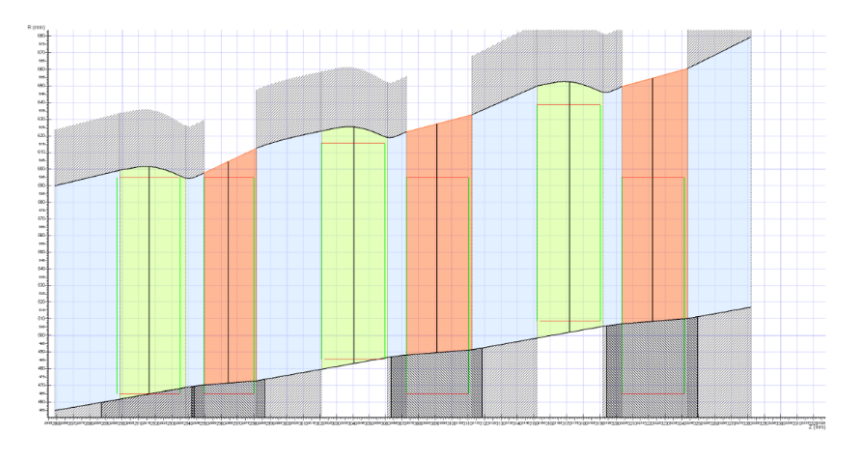


Figure 2-10 Meridional contouring (Russian kink)



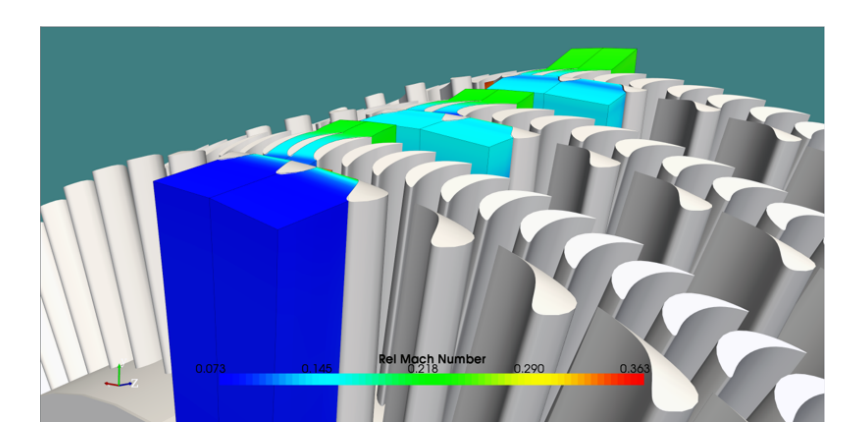


Figure 2-11 Three-dimensional turbine view

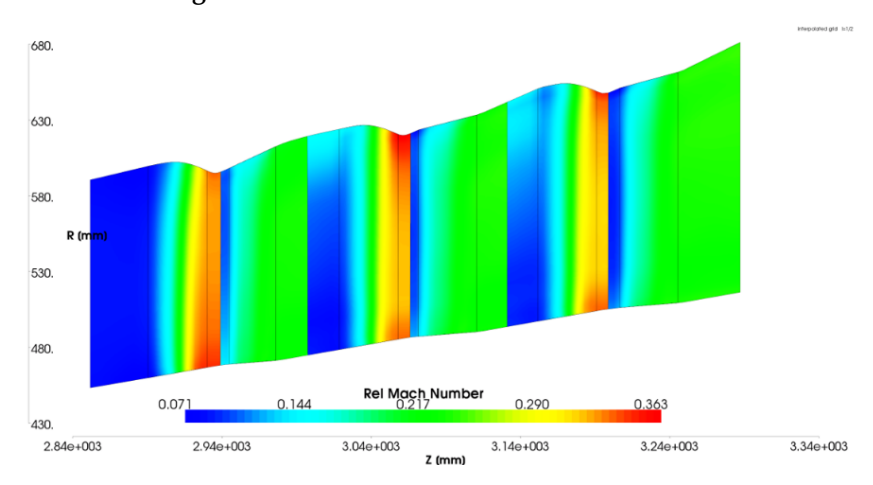


Figure 2-12 Relative Mach number levels

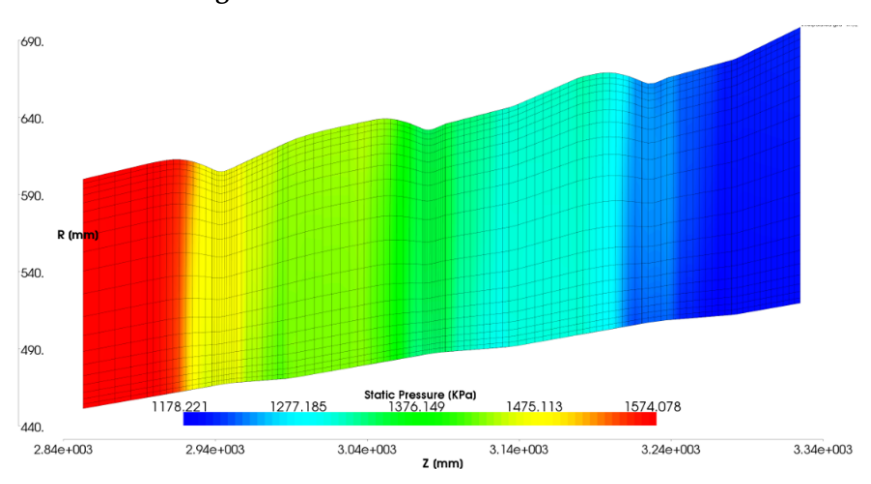


Figure 2-13 Static pressure field

One convenient and elegant way to demonstrate the impact from lean and channel contouring is presented in [4] and [5]. It starts from the intermediate form of the radial equilibrium equation:



$$F_r + \frac{1}{\rho} \frac{dp}{dr} = \frac{C_\theta^2}{r} + \frac{C_m^2}{r_c}$$

The previous equation is "valid" for the case of lean whilst the ealier Euler-n will be valid for a case of $F_r = 0$ and $r_c = \infty$ (i.e. straight streamlines). If one now assumes that, the swirl level (C_θ) stays the same then the change (due to lean) will be:

$$F_r + \frac{1}{\rho} \frac{d\Delta p}{dr} = \frac{C_m^2}{r_c}$$

Where Δp is the change in static pressure (from the blade force in the direction of the wall) introduced by lean. The subsequent change in end-wall velocity then becomes:

$$\Delta p_{end-wall} = -\frac{\rho \cdot C_m \cdot \Delta C_{m,wall}}{\cos^2 \alpha}$$

If the previous equation is solved for the change in velocity, then one can calculate the radius shift from the continuity equation for the mid-streamline:

$$\Delta r \approx -\frac{h}{4} \frac{\Delta C_{m,wall}}{C_m}$$

The associated change in streamline curvature, by assuming a parabolic form, is approximated from a parabola:

$$\Delta\left(\frac{1}{r_c}\right) = K \cdot \frac{\Delta r}{Chord_{ax}^2} \approx 10 \cdot \frac{\Delta r}{Chord_{ax}^2}$$

Combining the equations results in:

$$F_r = \underbrace{\frac{2 \cdot \Delta p}{\rho \cdot h}}_{pressure} + \underbrace{\frac{\Delta p}{\rho} \cdot \frac{10 \cdot h}{4 \cdot Chord_{ax}^2} \cdot \cos^2 \alpha}_{streamline\ curvature}$$

The ratio between the effect on the curvature term and the pressure gradient term from lean (F_r) is then:

$$\frac{\textit{Change in streamline curvture term}}{\textit{Change in pressure gradient term}} = 1.25 \cdot AR_{ax}^2 \cdot \cos^2\alpha_2$$

Therefore, at high values of aspect ratio (AR), the curvature term will dominate – and vice versa. This means that a high value of AR will lower the reaction gradient (because of the convex streamlines) whereas low AR will affect the hub- and tip-loading. However, it is possible to combine lean with contouring¹⁰ [6] in order to get an effect on the reaction gradient (i.e. streamline "convexing" by the wall contouring). This has been an extremely successful design approach by Siemens. This goes back to an invention by Allan Person (at that time ASEA-STAL) that was introduced in the early 90s in the VAX-II series.

A further support of the reasoning is by the derivation of the equation for span-wise reaction variation [7]:

$$\frac{1 - \Lambda(r)}{1 - \Lambda_{RMS}} = \left(\frac{r_{RMS}}{r}\right)^{2 \cdot Q_1 \cdot (1 - \varsigma) \cdot \cos^2 \alpha - \frac{2.5 \cdot Q_2 \cdot \sin(2 \cdot \alpha) \cdot r_{RMS} \cdot \sin \gamma}{C hord_{ax}}}$$



¹⁰ May also reduce the secondary losses because the outer part of the vane is off-loaded

In the previous equation, the blade lean angle is denoted " γ " and the influence from the chord is explicit. Note that the tangential angle definition from the original source [7] is retained.

It is interesting to note that "inverse twisting" or damped¹¹ forced vortex type of blade twists also increases the reaction at the hub – by introducing a force component from streamline shift.

Compound lean blades are, in principal, localized lean near the end-walls. Everything said on lean applies but the off-loading effect is directed towards both walls. No direct streamline curvature shift occurs – hence, the off-loading effect is solely due to the blade force component in each direction.

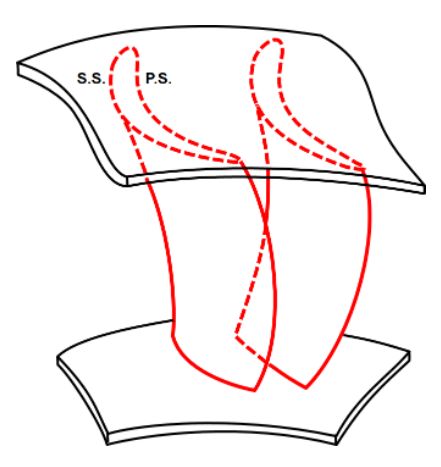


Figure 2-14 Guide vane with compound lean

The potential benefits from having compound lean may be summarized as [8]:

- Increase in load at mid-span and reduction near the end-walls causes more work to be done by the most efficient part of the blade, i.e. near mid-span
- Redistribution of the low-energy fluid. This may prevent loss accumulation and local separation near the end-walls.
- Reduction in velocity where the wet-surface is higher (end-walls) and an increase in velocity where the wet-surface is smaller (mid-span). This is probably best evaluated using Denton's U-cube method i.e. $\int C^3 dA$.
- More uniform flow for the next row (reduced over- and under-turning)

One drawback, however, is migration of lower-momentum fluid towards the midpassage. This may actually render in severe disturbance effects where the resulting efficiency is lower than intended. One possible cure is to lean the suction-sides towards the end-walls. This has to be in concert with reduced turning¹² near the end-walls (in order to reduce the loading).

A caveat is in place, the reaction of a stage is, in principal, determined by the bulk flow properties. Therefore will "local" features only will have minute effects for most cases.

¹² Brand-X type of blade



¹¹ Typically to 5...6°

3 Methodology – turbine design

The two dimensional numerical analysis of the airfoil section was done using in-house design tool from Siemens Industrial Turbomachinery, Finspong. Cascade analysis and design system CATO with MISESTM is used extensively for design, initial loss prediction and to achieve target Mach number distribution. The default intrinsic grid system from the MISES package is used. The key parameter to be retained is the flow exit angle from the baseline base. Due to unavailability of interface of steam table with MISES, an equivalent gamma model was used to arrive at correct specific heat values and their ratio to represent steam. Equivalent gamma and specific heat values were calculated from inlet and exit steam conditions. Inlet and exit steam conditions were inputs to present work provided by one dimensional turbine design tool.

The three dimensional numerical analysis of the stator and rotor was performed using commercial software CFX 15.0. CFD context models were built using commercial software NX. Steady state RANS simulations were carried out on single stage modeled using hexahedral mesh. ANSYS TurbogridTM was used for meshing. Mixing plane approach with stage interface was used with specified pitch values. In this approach, the flow variables are tangentially averaged out at the interface of rotating and non-rotating domain. This sears out the unsteady effects of wake on the performance of downstream blade row. However, with the limitations on resources, unsteady calculations were not performed. The mesh size for both stator and rotor was approximately 5 million. Also, the boundary layer refinement with a target y⁺ on all wall boundaries to be unity was maintained. Values of post analysis numbers for y⁺ was less than 1 in all the cases at all wall boundaries. Turbulence model used was $k-\omega$ SST. Furthermore, for all the runs, mass and energy imbalance was maintained below 0.001%. Standard "real gas" steam was used as fluid medium. Figure 3-1 illustrates CFD context model of a typical stage analyzed. Boundaries in the CFD domain were as indicated. Inlet boundary was located at distance of one axial chord length upstream of stator. Exit boundary was located 1.5 times axial chord length downstream of rotor. Interface was located at the point for least radius on the axi-symmetric endwall contour on the casing. Location of interface was decided in order to avoid sudden expansion region or compression region at the downstream of stator exit or upstream of rotor inlet respectively. In order to capture the effects of laminar to turbulent boundary layer transition, gamma-theta transition model was incorporated in the numerical simulation.

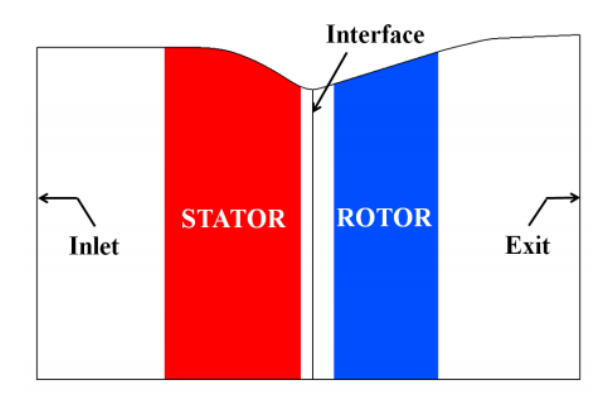


Figure 3-1 CFD domain



3.1 BOUNDARY CONDITIONS

A three dimensional numerical analysis of a three stage run with the target stage at the center was performed. This preliminary analysis has the only purpose of attaining the boundary conditions for the target stage. The stagnation profiles and direction cosines feeding into the target stage were extracted and used as boundary condition for inlet. At the exit, a single value of mass flow was used a boundary condition. This is done so that the design intent is not affected when vortexing methods are considered for further improvement. With the inlet and exit boundary conditions fixed, the three dimensional CFD was run for baseline stage. Mid span flow parameters of this run were extracted and used as boundary condition for the two dimensional MISES run. The boundary conditions were maintained for the airfoil design trials.

3.2 ASSUMPTIONS AND SIMPLIFICATIONS

Since the work presented here is in initial phase of a turbine design cycle, the complex three dimensional flow in a turbine is simplified and several assumptions have been made. These aspects need to be relooked in the later part of design cycle. Unsteady flow phenomenon which is inherent in turbine flow was not considered in present study. The number of stator blades and rotor blades (for the tall stage) in the baseline case being 60 and 125 respectively, calls for a full wheel analysis of stator blade row and rotor blade row. Due to limitation on resources and study being in initial phase of design cycle, unsteady calculations were not carried out. Wake effect from the stator blade row into the rotor is nullified as the flow variables are tangentially averaged out in a mixing plane approach.

At present, aspects of heat transfer analysis and structural analysis inputs are not considered for the modified design. These are of paramount importance in design cycle of turbine stage. Since the study involves numerical work, relating the same to actual flow physics should be backed up by experiments. Significant predictions of efficiency gain in numerical work will justify the possibilities of experiments to be carried out. This forms a part of future work. However, the present work is aimed at predicting qualitative trend in improvement or otherwise.

3.3 MESH DETAILS

Structured hexahedral mesh for the airfoil and flow passage was generated using commercial tool ANSYS TurbogridTM. Mesh sensitivity study was done for all the design cases. Mesh size was around 3 million for each blade row in the design iterations. Boundary layer was refined with a target y^+ of unity at all wall boundaries. Post analysis numbers for y^+ were maximum of unity for all the cases at all wall boundaries.



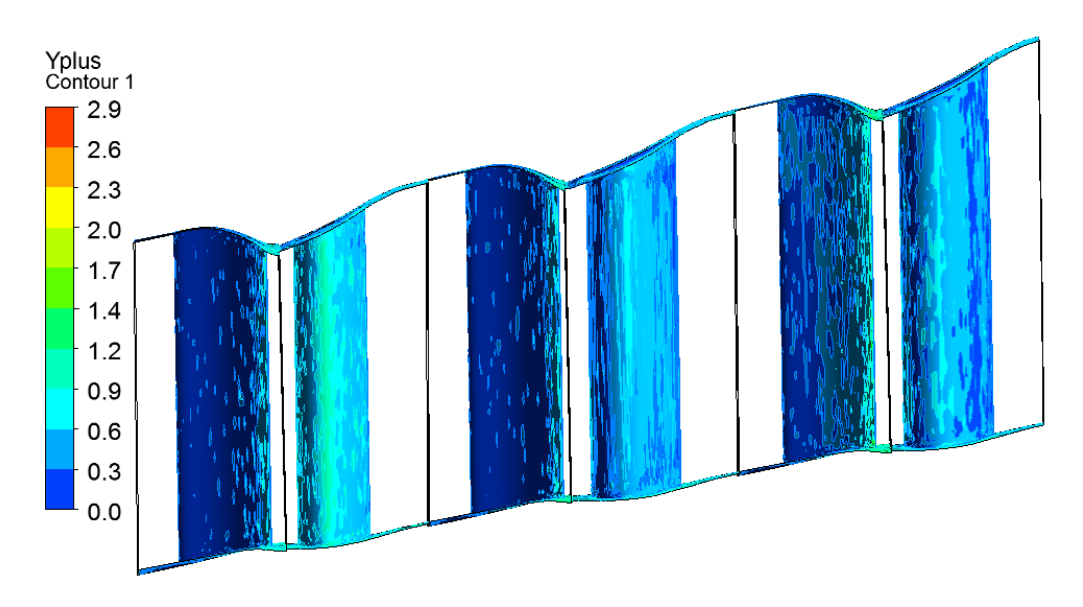


Figure 3-2 Smoot end-wall stage #11

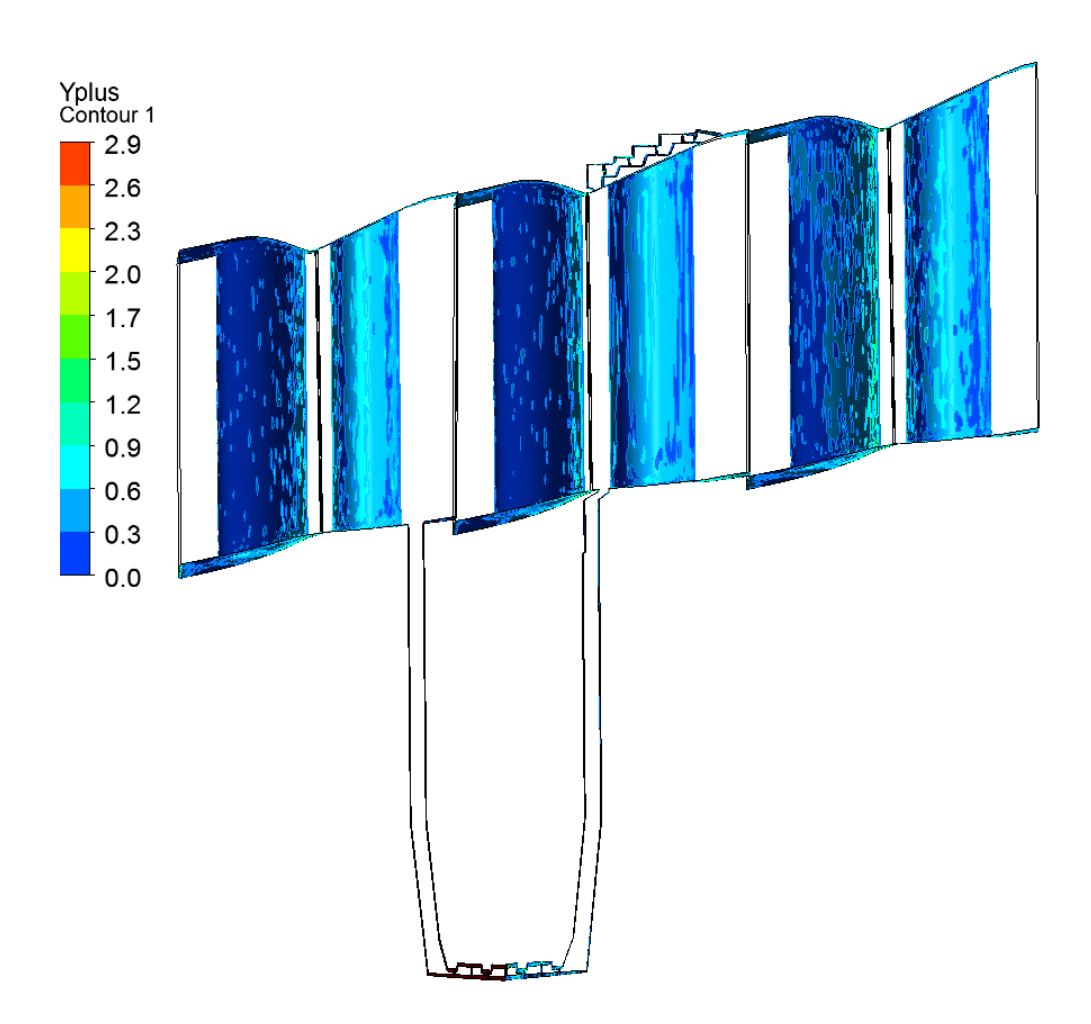


Figure 3-3 Extended geometry stage #11



3.4 GRID SENSITIVITY STUDY

Firstly, the results had to be grid insensitive. In order to accomplish this, the CFD domain of the stator and the rotor was run with different grid sizes. Stator and rotor grid sizes were varied in steps of 25 percent increase in mesh size. Changes in the results for the stator were monitored by total pressure loss coefficient (Y), while for the stage, changes in results were monitored by efficiency and hence, taking care of grid sensitivity in the rotor. Delta in Y and efficiency are computed as difference value from that of the first analyzed grid. The results are shown in Figure 3-4. The size of the first mesh for the stator was 2 million and for the rotor, it was 1 million. After grid increasing factor of 1.5, no significant changes in Y and efficiency were observed as shown in Figure 3-4. Hence, 1.5 grid factor was chosen making a final analyzing grid for the stator and the rotor to be around 5 million. The grid sensitivity study was performed on the baseline case as well as the first rotor modification case when rotor incidence was changed. From this study for the considered geometry, it is assumed that performance of the stator and rotor are insensitive to number of grid points.

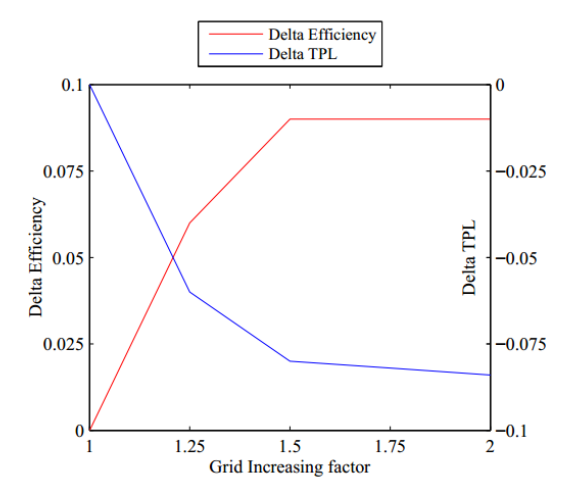


Figure 3-4 Grid independency study

3.5 BOUNDARY CONDITIONS

At inlet of CFD domain, stagnation conditions were provided as boundary condition. Total pressure profile imposed at inlet is shown in Figure 3-5. This inlet profile was built in comparison to the profile obtained from multistage analysis. At exit of domain, single value of mass flow was used as boundary condition. The purpose was not to impose a static pressure value or profile that would affect the design intent.



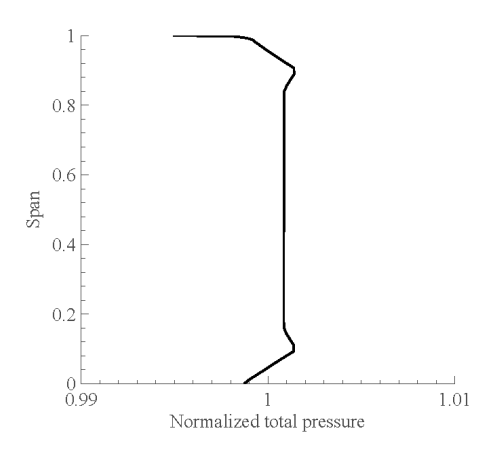


Figure 3-5 Inlet total pressure profile

3.6 OBJECTIVE FUNCTIONS

The total pressure loss (Y) is considered to be an objective function and defined as a ratio of difference of the total pressure at inlet and exit of blade row to dynamic pressure at the exit of the blade row.

$$Y = \frac{\Delta p_t}{q_{exit}} = \frac{p_{t(inlet)} - p_{t(exit)}}{p_{t(exit)} - p_{s(exit)}}$$

For calculation of Y for rotor, properties in relative frame of reference are considered.

The rationale behind the selection of the total pressure loss parameter is its direct coupling to entropy:

$$T_t \cdot ds = \overbrace{dh_t}^{=0} - v_t \cdot dp_t \\ v = \frac{R \cdot T}{p} \end{cases} :: \delta s = -R ln \left(1 - \frac{\delta p_t}{p_t} \right)$$

If the value of δ is small, then one can apply a Taylor series to yield:

$$\frac{\delta s}{R} \approx -\frac{\delta p_t}{p_t}$$

Secondary losses being also the focus in the work done, CSKE and SKEH are used to quantify the improvement in secondary losses. CSKE quantifies the amount of flow deviating from the primary flow direction. There are two definitions of CSKE considered for analyses in present work. One by Germain et al [9] and another by Corral et al [10].

In the method proposed by Germain et al [9], a plane at the exit of stator is considered with velocity field of $c(r,\phi)$ as shown in Figure 3-6. First \overline{c} is found at each radius by averaging the tangential component. Next step is to find c'. In the field of c' at stator exit, a window from hub to tip of the plane is considered and velocity values are averaged spanwise. This gives \overline{c} . Difference of c' and \overline{c} gives c''. This is considered for all three components of velocity to calculate secondary kinetic energy as shown in Figure 3-6 and in the equations below.



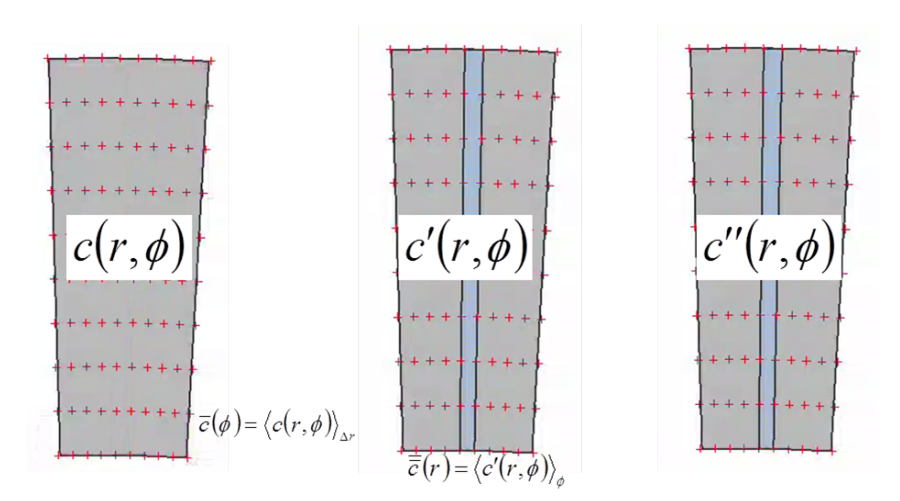


Figure 3-6 Secondary kinetic energy

$$\begin{split} &\bar{c}(r) = \langle c(r,\phi) \rangle_{\Delta r} \\ &c'(r,\phi) = c(r,\phi) - \bar{c}(\phi) \\ &\bar{\bar{c}}(r) = \langle c'(r,\phi) \rangle_{\phi} \\ &c''(r,\phi) = c'(r,\phi) - \bar{\bar{c}}(r) \\ &\bar{c}(r) = \langle c(r,\phi) \rangle_{\phi} \\ &c''(r,\phi) = c(r,\phi) - \bar{c}(r) \\ &SKE = \frac{\dot{m}}{2} \cdot \left\{ (c''_x)^2 + \left(c''_{\phi}\right)^2 + (c''_r)^2 \right\} \end{split}$$

Definition of CSKE by Corral et al [10] follows the equations

$$CSKE = \frac{\left(v_i - v_{pi}\right)^2}{v_{exit}^2}$$

Dot product of two vectors viz. local velocity vector and circumferentially averaged velocity vector is computed. A plane comprising 100 span wise points and 50 tangential points at the exit of stator is considered. Circumferentially averaged velocity direction at each span wise location is considered to be the primary flow direction. At each node point, the velocity vector is compared to the average velocity and the portion of local velocity vector contributing in the primary flow direction is determined by projection of vectors. The remaining portion of local velocity vector is quantified as secondary flow velocity contributing to secondary kinetic energy. This is normalized by nozzle exit dynamic pressure and coefficient is termed as CSKE.

$$v_{pi} = \frac{v_i \cdot v_m}{v_m^2} \cdot v_m$$

Once the CSKE is calculated, procedure to calculate SKEH is as defined by Corral et al [10], wherein the definition of non-dimensional helicity is given by

$$H_i = \frac{|v_i \cdot \omega_i|}{\frac{v_{exit}^2}{c}}$$



where v_{exit} is the mass averaged exit velocity, ω_i is the local vorticity vector and c is the blade chord. Finally, SKEH can be written as,

$$SKEH = CSKE_i \cdot H_i$$

Pictorially, helicity can be conceived from Figure 3-7. The secondary flow image is taken from VKI lecture series by Haller et al [11]. There are two vectors, viz, vorticity vector and velocity vector. If both are aligned to each other, that is the case of streamwise vorticity. If there is some angle between two vectors, the magnitude of dot product is an indicative of relative positions of vectors.

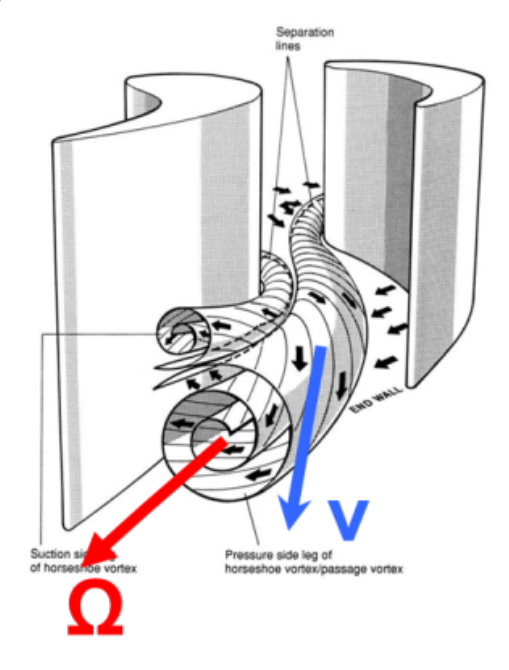


Figure 3-7 Helicity

Isentropic efficiency is the third objective function and is defined as ratio of actual enthalpy drop to ideal (or isentropic) enthalpy drop:

$$\eta_s = \frac{\Delta h}{\Delta h_s} = \frac{h_1 - h_3}{h_1 - h_{3,s}}$$

3.7 DESIGN LIMITATIONS

The work has been carried out with a certain turbine technology in mind and this imposes limitations in terms of:

- Unchanged thrust force i.e. no change in bulk reaction
- "Standard stages" with modest intra-stage swirl level
- Same stress levels

The mentioned limitations narrows down the design space considerably – simply because the throat areas for the stators and rotors have to be retained. A future



continuation of the present work should include a variable reaction and loading philosophy.



4 Results

4.1 IMPROVEMENTS IN AIRFOIL DESIGN – STAGE #16

In this chapter, airfoil design for the stator and rotor blade rows is discussed. The objective is to reduce the profile losses and hence increase the efficiency.

The fluid flow in turbomachine is, indeed, complex can be assumed to be comprising of two components - flow over airfoil sections and unintended flow e.g. along the end-walls associated with turning flow in airfoils. The leakage flows add to the complexity and losses to the flow along the end-walls. Local flow behaviour on an airfoil section in a turbomachine is influenced by local airfoil section parameters as well as pressure fields existing from adjacent airfoil sections. This is commonly referred to as blade-to-blade (or S1) flow field. Design of airfoil sections is in turn the design of the flow passage between airfoils because of the strong influence of blade-to-blade flow field. The losses associated with the blade-to-blade flow field are typically coined as *profile losses*. The discussion in the present chapter is about the airfoil design and associated profile losses specific to the stage under consideration i.e. the stage from intermediate pressure section of SST-900.

From the stagnation point at the leading edge, the flow starts from zero velocity and boundary layer starts growing as shown in Figure 4-1. The figure highlights the suction side of the airfoil because more than 80% of the losses occur on the suction side of the airfoil in turbine flows [8]. Initially, the boundary layer is (or may be) laminar. The changes in the boundary layer are significant and contribute towards loss patterns. In order to reduce skin friction loss on the suction side, the fraction of laminar boundary layer length has to be increased to the maximum possible extent. This is because, it is reported that the friction loss is almost proportional to the square of velocity in the laminar region and to the cube of velocity in the turbulent region [3]. A laminar boundary layer, however, stands a risk of separation bubble towards the trailing edge of airfoil because of increased diffusion factor. Hence, such profiles should be carefully designed to ensure turbulent reattachment before reaching the trailing edge. Shape factor is a non-dimensional parameter, which is indicative of the location of transition point. The shape parameter is defined as:

$$H = \frac{Displacement\ thickness}{Momentum\ thickness} = \frac{\delta^*}{\theta}$$

A sudden dip in the value of shape factor shown in Figure 4-1 indicates the transition point.

For given boundary conditions of inlet and exit Mach numbers, a turbine airfoil can be designed to be either a front-loaded airfoil or an aft-loaded airfoil. Front-loaded airfoils are also called to be flat-roof-top designs owing to the Mach number distribution on the suction side. A schematic representation of airfoil designs is shown in Figure 4-1. The decision for an airfoil to be front-loaded or aft-loaded depends on free stream Reynolds number, amount of expansion in the blade-to-blade passage and boundary layer patterns on the airfoil. Extent of profile loss numbers are vastly dependent on the path taken by surface velocity distributions from inlet Mach number to exit Mach number as shown in figure. Coull et al. [12], [13] studied the effects of front-loaded and aft-loaded airfoils on profile losses of turbine blades. It was *reported* that front-loaded airfoils are more robust



for various incidence angles¹³. However, in both the designs, loss is a strong function of diffusion factor. Diffusion factor is a measure of diffusion gradient in the blade-loading diagram. Experimentally, it was observed that front-loaded airfoils cause higher secondary losses¹⁴ [14]. Even the leakage losses increase with front-loaded airfoils – if the row is unshrouded [15]. These factors further add to complexity of design philosophy for optimum airfoil loading.

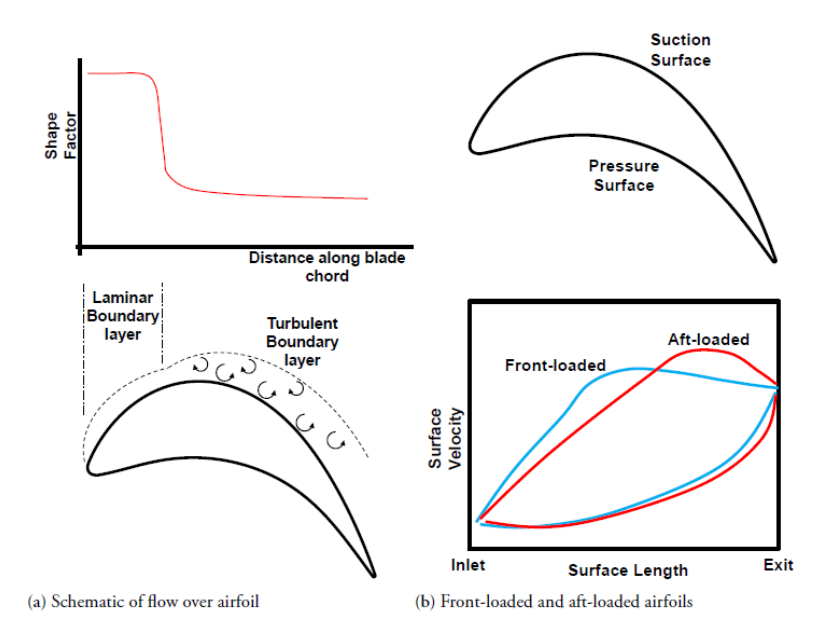


Figure 4-1 Cascade aerodynamics

Dependence of airfoil section performance on the incidence angle is another aspect that is analysed in present work. Effect of incidence angle on the profile loss is reported by many researchers [16], [17], [18]. Effect of incidence is also mentioned in prediction models proposed by Moustapha et al [19]. The general conclusion drawn from these reports is, profile losses increase quite rapidly as the incident flow vector tends to move from the pressure side of airfoil towards the suction side of airfoil. As this process takes place, a separation bubble starts to form on the pressure side of airfoil and causes gradient of loss with incidence angle. In the context of present work, changes in flow behaviour towards the leading edge is one of the points to focus.

High performance airfoil designs require good control on the curvature distribution on airfoils. Effect of smooth curvature on airfoil performance is discussed by Korakianitis et al. [20], [21]. The curvature and the slope of curvature are highlighted as controlling parameters to avoid undesirable loading distributions, local acceleration and deceleration. The curvature controls the local flow velocity levels. Theoretical and experimental evidences are provided for dependency of blade performance on curvature distribution of the airfoil. When comparing the difference in performance between designed blade and actual manufactured blade, curvature and its slope being maintained rather than every point being maintained, is projected as an important aspect.

43



¹³ This is highly questionable and the general perception is that aft-loaded blades are less sensitive. This is due to the "forgiving" effect of having acceleration after local diffusion, which in this case is caused by a miss-aligned stagnation point (cf. the earlier discussed "nose loading" rule).

¹⁴ One convenient way is to introduce the Marchal number which yields a qualitative gauge of the coupling between the loading philosophy and secondary loss.

The primary research objective here is to decide design philosophy for stator and rotor airfoils i.e. front loaded or aft-loaded. The Reynolds number for the present geometry being high (~106), the design philosophy is not obvious and needs to be established for the geometry considered. The degree of reaction being low is another factor to be considered. Designing better airfoils for the stage also means addressing issues like incidence and curvature distribution if any.

In the work presented here, modifications made to airfoil sections of stator and rotor are discussed.

4.1.1 Rotor improvements

From the non-dimensional numbers that define the stage parameters i.e. work coefficient, flow coefficient and reaction, the flow angles and velocity vectors were first calculated. The velocity triangle which serves as input to airfoil design was first checked. The velocity triangle calculated is shown in Figure 4-2 (a). The values of the velocities are not shown for proprietary reasons. The focus here is on the rotor inlet flow angle. The calculations show that there is difference in the rotor inlet flow angle and the rotor inlet metal angle. In the figure, calculated flow angle and actual metal angle are shown to be 38.82° and 35.27° respectively. There is a negative incidence of 3°. This being negative incidence, the first objective was to check for efficiency gain by correcting the incidence. Rotor inlet metal angle was corrected by 3° to match the incident flow angle. Elaborate results and methodologies from this study are presented in Paper I. It was observed that due to change in incidence, a gain in total a total stage efficiency of 0.17% could be obtained.

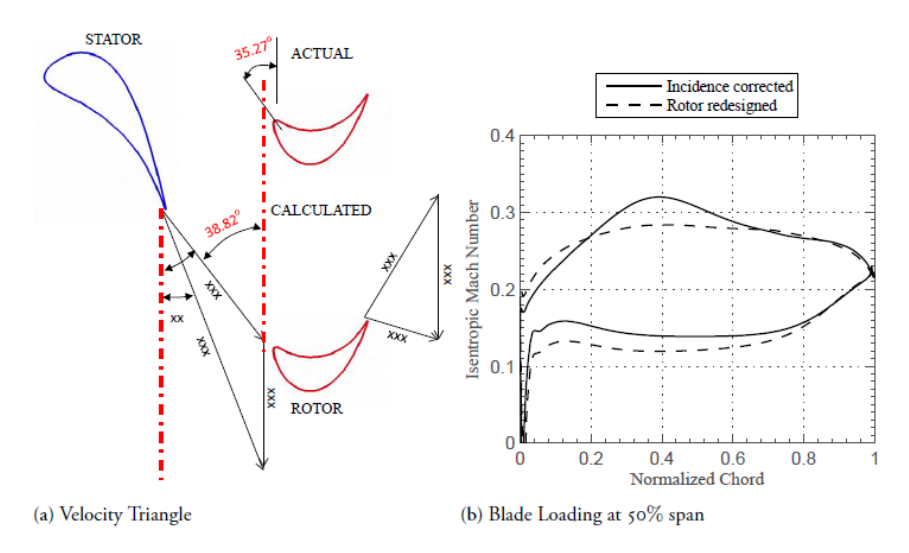


Figure 4-2 Modified rotor design

Figure 4-2 (b) shows the blade-loading for rotor with incidence corrected. It can be observed that from the leading edge there is initial acceleration to Mach number 0.32 at a distance of 0.4 axial chord. And from there on, flow is diffusing to exit Mach number. The reaction of the stage being low, the expansion of flow in the rotor is relatively less. Hence the acceleration to 0.32 Mach number and then the diffusion could be avoided. This was attempted and result is shown in Figure 4-2. The redesigned rotor shows flat top Mach number distribution with reduced peak Mach number. With the Mach number



levels reduced, the losses are also reduced. With the rotor redesigned, the stage efficiency further increased by 0.06%. Observing the streamwise vorticity distribution at the exit of rotor, it was verified that the improvement was only from profile losses and there was no changed in the secondary loss pattern due to changes in rotor redesigns. Overall increase in efficiency due to rotor airfoil redesign was 0.23%.

4.1.2 Stator improvements

As the reaction of the stage under consideration is low, relatively higher acceleration can be expected in stator. The blade-loading of the baseline stator is shown in Figure 4-3 (a). It can be observed that the baseline stator has two slopes of acceleration on the suction side. With an intent to make the acceleration smoother and to make the flow accelerating till further downstream on the airfoil surface, stator was redesigned. The overlap of resulting blade-loading over baseline blade-loading is shown in the figure. The acceleration is more gradual and smooth in the redesigned stator. Also, the airfoil is relatively more aft-loaded. In the redesigned stator, the shape factor was checked for laminar to turbulent boundary layer transition. As a result of redesign, the transition from laminar to turbulent boundary layer is delayed. These two aspects of gradual acceleration and delaying the transition are favorable to reduce the profile losses. However, it can be noted that the diffusion patterns in the baseline and the redesigned stator are similar. Another important factor contributing in the redesigned stator is the curvature distribution. The baseline airfoil, the redesigned airfoil and the curvature distribution on suction side of redesigned airfoil are shown in Figure 4-3 (b). The curvature is maintained smooth on the suction side of modified airfoil. The total to total stage efficiency of the stage further increased by 0.15 due to changes in the stator airfoil design.

Significant improvements are seen due to incidence correction in rotor; 0.6 in total pressure loss and 0.17 points in efficiency. Changes in airfoil design for stator and rotor resulted in overall efficiency improvements of 0.33%.

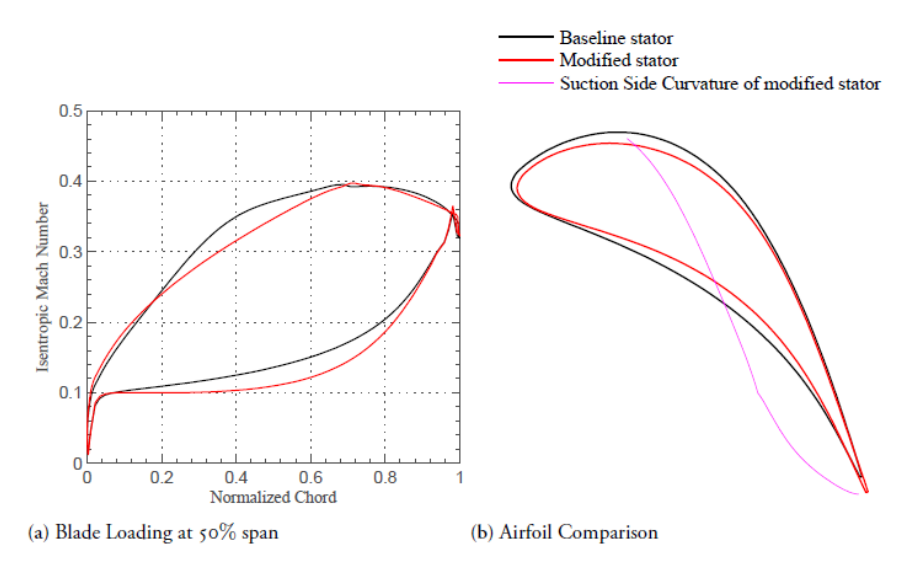


Figure 4-3 Modified stator design



4.2 PERFORMANCE WITH MODIFIED PITCH-TO-CHORD RATIO

In turbomachines, as mentioned, there is a strong influence of adjacent airfoil section on the blade to blade flow field rather than flow over blade in isolation. This flow field is strongly influenced by the pitch-to-chord ratio. Figure 4-4 shows the definition of pitch-to-chord ratio and typical trends in loss behavior depending on pitch-to-chord ratio. It can be understood from the figure that an optimum pitch-to-chord ratio is a break even between viscous and turning losses. Higher the number of blades (low pitch-to-chord ratio), higher is the wetted region and higher is the viscous loss (cf. $\int C^3 dA$ discussed earlier). With the pitch-to-chord ratio being low, there is a possibility of redundancy of metal used.

Lower the number of blades, higher is the lift force per airfoil section for fixed boundary condition. Due to less number of blades, the lift force per blade increased and hence velocity levels are higher. These factors lead to higher losses. An optimum pitch-to-chord ratio is a choice of the designer for minimum losses. During the initial design phase, there are loss models to select the pitch-to-chord ratio [22], [23], [24], [2], [25]. The loss models help the designer a great deal to select the preliminary pitch-to-chord ratio. However, enough care should be taken at later design phase to check for performance with selected pitch-to-chord ratio.

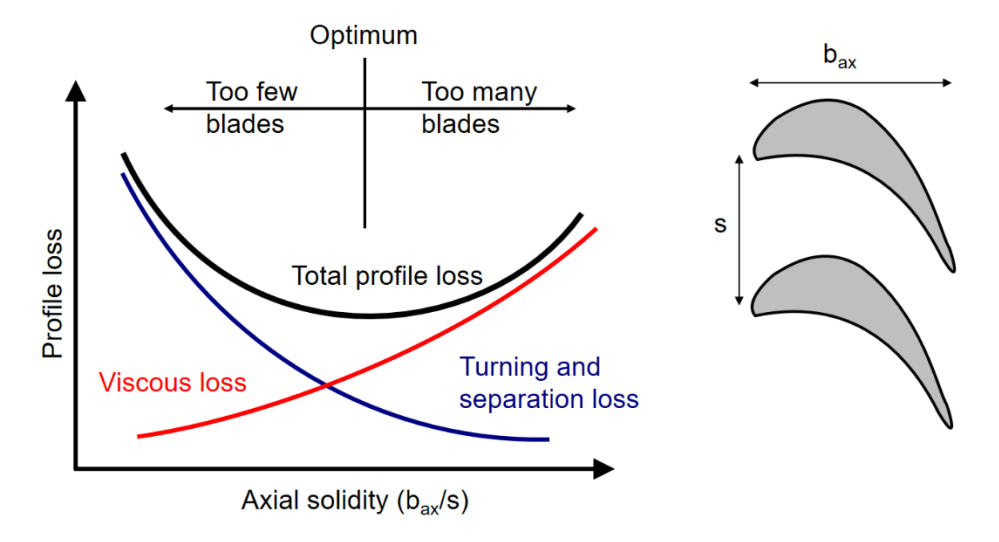


Figure 4-4 Pitch-to-chord ratio

4.2.1 Pitch-to-chord ratio of stator

Performance improvements in stator by modifying the pitch-to-chord ratio was done in two steps. First, the blade count was reduced from 60 to 50 where in the pitch-to-chord ratio increased from 0.75 to 0.82. Second, the pitch-to-chord ratio was further increased by decreasing the axial chord by 3 mm. Final pitch-to-chord ratio of the stator that was studied was 0.86. The blade-loading comparison for the three cases are shown in Figure 4-5. Since the boundary condition was maintained, it can be observed that blade-loading increased with each iteration of increased pitch-to-chord ratio. The area covered by the blade-loading curves on the suction and pressure side is indicative of the lift force or the work done by the airfoil section. This area covered by blade-loading curve can be seen to increase by increase in pitch-to-chord ratio. The location of peak Mach number shifts upstream on the suction side of the airfoil. This shift in peak Mach number also means that there is relatively larger surface length available for the flow to catch up to the exit



Mach number. Hence reducing the diffusion losses. The total-to-total efficiency of the stage increased by 0.52% with the reduced blade count and further increased to 0.66% with decreased chord. These efficiency numbers include the airfoil design iterations that were discussed in previous sections of this chapter. The comparison in airfoil sections are shown in Figure 4-5. The increase in efficiency indicated that the airfoil section can still handle the turning for the given boundary condition.

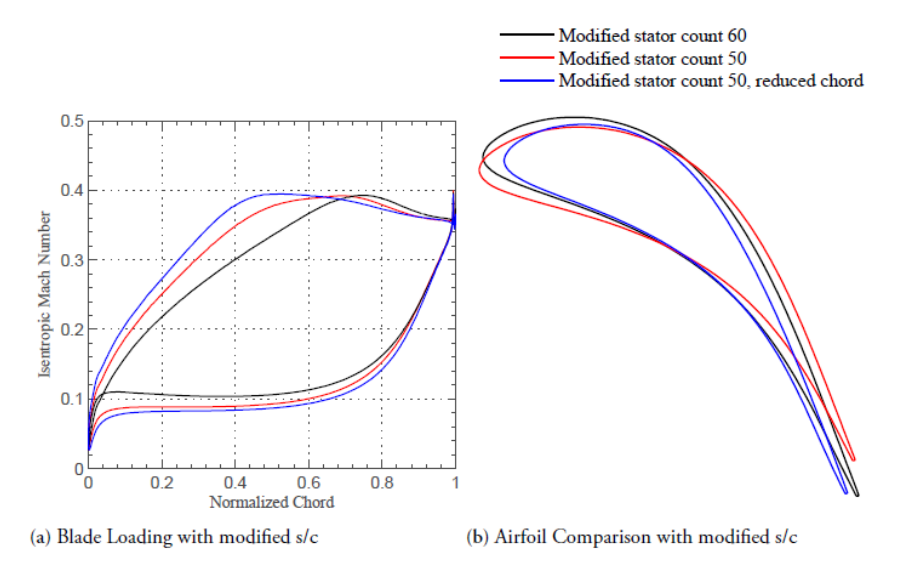


Figure 4-5 Stator pitch-to-chord ratio

The increased loading was shown to be beneficial because of the reduced rate of diffusion – cf. Figure 4-6 for further information. The result is a trade-of between the velocity level per se, the state of the boundary layer and the subsequent diffusion process. If one reverts to the U-cube reasoning ($\int C^3 dA$), then it is apparent that this case gains from the reduced rate of diffusion rather than just the velocity level.

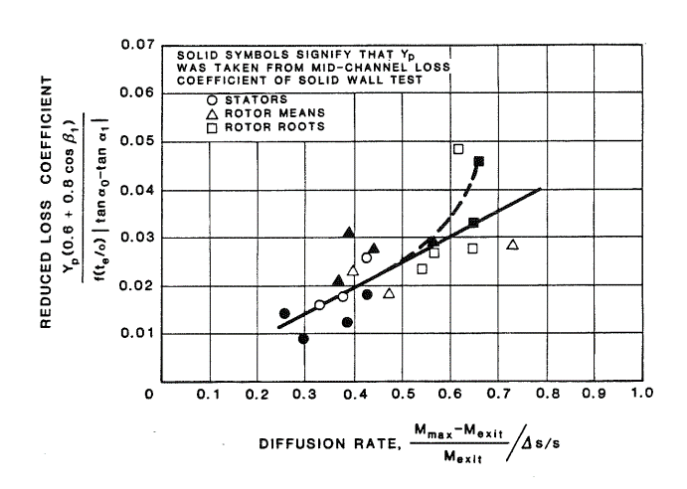


Figure 4-6 Losses vs. the diffusion rate parameter

One caveat is, however, in place because higher blade loading tends to increase the amount of front loading. This could render in higher secondary losses and should therefore be carefully further evaluated before implementing.



4.2.2 Pitch-to-chord ratio of rotor

Pitch-to-chord ratio variation in rotor is more complicated as the mechanical requirements are more stringent in rotating parts. Hence, not many modifications were tried on rotor. Axial chord of the rotor was reduced by 2 mm while retaining the blade count. Comparison of airfoils is shown in Figure 4-7. Overall efficiency gain with airfoil improvement and pitch-to-chord ratio study on stator and rotor was 0.74%.

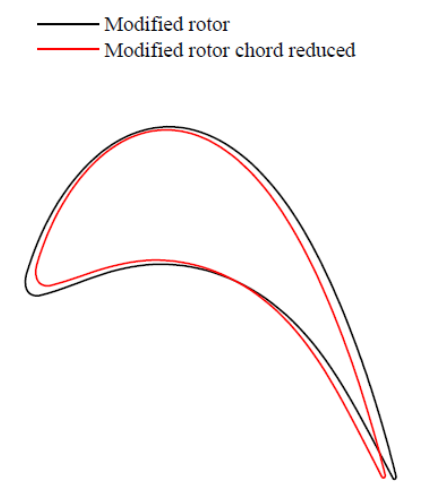


Figure 4-7 Rotor pitch-to-chord ratio

4.3 PROFILING SUMMARY

The SST-700 and -900 units are mature products but despite of that fact, some room for improvement still exists. The work reported in this chapter is for tall stages, where the aspect ratio is high. This means that the profile loss is high when compared to the end-wall losses.

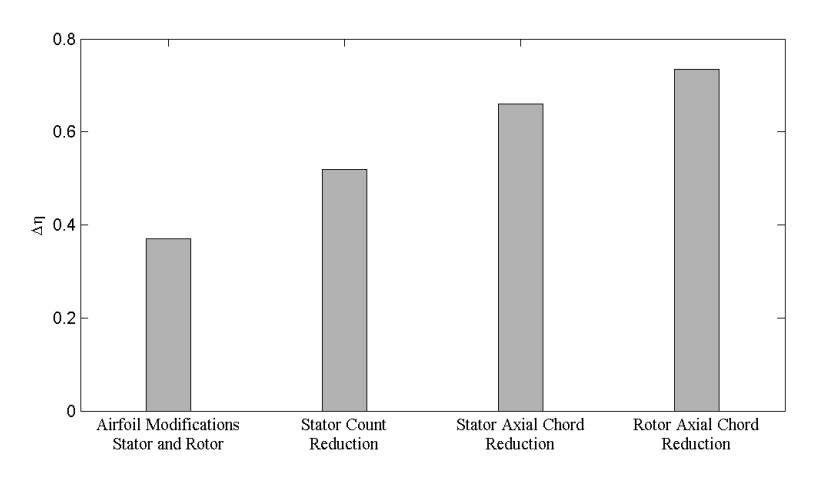


Figure 4-8 Efficiency gain with airfoil redesign

The efficiency improvements due to redesign of airfoil sections for high aspect ratio blades were found to be significant. The overall improvement is 0.74%. Figure 4-8 shows the incremental improvement in efficiency by each design iteration performed. This



improvement, verified numerically by RANS simulations is significant for the design to be relooked at. It is understood that these numbers that are being looked at aerodynamic perspective, needs to be endorsed by other disciplines too. But the amount of efficiency improvement makes a strong case to be looked at from product perspective.

4.4 PROFILE CLONING

The presented work has been carried out on a certain stage in the turbine and there is a need to be able to create profiles with the same characteristics for other stages. As discussed in the introduction, the curvature is the main driver behind the velocity distribution. This means that one can create a library with suitable curvature distributions and then apply these wherever required. The word curvature has a strict mathematical definition for a curve (of arc length "s") where the coordinates are expressed in Cartesian curvilinear (t=0...t=1) form i.e. y(t) and x(t):

$$\kappa = \frac{1}{r_c} = \frac{d\varphi}{ds} = \frac{\frac{d\varphi}{dt}}{\frac{ds}{dt}} = \frac{\frac{d\varphi}{dt}}{\sqrt{\left(\frac{dx}{dt}\right)^2 + \left(\frac{dy}{dt}\right)^2}}$$

One can after considerable algebra rewrite the preceding equation into a more useful form in Cartesian coordinates (i.e. x and y), which yields:

$$\kappa = \frac{\frac{d^2 y}{dx^2}}{\left\{1 + \left(\frac{dy}{dx}\right)^2\right\}^{3/2}} \approx \frac{2\left[\left(\frac{y_{i+1} - y_i}{x_{i+1} - x_i}\right) - \left(\frac{y_i - y_{i-1}}{x_i - x_{i-1}}\right)\right] / (x_{i+1} - x_{i-1})}{\left\{\left[\frac{1}{2}\left(\frac{y_{i+1} - y_i}{x_{i+1} - x_i}\right) - \left(\frac{y_i - y_{i-1}}{x_i - x_{i-1}}\right)\right]^2\right\}^{3/2}}$$

The preceding equation cannot be solved analytically and one has to revert to iterative numerical methods such and curve fitting (or Bezier curves). The "next" value of y_{i+1} is numerically solved from known (x_{i-1}, y_{i-1}) , (x_i, y_i) , x_{i+1} and the required curvature (κ) . There are other possibilities and one may, for example, use a modified Bessel function for implanting a more analytical approach. In any way, one should recognize that there are several ways of creating a cloned profile. All, however, carries considerable analytical geometry and numeric analysis when implemented into a profiling tool.

It is also convenient to introduce normalized curvature in order to take into account different chords and camber angles. This means that one can calculate the blade profile coordinates for any combination of chords and camber angles. Normalized curvature is defined as:

$$ar{ar{\kappa}} = rac{1}{ar{ar{r_c}}} = rac{\kappa \cdot camber}{chord}$$

It should, however, be noted that the suggested cloning process does not take into account for Reynolds number effects.



4.5 DESIGN MODIFICATIONS TO REDUCE SECONDARY LOSSES

Secondary loss is the target area discussed in this section which arises due to secondary flows. Any flow behaviour not complying to primary (expected) flow behaviour is termed as secondary flow behaviour. In turbomachinery flows, the flow is expected to follow the airfoil guided path. This flow is termed as primary flow. Loosely stated, flow that deviates from the path guided by airfoil is the secondary flow. The mechanisms where discussed in section 2 but there is an additional explanation model. The other model is based on a flow kinematic point of view, which will be briefly discussed here. One of the main causes for secondary flow is the embedded vorticity in the incident total pressure profile impinging on the turbine airfoil along the blade height. Vortex lines tends to be stretched on pressure side and suction sides of airfoil giving rise to horseshoe vortices. These horseshoe vortices interact with the expected primary flow and generate a secondary loss mechanism. Amount of secondary loss is a function of many geometrical parameters such as aspect ratio of blade, turning on the blade, pitch-to-chord ratio and also the boundary conditions. It should, however, be noted that the described model by Sir Hawthorne only addresses the horseshoe vortex component. The "other" part is classic boundary layer migration driven by the cross-passage pressure gradient. This is one of the drivers behind the aft-loaded blade profiling approach – simply by moving the point, which has the maximum aerodynamic load as far back into the passage as possible.

During the present work, an attempt was made to reduce the secondary losses in the turbine stage considered. Vortexing methods and leaning of airfoil are well known three-dimensional modifications on the blade row to reduce secondary losses. Both these design modifications are discussed for the stage under consideration. Along with the non-intruding design modifications, intruding design modification like the boundary layer fence was also attempted. Introduction of boundary layer fence was based on hypothesis of breaking down horse shoe vortices.

Quantification of improvement in secondary losses was a challenge and a parameter Secondary Kinetic Energy Helicity was formulated from the available literature. SKEH and co-efficient of secondary kinetic energy discussed in the chapter *Numerical Methods* were the two functions used to monitor secondary losses for the design modifications considered.

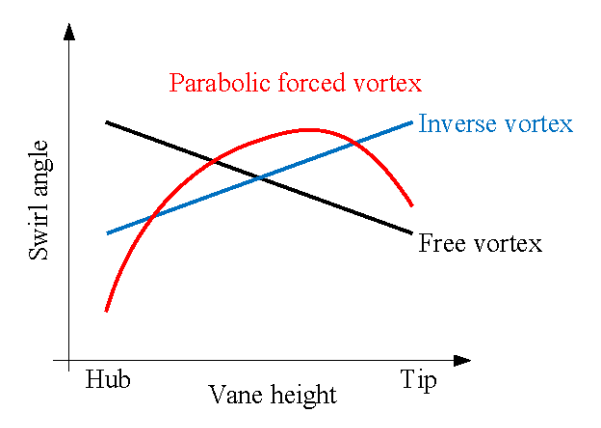


Figure 4-9 Vortexing philosophies



4.5.1 Vortexing methods

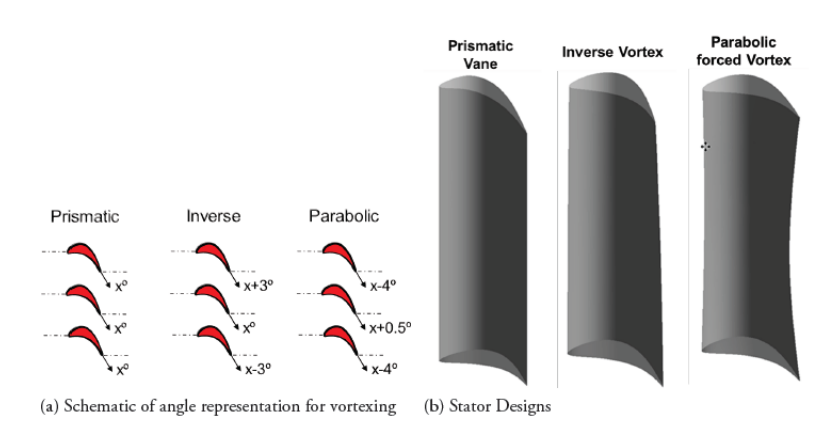


Figure 4-10 Vortexing designs

Vortexing methods primarily aim at reducing secondary losses. Also, there have been extensive research on using vortexing to produce desired pressure profiles at stator exit [8]. These desired pressure profile affects the radial distribution of reaction and can affect the leakage loss. Hence, vortexing influences the work and spanwise properties of a stage.

Three vortexing philosophies were adopted namely; constant section, inverse vortex and parabolic forced vortex. The constant section blade resembles a "free vortex design" because of the varying deviation angle.

In inverse vortex design, the intention is to aim at less expansion in stator at hub and more expansion at stator tip. The inverse design type resembles the forced vortex approach and the difference lies in the lower swirl angle variation. One important feature of the inverse vortex design is the rotor hub inlet angle, where one can show a significant reduction in gradient of incident swirl angle. The inverse vortex design also results in a fairly un-twisted rotor leading edge. The latter is indeed useful for cooled gas turbines but this is outside the current research work. The gain in efficiency due to the inverse vortex twist may be accounted to the reduced turning at the hub-section for both the stator and rotor.

Parabolic forced vortex aims at less expansion at hub and tip section. This is because the incoming flow in the boundary layer has embedded vorticity and less momentum at hub and tip. To maintain the same reaction and same work extraction, this calls for more expansion at the mid-section. It is clear from the figure that, for a parabolic forced vortex design, flow angles are reduced at the end-walls. This results in opening up of airfoils for a given pitch and hence increasing mass flow rate across end-wall sections. As a consequence, flow angles at mid span increases and throat area reduces. This reduces the mass flow at mid-section. So, parabolic forced vortex changes the mass flow distribution from hub to tip and thus affects efficiency.

The three discussed vortexing methods were attempted on the stage considered. Figure 4-10 (a) shows the design modifications on the stator in order to arrive at the desired vortexing method. The angles shown use tangential reference angles i.e. angles are measure positive clockwise from the axis of the blades.

For inverse vortex design, mid-span section was retained as it is. Tip section was closed by 3° and hub section was opened by 3° . For parabolic forced vortex design, both hub



and tip sections are opened by 4°each and mid span section is closed by 0.5°. These airfoil section rotations are shown in Figure 4-10 (a). Visual differences in three stator configurations can be seen in Figure 4-10 (b). Number of blades and hence the pitch was retained the same as in reference stator. With the constraint that flow coefficient, work coefficient and reaction of the stage to be the same as in baseline, the challenge was to maintain the same throat areas for all stator configurations. Both the stator configurations matched the reference stator area within 0.3% difference. Design modifications and airfoil creations were done using in-house airfoil design tool. Throat area measurement was done using commercial CAD tools. For all the three cases analyzed, rotor was retained the same. Rotor is again a prismatic airfoil for baseline case. Using the same rotor for all the cases is expected to have some incidence problems. But, the focus of present work is vortexing in stator.

The total pressure losses in stator reduced by 1% in inverse vortex design and 0.5% in parabolic forced vortex design. SKEH reduced by 6% in inverse vortex design and 5% in parabolic forced vortex design. The designs show reduction in secondary losses. However, the total-to-total efficiency numbers does not reflect the losses reduced in the stator blade row.

4.5.2 Compound lean

Three-dimensional shaping of stator to reduce losses in a turbine stage has a long history [26]. Straight lean, compound lean, sweep, localized blade twists are a few modifications to mention [5]. However, the exact working principle of lean is not clear yet, a very good theoretical perspective is conveyed by Denton summarizing the most important effects and explanations available [5]. The effect of pressure side leaning towards the end-walls is primarily to increase the pressure locally at the hub-side and hence push the flow towards the mid-span of airfoil where the flow is predominantly following the airfoil. If in stator, lean is incorporated at both end-walls, the configuration is termed as compound lean. As a consequence, lower loadings at end-wall can be obtained.

The compound lean design of stator is shown in Figure 4-11. The angle δ shown in figure is the measure of amount of compound lean. Two values of δ were incorporated in the study 15° and 30°. With the numerical analyses of the stage, it was found that the secondary losses were reduced significantly at the exit of the stator. The coefficient of secondary kinetic energy reduced in compound lean configuration by more than 30%.

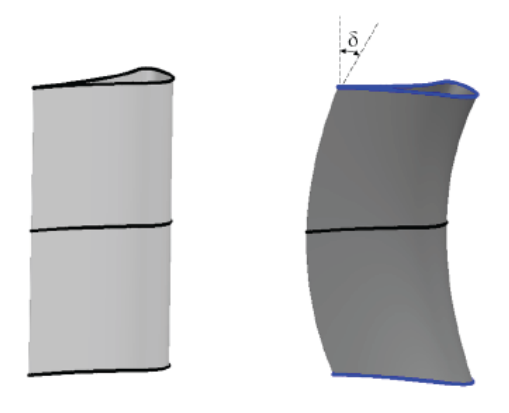


Figure 4-11 Twisted vs. compound lean stator



All the effects of compound lean reported in literature like off-loading of end-wall sections and migration of flow towards the mid-span region could be captured by numerical approach. However, the efficiency gains to the magnitudes reported in literature, due to compound lean could not be achieved. Improvements in flow reflecting in total-to-total efficiency could not be seen. There could be two reasons for losses not reflecting in improvement in efficiency. One, advantage obtained in stator blade row is nullified by the addition of losses in rotor blade row or two, may be a limitation in the prediction methodology adopted.

4.5.3 Boundary layer fence

Boundary fence is a design configuration which intrudes into the flow path to reduce the major secondary loss mechanisms. Figure 4-12 shows typical boundary fence that was tried on T106 cascade for study purpose [27]. This cascade was chosen from open literature. The selection of boundary fence is based on two hypotheses. First hypothesis is to cut the vortex line incident on the blade row and hence reduce the strength of the horseshoe vortices. Second is to reduce the cross flow between airfoil due to blade-to-blade pressure field.

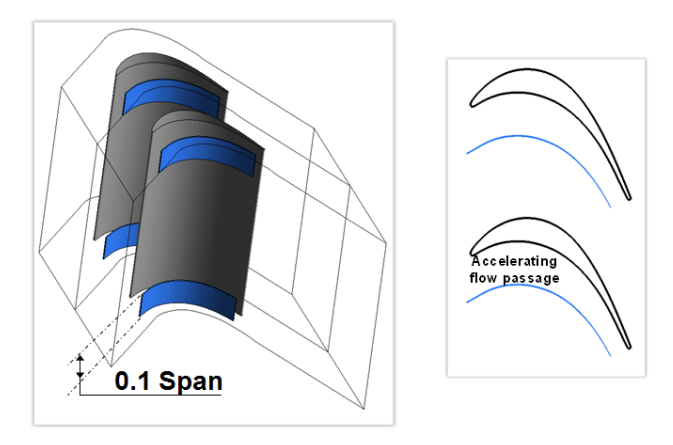


Figure 4-12 Schematic representation of boundary layer fence

Coefficient of secondary kinetic energy and SKEH evaluation of the design modification showed significant improvement in secondary losses. CSKE reduced by 30% and SKEH reduced by 40% in the presence of boundary fence. Total pressure loss also decreased indicating that added loss due to intrusion in flow path does not surpass the gain obtained due to reduction in secondary losses. Figure 4-13 shows the total pressure loss contour at the exit of the cascade overlapped with the vortex structures. Reduction of vortex strength in presence of boundary fence can clearly be observed in figure Figure 4-13.



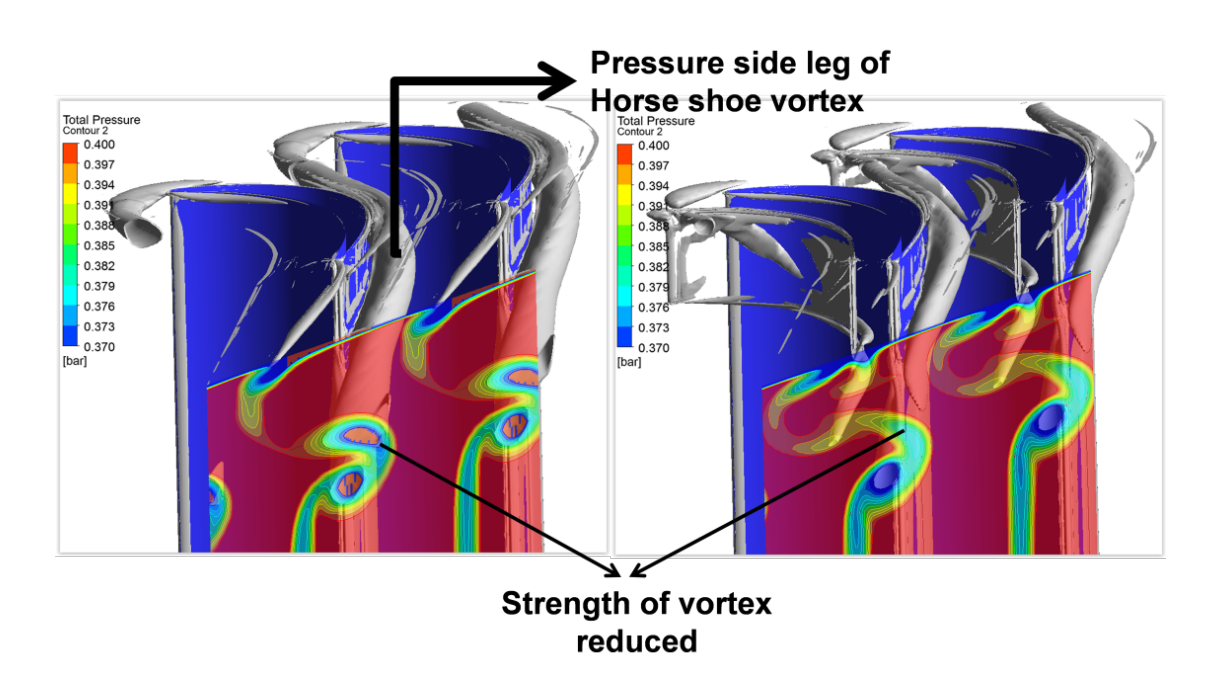


Figure 4-13 Reduction of vortex strength by boundary layer fence



4.6 MERIDIONAL FLOW PATH MODIFICATIONS

The domain of the target stage is shown in Figure 4-14 for reference. Axisymmetric end-wall contouring incorporated at the casing in the baseline flowpath shown is historically referred to as Russian kink. Main task here is to assess the significance of end-wall contouring on the performance of the stage. Given the three main loss mechanisms in turbomachinery flow *viz* profile loss, secondary loss and tip leakage loss, understanding as to which component is being addressed by the presence of end-wall contour in the present target stage is sought.

Static pressure changes that can be induced by curving the streamlines in meridional direction is one of the avenues to influence local loss mechanisms. End-wall contouring is one such design modification. To authors' knowledge, end-wall contouring was first introduced by Deich et al [6]. The purpose of axisymmetric end-wall contouring was to create a local radial pressure gradient in the meridional plane. This phenomenon of affecting the pressure by axisymmetric and non-axisymmetric end-wall contouring is studied extensively [28], [29], [30], [31]. The spanwise pressure distribution at stator exit also affects the tip leakage losses and can be used to reduce the same. As a consequence, the reaction gradient for the entire stage can be reduced using end-wall contouring.

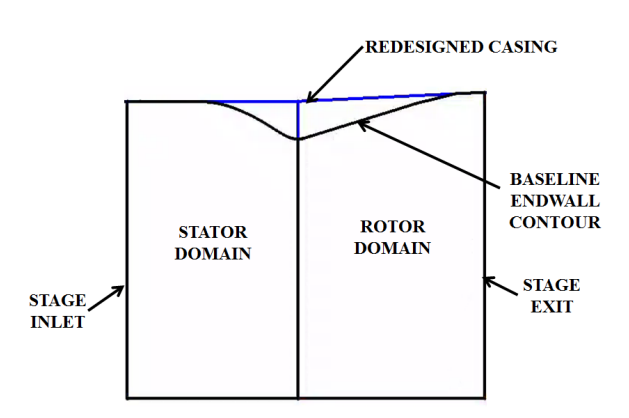


Figure 4-14 Flow path modifications

4.6.1 Flow path modifications

Design parameters of turbine stage being retained, redesign of the flow path to remove endwall contouring in the tip region is done. In order to maintain the stage loading and the degree of reaction, turning on the stator and rotor is increased. The changes in the flowpath are made from a retrofit point of view, i.e inner and outer radii at the stage inlet and the stage outlet are retained so that the stage fits into the flow path with upstream and downstream stages. This also enables design verification in multistage environment. Airfoil sections developed in earlier chapters are considered. The stage with modified airfoil design is considered as baseline for flowpath study. Throat areas of stator and rotor for new flow path are reduced in order to match the reaction. Degree of reaction was matched by trial and error and verified by three-dimensional viscous CFD analyses.

To represent the distribution of local pressure at stator exit, a term non-dimensional static pressure is used which is defined as:



Non – dimensional static pressure =
$$\frac{p_s}{p_{t,inlet}}$$

End-wall contour on the baseline flowpath was removed. Comparison of baseline flowpath and modified flow path is shown in Figure 4-15. Stage design parameters were retained from baseline. The annulus area after the stator in the flowpath is increased in the modified flowpath. Hence, the bulk velocity levels are reduced. In order to maintain the same reaction, the velocity level had to be increased. This was achieved by closing the stator by 2°. Airfoil profile thus obtained is shown in comparison with the baseline stator in Figure 4-15. As the baseline airfoil is rotated by certain amount, axial width of the airfoil is reduced. This rotation affects the blade-loading on the stator airfoil.

Comparison of blade-loading at the mid-span of stator blade row is shown in Figure 4-15 (b). Movement of throat point on the suction side of airfoil due to closing of airfoil was less than 1% of axial chord. This was calculated and verified using CAD tools (NX). Because the throat point movement on the suction surface is relatively less, the location of peak Mach number is almost the same for both baseline and the new stator without end-wall contouring. Since the downstream pressure levels and Mach numbers are fixed from baseline, there is not much difference in the blade-loading patterns at mid-span. The peak Mach number for new stator is slightly higher than the baseline case at mid-span.

Since the end-wall contouring was removed in the tip region, blade-loading plots are also compared at tip region for the stator in Figure 4-15. Blade-loading in the baseline case is relatively higher by virtue of reduced pressure at stator exit because of end-wall contouring. End-wall contouring is typically done to reduce blade-to-blade loading towards end-wall. The fact that blade-to-blade loading is increased in this case is due the axial position of the end-wall contour which drives low pressure being present at the stator exit tip location.

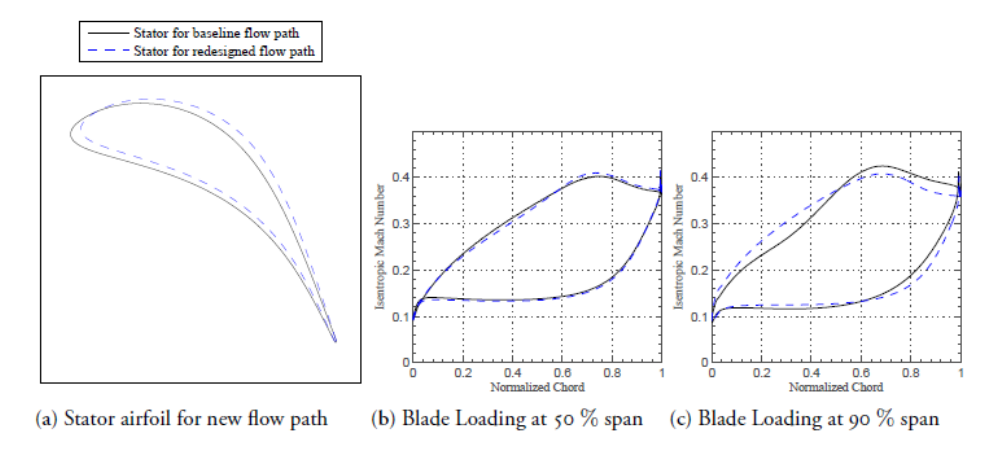


Figure 4-15 Blade loading comparison



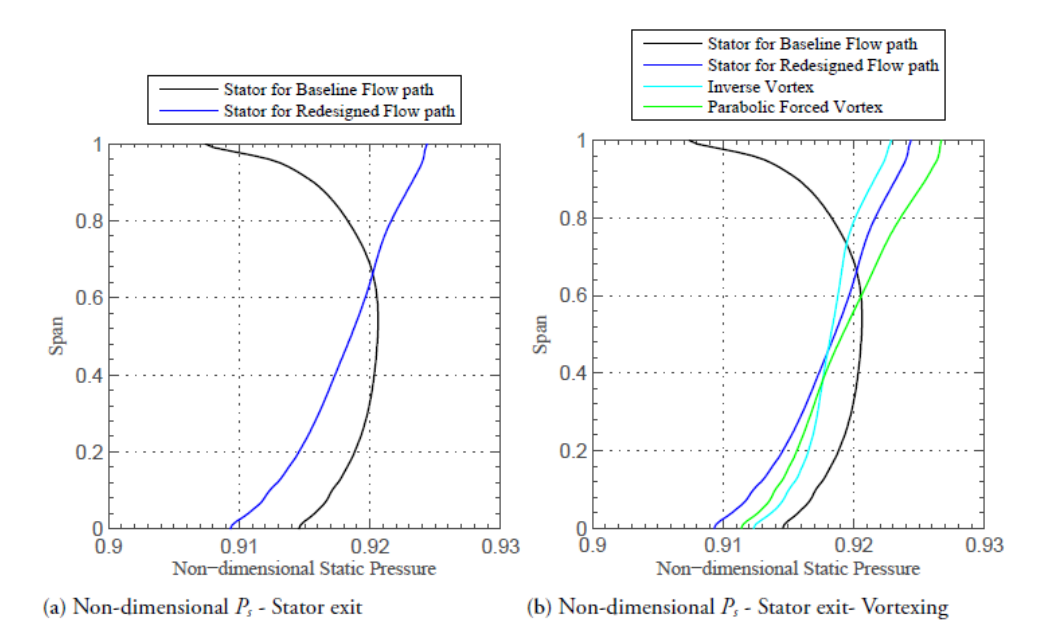


Figure 4-16 Vortexing designs

One of primary reasons for the presence of end-wall contour in baseline flow path is to obtain desired pressure profile at the stator exit. The pressure profile in turn controls the leakage flows and hence the leakage losses [8]. Static pressure profiles at the exit of stator in the form of non-dimensional static pressure are shown in Figure 4-16 (a). Local reduction in pressure in presence of end-wall contour is evident in the baseline flow path case at the tip. In case of new flow path, static pressure value at the tip is increased and hence, increasing the pressure difference across the tip seal region. This is not favourable as the leakage flow increases with higher pressure gradient.

In order to reduce the pressure locally with the redesigned flowpath, vortexing was incorporated in the stator. Vortexing methods adopted were in line with the philosophies discussed in the section *reduction of secondary losses*. It can be observed from Figure 4-16 that low pressure as obtained by end-wall contouring could not be obtained by any of the vortexing methods attempted.

It is well understood and explored phenomenon that leaning the stator with pressure side towards end-wall would increase the pressure locally [5]. A counter thought to this fact would be, to lean suction side towards end-wall to reduce pressure locally. This was attempted with suction side lean designed at the tip. This is termed as negative lean in literature. Advantages and disadvantages of negative lean are reported by Haller et al [11]. In the context of present work, negative lean is used to decrease the pressure values locally at stator exit tip.

After several iterations, configuration shown in Figure 4-17 was obtained. This was done by tangential movements of airfoil sections resulting in suction side lean angle of 12 degrees at the tip. With the suction side lean at the tip, spanwise distribution of pressure at exit of stator was extracted and compared with the previous results. Comparison is as shown in Figure 4-17 (b). The static pressure gradient is further reduced when compared to the vortexing methods, to the extent that static pressure has nearly a constant value from root to tip. By introducing suction side lean at tip, pressure side leaning in the hub region evolves as a consequence. This pressure side leaning at hub adds to already



existing straight positive lean at hub which in turn assists in reducing the spanwise static pressure gradient.

With the changes in the flow path and the stators discussed, isentropic total to total efficiency numbers were extracted and compared. Close to 0.2 percent improvement in total-to-total efficiency can be shown by changing the flow path.

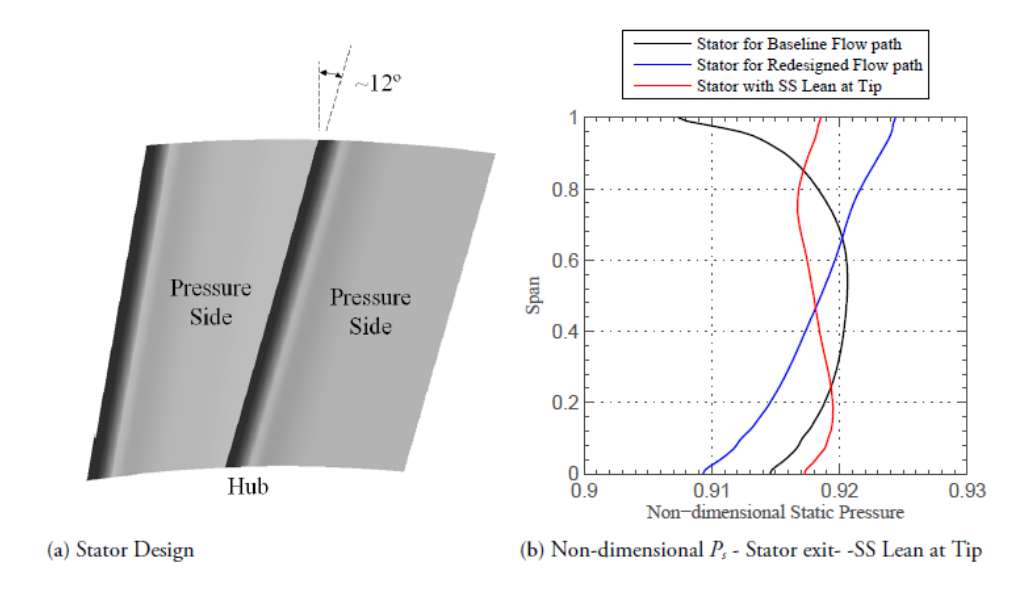


Figure 4-17 Suction-side lean at the tip

4.6.2 Tip shroud implementation

With the significance of stator exit static pressure profile discussed earlier with reference to tip leakage losses, it is important to check the performance of the modifications with tip shroud. Two tip shroud configurations were considered, one for baseline flow path and other for modified flow path as shown in Figure 4-18 (a). These were designed purely from a study perspective and have no similarities to geometry in actual turbine stage. Tip clearance was maintained to be the same in both the cases. The thought to retain the tip clearance distance rather than tip clearance area was to consider mechanical constraints to maintain gap between rotating and non-rotating components to avoid rubbing. Two seal strips were considered. It is reported that the tip leakage losses decrease by increase in number of seal strips [32]. For ease of meshing and numerical calculation, two seal strips were finalized. Also, since the difference in performance numbers are reported, it is assumed that number of seal strips will not have impact on the conclusions.



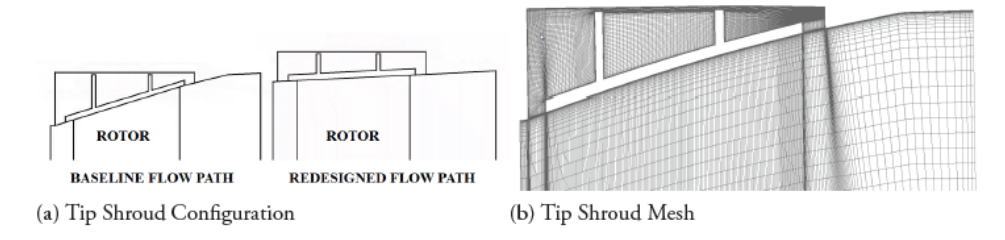


Figure 4-18 Tip shroud study

Rotors were meshed along with the tip shroud using ICEMCFD. Hexahedral mesh was generated without interface between rotor and tipshroud geometry. y⁺ of unity was targeted at all wall boundaries. A typical tip shroud mesh is shown in Figure 4-18 (b). The outer walls of the tip shroud i.e. the tip cavity was defined as stationary wall in the analysis.

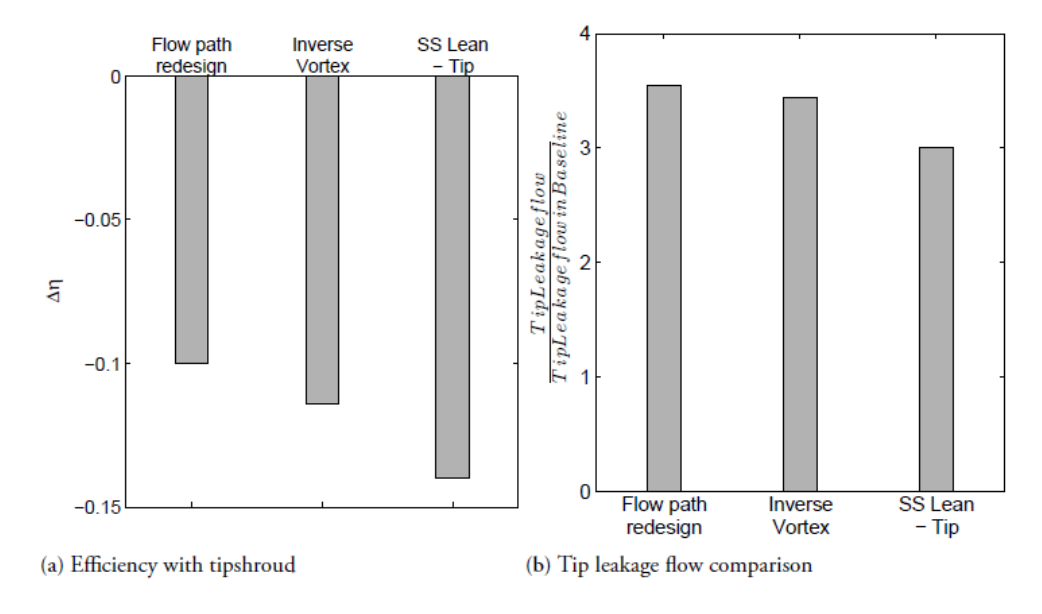


Figure 4-19 Efficiency with tip shroud

With the tip leakage flow modelled, difference in efficiency numbers are shown in a. CFD was done with stator and re-meshed rotor with tip shroud. Delta efficiency values with reference to baseline case with tip shroud are shown. Efficiency numbers of new flow path and corresponding stator modifications are less than the baseline flow path with tip shroud. There is a change in scenario in terms of efficiency numbers with and without tip leakage in the analyses. Efficiency numbers of baseline flow path with tip shroud is better than the other modifications attempted.



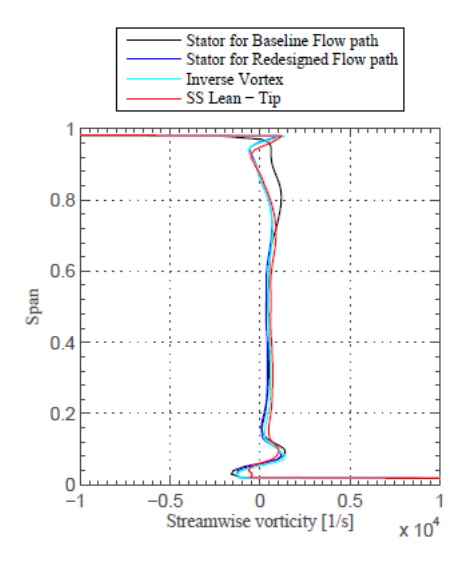


Figure 4-20 Streamwise vorticity - stator exit

In order to understand the effect of stator exit pressure profile on the tip leakage flow, the leakage flow values were extracted from numerical analyses and plotted in Figure 4-19 (b). Tip leakage flow in the baseline flow path case is around 0.25 kg/s and this is taken as reference. The leakage mass flow is approximately 0.2% of the primary mass flow through the stage. Other tip leakage flows are shown as multiples of reference case. Tip leakage flow increased with the increase in pressure at the tip of stator exit. It can be observed that low pressure at the tip in baseline case has a significant effect on the leakage flow. Also, the modification to reduce the pressure at the tip does not reveal significant impact on the tip leakage flow.

To segregate if the penalty in efficiency is by virtue of tip leakage loss alone, the indications from secondary losses had to be studied. For this reason, spanwise distribution of streamwise vorticity direction at the stator exit for the cases analysed are extracted in Figure 4-20. Streamwise vorticity is calculated using the equation:

$$\omega_{streamwise} = \omega_{axial} \cdot \cos \alpha_2 + \omega_{tangential} \cdot \sin \alpha_2$$

In the flow path and stator modifications attempted, vorticity values have either decreased or remained at same levels as the baseline case. This indicates that the loss in efficiency in the modified cases is a strong function of tip leakage loss.

To reconfirm the effects of stator exit static pressure profile, another check with CFD analysis was performed. Stator was removed from the stage CFD analysis of the baseline stage with the tip shroud. Static pressure profiles at stator exit from the stage analysis were extracted. Stand-alone rotor with tip shroud was analysed with stator exit pressure profile. Boundary conditions imposed at inlet were the two static pressure profiles - one from baseline stage analysis and the other from the modified flow path stage analysis. Both the profiles are shown in Figure 4-20. With rotor alone analysis done, performance was monitored as isentropic efficiency across rotor alone. Difference in efficiency numbers between the two profiles was around 0.25% with baseline flow path profile performing better. For the case with baseline pressure profile, the leakage flow was relatively lesser than the case with static pressure profile from modified flow path. This confirms the importance of stator exit static pressure on rotor performance with tip shroud.



4.7 SHORT STAGES – SST700 STAGE #2

Analysis done thus far was on stages with high aspect ratios (i.e tall stages). In these stages, the most prominent loss mechanism was profile losses. In order to reduce profile losses, pitch to chord ratio and Mach number distribution on airfoil influenced the efficiency significantly. Loss mechanisms due to secondary flows are significant in stages with low aspect ratio (i.e. short stages). The below geometry with the details in the table was the vehicle for the research work.

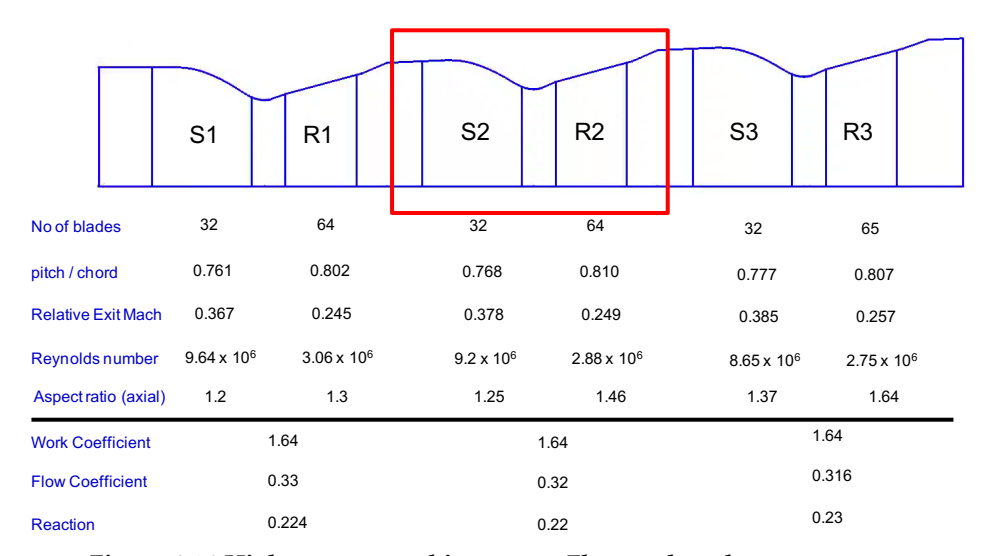


Figure 4-21 High pressure turbine stage - Flow path and stage parameters

It can be observed from Figure 4-21 that, reaction of the stages are of the range of 0.2. Mach number levels are the exit of stators of the order of 0.35 and rotor exit Mach numbers are of the order of 0.24. Important parameter with respect to present study is the aspect ratio of the stages which are of the order of 1.2 for stator. At this aspect ratio, the expectation is that the secondary losses would be dominating over other loss mechanisms like profile losses and tip leakage losses. The target stage is the second stage. Upstream and downstream stages are considered to study if the changes made in stage 2 affects the performance of stage 1 and stage 3. All the geometry and flow discussion in the report are for stage 2.

4.7.1 One-dimensional parameters of baseline geometry:

Pitch-to-chord ratio and Zweifel loading number were calculated for the baseline geometry in order to investigate the scope for improvement. Also, the pitch-to-chord ratio on the machine was compared to the recommended pitch to chord ratio by various loss models. Below table gives the comparison. It can be observed that, the Zweifel number of the stator being of the order on 0.5, there is certainly scope to further improve on this – from an aerodynamic standpoint¹⁵. Pitch-to-chord ratio on machine matches well with the highlighted pitch-to-chord ratio obtained from the loss models. Improvements in efficiency can be aimed by further loading the airfoils – cf. the work on taller stages.

¹⁵ The vanes are part of the structural integrity of the diaphragms and cannot be changed without e.g. introducing bridges etc.





Model	Pitch-to-Chord ratio		
	Stator	Rotor	
Mamaev	1.02	0.81	
Ainley-Mathieson16	0.65	0.6	
Denton U3	0.75	0.6	
Traupel	0.71	0.66	
Actual numbers	0.77	0.79	

The calculated Zweifel numbers are 0.58 and 1.1 for the stator and rotor, respectively. The velocity triangles were calculated and the airfoils were checked for the amount of incidence. From previous studies, it was established that incidence angles should be properly designed more so for the rotors for the stator exit flow angles. The results of this calculation is shown in Figure 4-22. Velocity triangles and airfoil angles are shown at midspan. It is seen that, there is a small incidence of 2 degrees on the rotor.

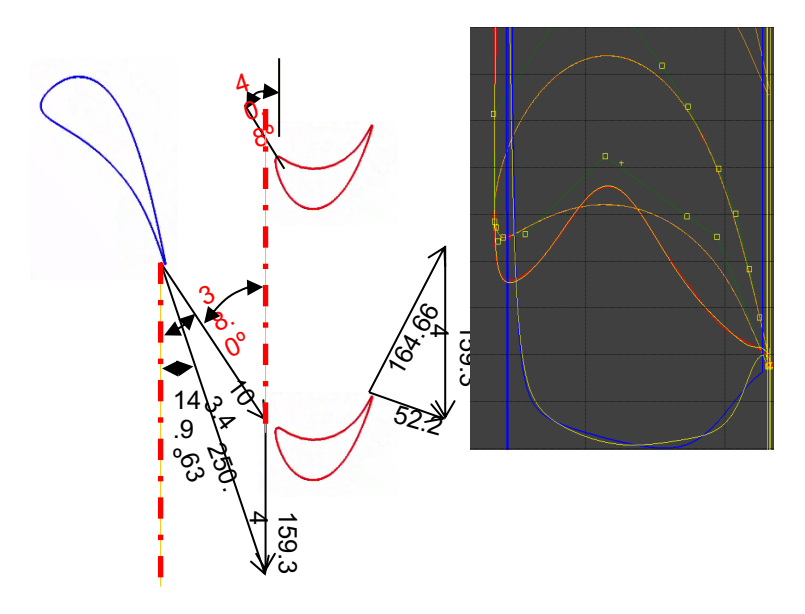


Figure 4-22 Velocity triangles - Stage #2

The CFD work revealed a rather large capacity problem (too large) that indicates that the angle models are off by approximately one or two degrees – or deliberate extra flow margin. From two-dimensional MISESTM analysis, the profile loss numbers (with the Traupel trailing edge loss model) are 3.6 % and 5% for stator the rotor, respectively.

4.7.2 Three-dimensional features in baseline design

A straight lean (as for the tall stage) on the stator with pressure side towards the hub is a feature present in the baseline geometry. The meridional view also shows the presence of significant axisymmetric end-wall contouring (normally referred to as a "Russian Kink"). The pitch-to-chord ratio on the stator is also maintained constant from hub to tip. This is enforced for ease of machining and structural purposes.

-



¹⁶ Obsolete model

In order to establish the performance of the baseline geometry, three-dimensional CFD analysis was performed. All the blade rows were meshed using Turbogrid™ except for rotor 1 and rotor 2. Rotor 1 and rotor 2 were meshed using ICEMCFD™ in order to bring in the effect of leakage losses – see Figure 4-23 for information. Root cavity and the tip cavities were modeled using structured grid in order to capture the effects of leakage flow and main flow interaction.

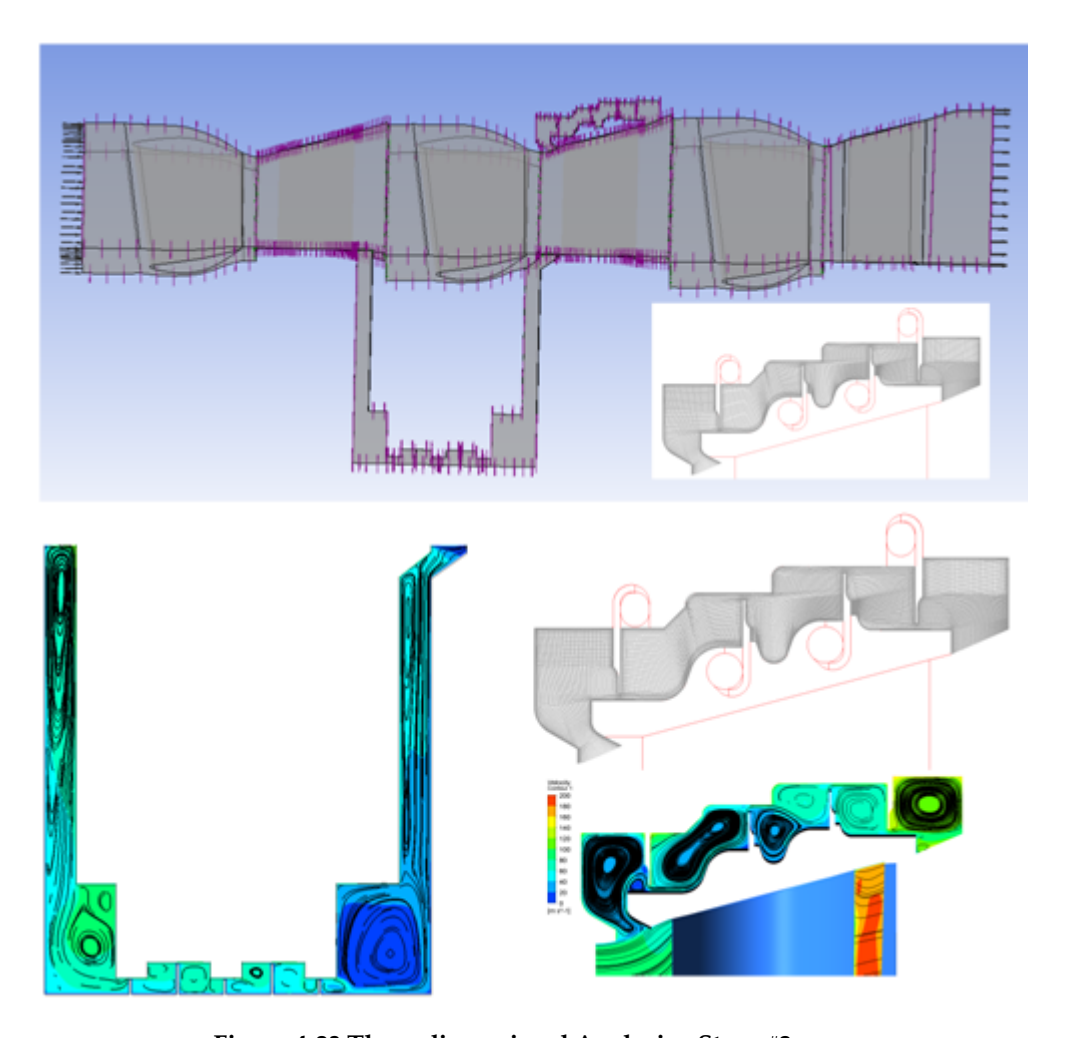


Figure 4-23 Three-dimensional Analysis - Stage #2

Figure 4-23 briefly describes the mesh for the three stage model with the target stage in the center. Both root cavity and tip cavity are modeled for the target stage. The flow patterns in these cavities are also shown. Flow patterns seem to make good sense as to location of vortices and flow structure. Efficiency improvements will be focused on this stage from one, two and three-dimensional perspectives.

4.7.3 Three-dimensional rotor design

In order to explore the design space, a number of different design configurations were designed and analyzed. The work is based on a back-to-back analysis in order to minimize the effects from CFD imperfections. The first step was to introduce the datum geometry that is shown in Figure 4-24.



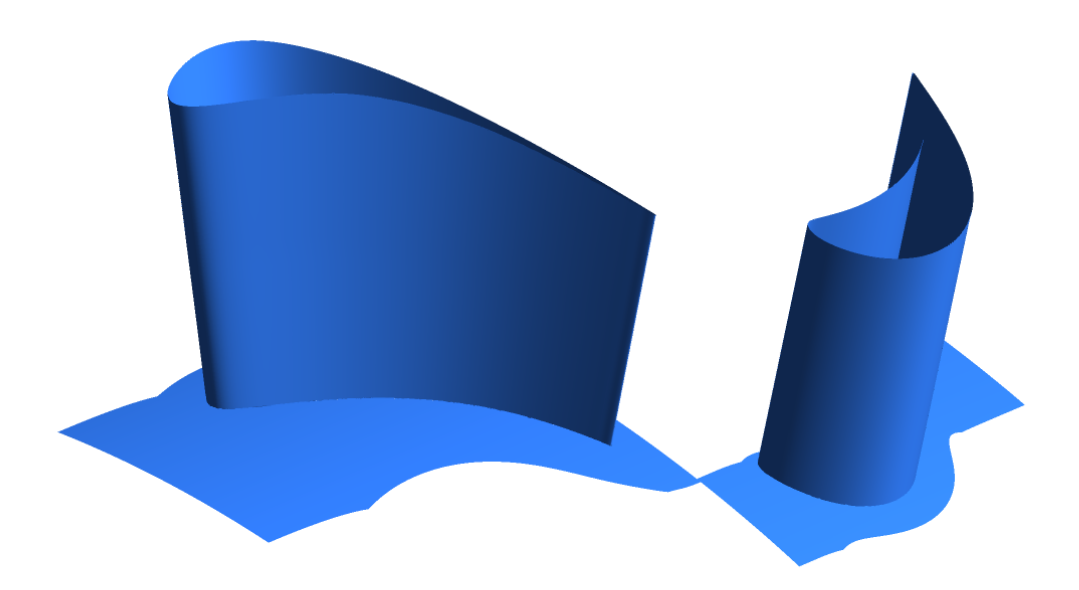


Figure 4-24 Datum stage #2

The datum (or baseline) geometry was used as the reference level for the study, which incorporated:

- Datum stator and 3D rotor (Figure 4-25)
- Compound lean stator and datum rotor (Figure 4-26)
- Compound lean stator and 3D rotor (Figure 4-27)
- C-shaped compound lean stator and datum rotor (Figure 4-28)
- C-shaped compound lean stator and 3D rotor (Figure 4-29)

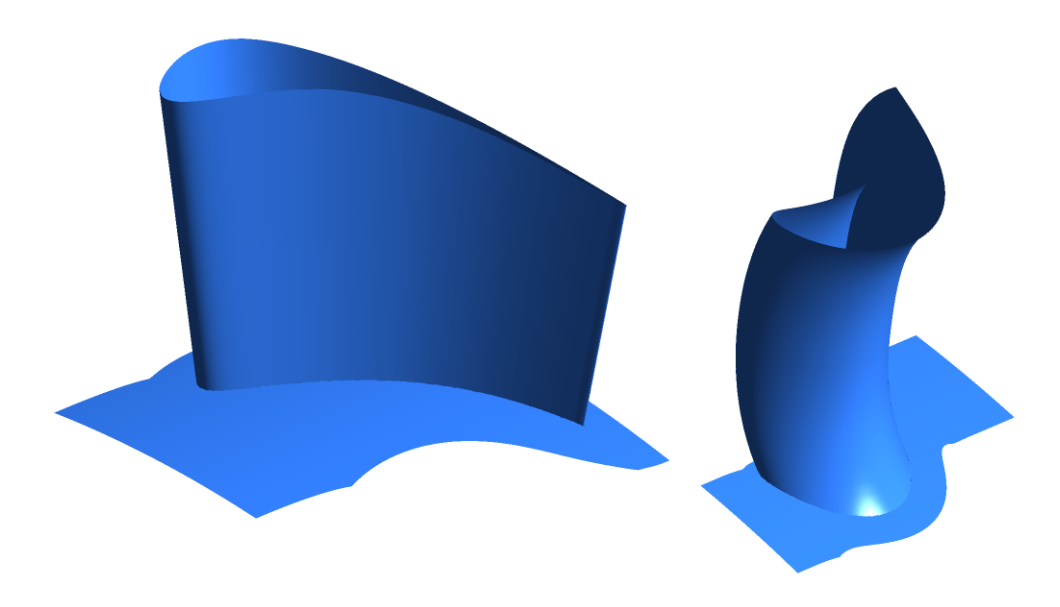


Figure 4-25 Datum stator and 3D rotor



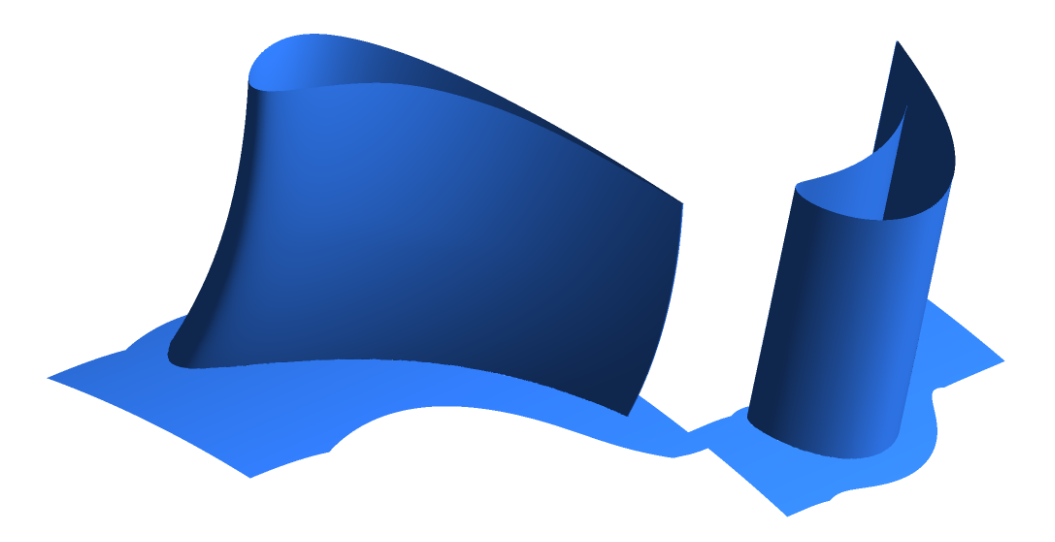


Figure 4-26 Compound lean stator and datum rotor

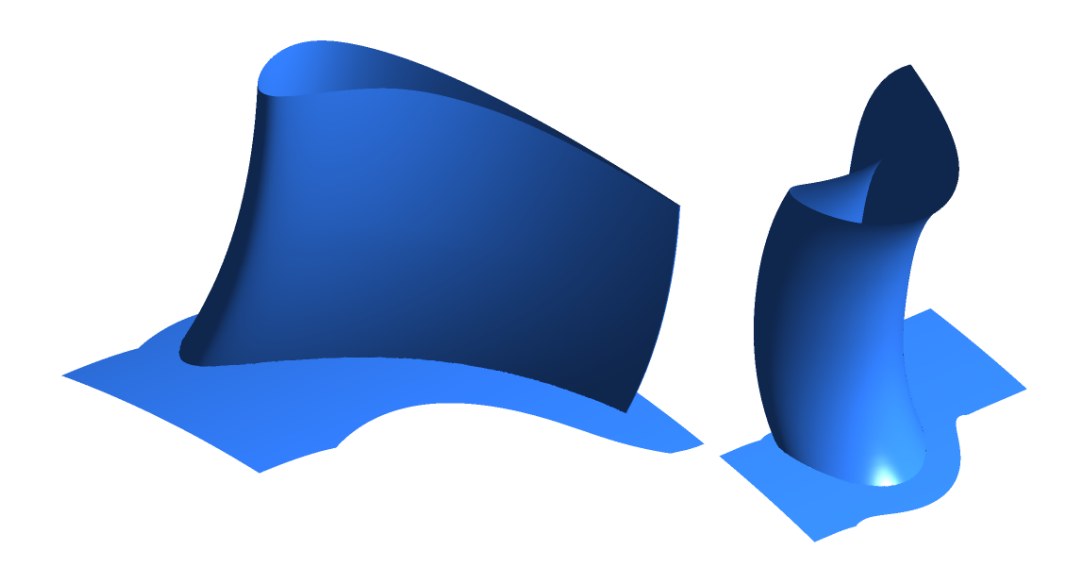


Figure 4-27 Compound lean stator and 3D rotor





Figure 4-28 C-shaped compound lean stator and datum rotor

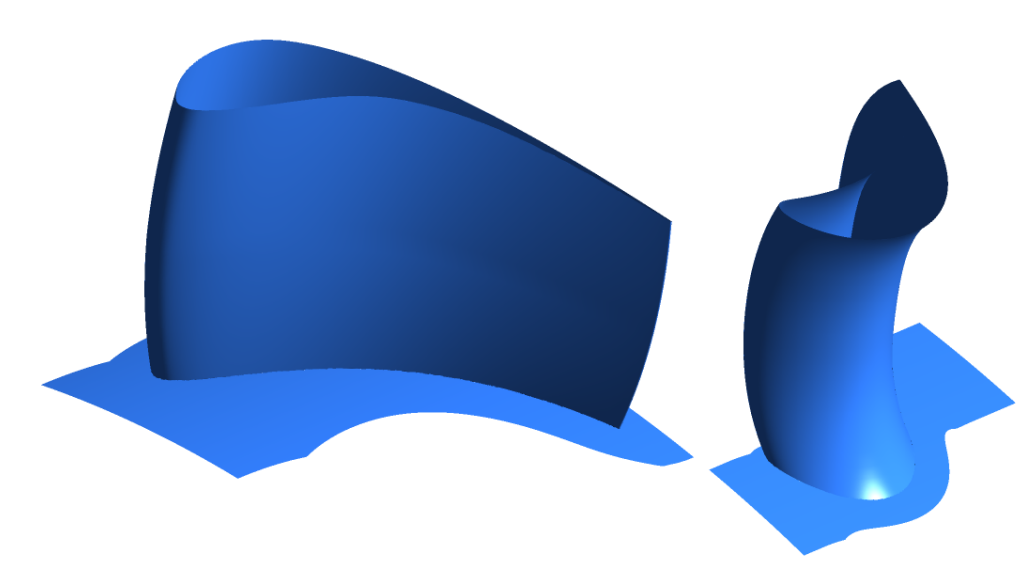


Figure 4-29 C-shaped compound lean stator and 3D rotor



The sole purpose of introducing C-shaped compound lean and 3D-roters was to reduce the secondary losses. The 3D rotor is actually a compound lean stacking and the nomenclature is selected for clarity reasons. As discussed earlier CFD has problems in quantitatively assessing the impact from secondary losses. This work also showed that there are qualitative issues. It is established practice to assess secondary loss features by introducing a vector quantity called "helicity" in order to capture some quantitative aspects of design modifications.

Stator	Rotor	Stage efficiency	Figure
Datum	Datum	94.8	Figure 4-24
Datum	3D	94.3	Figure 4-25
Compound lean	Datum	94.4	Figure 4-26
Compound lean	3D	94.2	Figure 4-27
C-shape compound lean	Datum	93.7	Figure 4-28
C-shape compound lean	3D	93.7	Figure 4-29

The results shows that CFX does not capture the expected effects and the calculated efficiency for the most "advanced design" is one percent lower than for the datum level. There may be several reasons behind this result and the most prominent is most likely that the CFD per se fails to capture some of the effects. The latter has been confirmed during the test campaign at IIT. The purpose of using a C-shaped blade is to counteract the migration of lower momentum fluid into the passage and this effect was not captured by CFX in the post-test analysis. This renders further optimization with CFX questionable and more work has to be done in order to bring in the full scope of all leakage flows etc. The latter is especially important for the leakage flow from the diaphragm seal flow which has a very big impact on the rotor end-wall losses.

It should be empathized that CFD is not an exact science and carries many modelling assumptions. Two important such parts are turbulence- and transition models which both has a profound impact on the results. Experience has also shown that the only way to get certain answer is to run campaigns in a test turbine.



5 Test campaign

In order to further understand aerodynamic flow behaviour relevant to the turbine stage in consideration, experiments were conducted in Turbomachinery Laboratory, Indian Institute of Technology, Bombay. The details of the experiments conducted are discussed in the present chapter and the results are briefly shown in next chapter.

Figure 5-1 shows a stator and rotor in high pressure section of SST-700 (or -900) industrial steam turbine. It can be observed that the stator has varying chord along the height of the blade. The variation of chord along blade height was due to ease of manufacturing rather than aerodynamic purpose as the pure design intent.

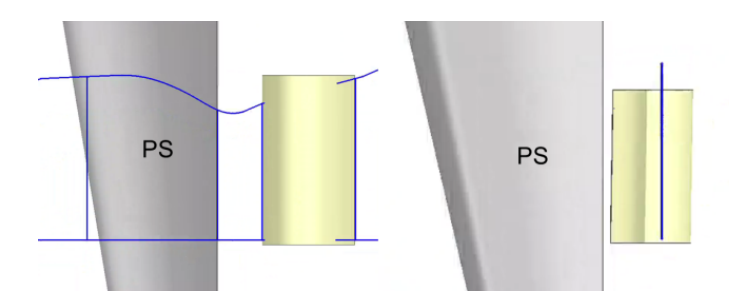


Figure 5-1 HP-section of SST-700 and -900

With this background, the research objective was to investigate the differences in aerodynamic behaviour between two designs, viz. constant chord along the span and varying chord along the span. The aim was to quantify the total pressure losses, to study the blade-loading patterns and to investigate the effects on secondary flows.

In order to foster to the research objective stated, both experimental and numerical works were carried out. The two designs to be compared, viz. constant-chord design and varying-chord design, were manufactured and tested in a linear cascade wind tunnel. The same cascade is also numerically analysed using commercially available CFXTM software. Both the experimental and numerical studies are compared.

5.1 METHODOLOGY AND INSTRUMENTATION

The experimental investigations were carried out in a low speed, open circuit linear cascade wind tunnel at the Turbomachinery Laboratory, Indian Institute of Technology, Bombay. A schematic representation of the experimental facility is shown in Figure 5-2. The air entering the blower is filtered by a filtering screen. The exit flow from the blower enters the settling chamber, where it passes through a honeycomb followed by a series of screens. At the exit of the contraction, uniform flow is available, which enters the cascade test section. The test section is a rectangular duct of 398 mm x 150 mm at the entrance of the cascade. The cascade consists of eight blades with the end blades forming the two ends of the test section as shown in Figure 5-2. At the exit of the blade, the test section follows the camber line path.



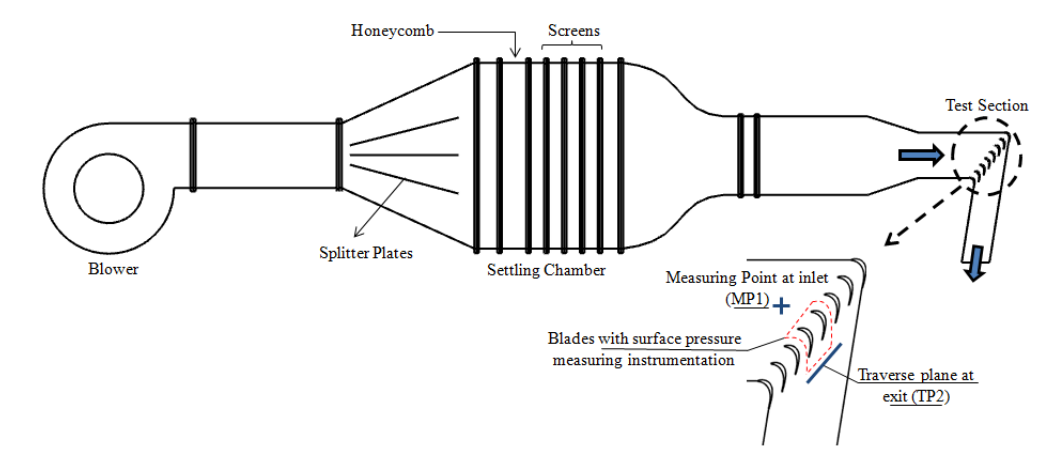


Figure 5-2 Schematic of test-section

The inlet flow conditions are measured using manual traverse with pitot tube at approximately one chord length from the leading edge of the cascade. This location is marked as MP1. The stagnation pressure profile required as boundary condition for the numerical analysis is also extracted at this location. An auto-traverse mechanism at the exit of the blade row enables a seven-hole probe (from Aeroprobe Inc, USA) to be traversed in order to measure the flow conditions. The least count of the traverse mechanism is 1 mm. Also, a traverse of 4 mm with one revolution of the lead screw could be achieved. The 7-hole probe can measure the flow speed over a range of Mach 0.02 to Mach 2. The flow angle of receptivity is 70 degrees. The sampling rate of data acquisition is 250 Hz and the sample size is 500. The seven-hole probe is connected to 16 channels Digital Sensor Array (DSA 3217 from Scanivalve Corp, USA). The traverse plane is approximately one third of the chord length downstream of trailing edge. This traverse plane is shown as TP2. The matrix to be traversed by the seven-hole probe covers one full tangential pitch of the cascade.

The instrumentation necessary for surface pressure measurements on the blade to evaluate the blade-loading is made available on the two blades at the center of the cascade as shown in Figure 5-2. The 0.3 mm static pressure taps on the blade surfaces are connected to the computer through 16 channel digital sensor arrays. The static pressure readings on the pressure surface and the suction surface are captured by two separate sensor arrays.

The cascade blades tested and analyzed in the present work comprise T106 airfoil sections. Two T106-based cascade designs are tested: constant-chord design and varying-chord design. As the name indicates, the chord of the T106 airfoil section is constant along the blade height in constant-chord design. However, in the varying-chord design, the mid-span airfoil section is retained from the constant-chord design. The tip and the root airfoil sections are scaled up and scaled down respectively. The cascade details for the constant-chord design are provided in Table 1 below.



Table 1 Cascade Details

Parameter	Value
Chord [mm]	100
Blade Height [mm]	150
Pitch [mm]	71.4
Aspect Ratio	1.5
Inlet Design Angle [degrees]	37.7
Exit Design Angle [degrees]	63.2
Reynolds number at exit based on blade chord	3.0 x 10 ⁵
Number of Blades	8

5.2 NUMERICAL APPROACH

The three-dimensional numerical analysis of a single cascade blade passage is carried out using the commercial software ANSYS CFX. Steady state RANS simulations are performed using the k- ω SST turbulence model.

The boundary conditions for the analysis are derived from the experimental data measured. At the inlet, the stagnation pressure profile obtained at MP1 is used. At the exit, an area averaged static pressure value from the experimental data at traverse plane is imposed as the boundary condition. A single cascade blade passage is analysed assuming a periodic flow.

The periodic flow assumption in the single passage analysis is justified by CFD and experiments. In order to check if the flow is periodic in reality, total pressure readings were taken at traverse location TP2. At mid-span of the blade row, readings were taken for approximately three blade passages. The resulting ratio of P_t to mass averaged P_t is shown in Figure 5-3. It can be noticed that the flow is periodic in reality with the constructed test section. A three-dimensional CFD analysis of all the eight blades and the hardware of the test section is performed. The entire test section is modeled with hexahedral mesh. Iso-Mach contours from this CFD run are shown in Figure 5-3 (b). The CFD reveals that the number of blades and the hardware are sufficient to generate periodic flow.

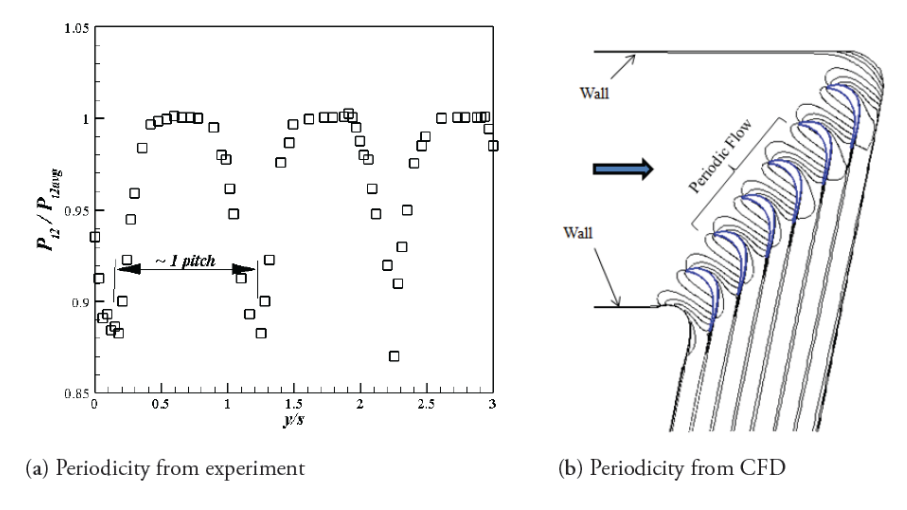


Figure 5-3 Periodicity check



5.3 RESULTS FROM MEASUREMENTS

This section starts with a discussion of the effect of spanwise variation of chord on the blade-loading. Figure 5-4 shows the comparison in blade-to-blade loading for the two designs. Both experimental and CFD results are compared.

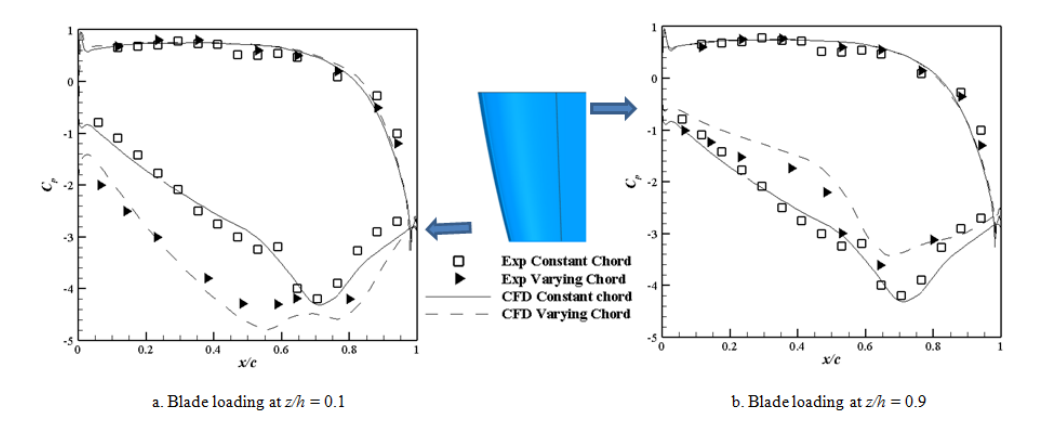


Figure 5-4 Blade-loading comparison

Figure 5-4 (a) shows the blade-loading at *z/h*=0.1, where the chord in varying chord design is relatively small when compared to the constant-chord design. It can be observed that due to the decreased chord and the maintained pressure ratio, the blade-loading in the varying-chord design is increased. The gradient of acceleration on the suction side of the airfoil increased in the varying-chord design. The diffusion on the suction side after the peak Mach number is not smooth. The location of peak Mach number on the suction side in the constant-chord design is around 0.7 chord length. However, for the varying-chord design, the peak Mach number on the suction side is around 0.5 chord length.

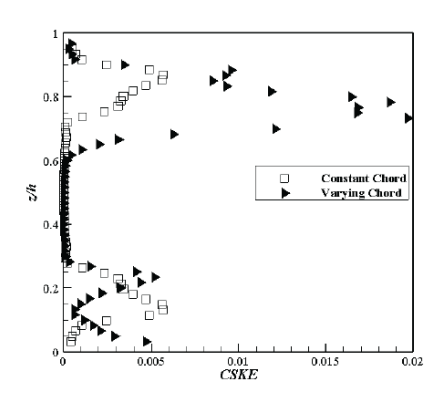
From the blade-loading plots at z/h=0.9 shown in Figure 5-4 (b), it can be observed that blade-loading for the increased chord in the varying-chord design decreases. The path of acceleration to the peak Mach number on suction side in the varying-chord design has two distinct gradients. One, mild acceleration till 0.5 chord length. Two, high acceleration from 0.5 to 0.7 chord length where the peak Mach number is reached. Importantly, the area covered by the curves is decreased in the varying-chord design by virtue of the increased chord.

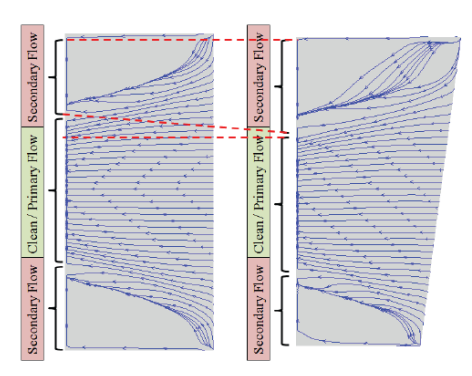
In order to study the secondary flow behavior in the constant-chord design and the varying-chord design, coefficient of secondary kinetic energy (CSKE) is used as the objective function. According to this definition of CSKE a zero value of CSKE corresponds to clean flow or primary flow or flow void of secondary flow. Any value of CSKE other than zero corresponds to deviation from the primary flow and can hence be termed as secondary flow.

Figure 5-5 (a) shows the CSKE comparison between the two designs from the extracted experimental data at the traverse location. In the mid-blade region (around z/h=0.5), CSKE values are zero, which reveals that the flow is void of streamwise vorticity. Towards the end-wall zone where z/h = 0, the region affected by secondary flow is almost comparable for the constant-chord design and the varying-chord design. However, in the region above z/h =0.6, the secondary flow patterns between the designs differ. In the



varying-chord design, the secondary flow patterns is significantly higher than that in the constant-chord design above z/h = 0.6.



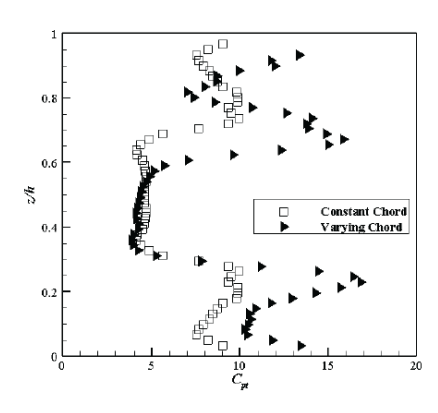


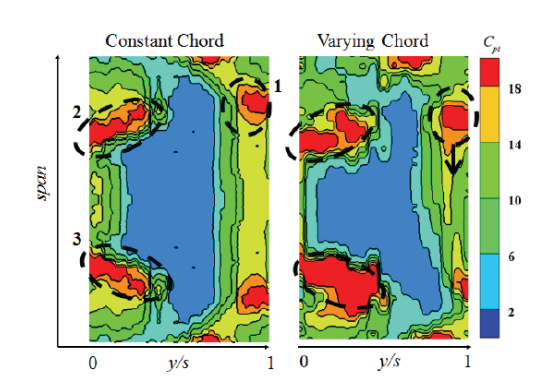
- (a) Secondary loss comparison from experiments
- (b) Streamlines on suction surface of cascades (CFD)

Figure 5-5 Secondary flow behavior

The trends seen in CSKE plot can be visualized by streamlines extracted from CFD simulations. Figure 5-5 (b) shows the surface streamlines on suction side of cascade designs. In the figure, approximate regions of primary flow/ clean flow are marked. Also marked are the secondary flow regions. In the varying-chord design, increase in secondary flow region, as seen in CSKE plots from experiments, is indicated. In the region towards z/h = 0, the region affected by secondary flow is almost comparable between the designs. From one-dimensional values, the CSKE value in varying-chord design is close to three times of CSKE value in the constant-chord design.

The variation of Total pressure loss along the blade height will be discussed for both the designs. The variation of loss along blade height is shown in Figure 5-5 (a). The values plotted are extracted from the experimental data.





- (a) Overall loss comparison from experiments
- (b) Contour at traverse plane from experiments

Figure 5-6 Overall loss behavior

In the zone above z/h=0.6, loss is higher for the varying-chord design. The overall losses being higher in this region suggests that secondary losses are the dominating losses in this zone for the existing setup.



In the zone below z/h=0.3, the overall losses in the varying-chord design is higher. The chord being lower in this region, the profile losses are observed to be higher. From the CSKE evaluation, the secondary losses in the varying-chord design below z/h=0.3 are comparable to the constant-chord design. Since the overall losses being higher with higher profile losses and comparable secondary losses, it can be stated that profile losses are more dominating in this zone. Hence profile losses contribute significantly to the overall pressure losses.

At the traverse plane, measurements are taken across a matrix to cover one blade passage and a blade height. Contours are generated calculating losses at each point measured. Figure 5-6 (b) shows the contours of loss at traverse plane from the measured data. There are three regions marked in the contour for constant-chord with numbers 1, 2 and 3.

Considering region 1 in both the designs, it can be observed that there is a shift in region downwards in the varying-chord design. The same is indicated by a downward arrow in the varying-chord design. This shows there is a hint of flow migration from the higher chord zone to the lower chord zone. The area covered by loss region also increases in varying-chord design in region 1.

In region 2 and region 3, the losses are higher in the varying-chord design compared to the constant-chord design.

With the effect of spanwise variation of chord discussed, it is clear that more investigations and enough care needs to be taken from the various loss mechanisms point of view. Profile losses and secondary losses have to be taken into account in the design exercise. From the present study and for the given test section, secondary losses are seen to be the dominating loss mechanism.

5.4 THE C-BLADE CONCEPT

One concept that was experimentally examined with a focus on reducing the secondary losses was the C-blade concept. Three blade configurations were examined *viz*. Prismatic, Compound lean and C-blade. The designs are shown in Figure 5-7. The designs were tested in a linear cascade wind tunnel. The experimental details remains the same as described in the previous section.

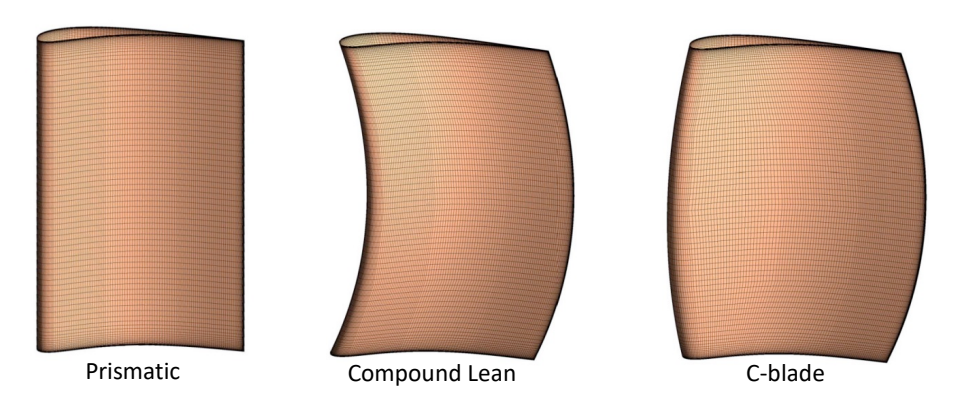


Figure 5-7 Design configurations

The basic idea behind the C-blade concept is to counteract one of the drawbacks of the compound lean stacking – namely spanwise migration of lower-momentum fluid



(towards the mid passage). One can easily realize that acceleration toward a solid wall is impossible; hence, any pressure gradient in that direction must be small. The principal features are shown in the figure below:

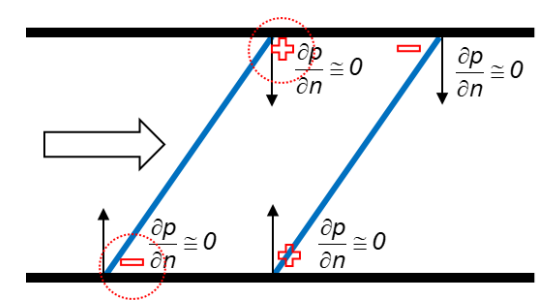


Figure 5-8 Blade sweep and loading

The top (i.e. casing or shroud) part at the leading edge has the same feature as for the C-blade. The rationale is simply that the loading is increased because the fluid below has loading because of the chord position. The increased loading lowers the pressure locally and "draws" high-momentum fluid towards the end-wall regions – hence preventing low-momentum fluid from being migrated upwards (from the blade lift component towards the end-walls). The figure below (Figure 5-9) shows the impact on the losses:

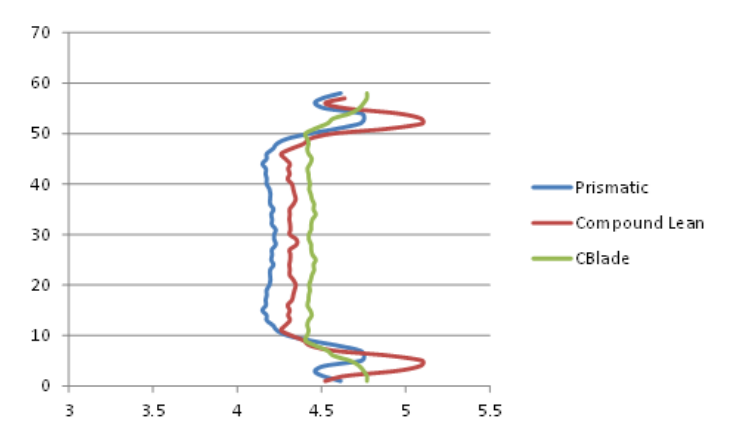


Figure 5-9 Measured total pressure loss distributions

With the three design configurations tested, results are summarized in Figure 5-9. It can be observed that secondary losses are significantly reduced towards the end-walls for the C-blade configuration. This was the intent while designing the C-blade configuration. However, towards the mid-span, it is seen that the losses have increased. This is assumed to be due to increased wetted area which is the consequence of increased chord. This design configuration is to be further optimized in the mid-span region for overall losses to reduce in this region. This remains as a part of future work to be accomplished.



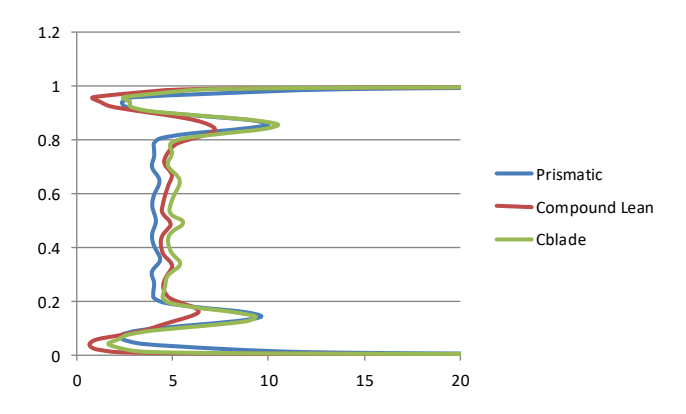


Figure 5-10 Calculated total pressure loss distributions

The post-test CFD analysis in Figure 5-10 shows a different behavior and the "secondary loss core" for the C-shape is quite different when compared to the measurements. The CFD calculation misses the described effect from the C-shaping (flow directed towards the end-walls) that prevents the loss core migration. This is clearly visible in the test results.

In summary – the C-shaped blade is a promising design feature but further refinement is necessary. The test also reveals limitations in the CFD methods



6 Conclusions

The results show that there is potential for improvement and that the amount of renewable electricity can be increased. The work has been focused on stage #11 and #16 in a SST-900 turbine and stage #2 in a SST-700 module. The former is an IP/LP module with tall stages whilst the latter is a HP module with short stages. For the tall stage, the work has been directed towards the profile- and end-wall losses and for the short stage mainly the end-wall loss.

The results show that the stage #16 profile loss can be reduced by 0.74 percent and that the secondary losses is reduced by the suggested means. The analysis shows that the reduction in secondary losses are high - on the order of 30 percent (expressed as secondary kinetic energy - SKE).

$$\Delta \eta = 0.74 + f(\Delta SKE)$$

The CFD analysis, however, does not capture the gain in stage efficiency, due to the reduced secondary loss, in firm numbers.

The suggested profile modifications may be cloned for other stages by the presented methodology. This approach is useful because one can abandon the old principle of having certain profile families and, instead, having a set of optimized curvature distributions. This means also that one can have stages with intra-stage swirl and thereby opening another level of optimization – with changing loadings, flow functions¹⁷ and reaction levels.

The work on the short high pressure turbine shows that there is room for improvement. The CFD analysis failed to capture the improvement associated with advanced blading – even fundamental fluid dynamics related to sweeping (i.e. C-shaping) vanes was missed in the CFD work. The latter was verified in a test campaign at IIT where significant reductions in secondary losses were measured. There is an established fact that, it is fairly easy to reduce a loss – just for increasing another. In this case, however, there was an expected increased increase in profile loss because of having both more wet surface and non-optimized mid-section of the blade. The design is promising but further work is required to realize the full potential.

In summary: the work has revealed that, despite the SST-700 and -900 are mature products, there are room for improvement.

¹⁷ May be impractical under certain circumstances





7 Goal fulfilment

The aim of the KME-707 is to reduce the cost of ownership by increasing the turbine efficiency and thereby the amount of power produced for a certain fuel input. The aim for KME-707 was bold with a 2 percent increase in efficiency. The results show clearly that the profile losses can be reduced by 0.8 percent and that the secondary losses can be significantly reduced. The exact magnitude of the loss reduction is still to be determined after implementation in an either a real turbine or a test turbine. The latter is preferred because a number of geometries have to be tested. The reason for the uncertainty originates from imperfections in the CFD methods. Denton¹¹8 states that "There are many things we cannot predict accurately with CFD, these include; (1) boundary layer transition (2) turbulence modeling (3) end-wall loss (4) leakage loss (5) compressor leading edge flows (N/A) (6) turbine trailing edge flow (7) effects of small geometrical features (8) unsteady losses".

The results show both reduced secondary kinetic energy and helicity – which is a gauge of the dissipation potential in the rows. In other words, reduced values should render in higher efficiency by basic flow physics. The test campaign also showed a very large difference between the measured loss profiles and the CFD-analysis for the same geometry. The test shows that the secondary flow loss core (and the flow) is forced to stay at the end-walls, whilst the CFD analysis fails to capture the behavior.

The work has revealed that, despite the SST-700 and -900 are mature products, there are room for improvement.



¹⁸ PCA 20th anniversary lecture, 2008

8 Suggestions for future research work

The work in KME-707 has been based on cascade testing and numerical analysis, using 1D, 2D, 2D blade-to-blade and full 3D tools. The work has shown that there is a potential to improve the steam turbine technology by introducing more advanced blading. The work has also explored weaknesses in the used state-of-the-art CFD tools and it is not uncommon to find that improved flowpath features does not turn into efficiency.

- 1. Expand the work on short stages to include leakage effects
- 2. Full three-dimensional high-fidelity in-stationary numerical optimization with supercomputers
- 3. Testing in a test turbine
- 4. Non-axisymmetric end-wall contouring where the contour is used to create lift and thereby off-load the profiles (locally at the end-walls).
- 5. Developing a fully flexible turbine design in terms of stage loading and reaction.

The items 1, 2 and 3 are related to the research method whilst 4 and 5 are turbine design features. Non-axisymmetric end-wall contouring was introduced on aero-engines for more than a decade ago, hence not a novel technology. During recent years, the technology has been introduced for usage on land-based gas turbines.



Figure 8-1 Turbine guide vane with non-axisymmetric end-wall contouring

A rather significant difference stems from the gas turbine design philosophy with its casted cooled vanes (and blades). Most OEMs uses casted pairs (or triples) for good leakage control (cf. Figure 8-1 Turbine guide vane with non-axisymmetric end-wall contouring. The castings may be modified in order to incorporate advanced end-wall features with reasonable efforts. For the low-reaction turbine, the situation is different, because of the EB-welding of the assembly of the outer part, outer band, the vanes, inner band and finally the inner part (that holds the seal). This is not to say that it is impossible but further research should be undertaken before further work in this direction.

The fundamental turbine philosophy with a certain reaction and low intra-stage swirl poses a severe limitation in terms of achievable efficiency levels. The design principle of having low levels of swirl between the stages should be looked at with today's manufacturing capacities. The rationale behind the philosophy is to minimize the kinetic



"carry-over" energy that potentially may be lost when entering the subsequent vane (and diaphragm inlet).



9 Literature references

- [1] A. Stodola, Dampf-und Gasturbinen: mit einem Anhang über die Aussichten der Wärmekraftmaschinen, J. Springer, 1922.
- [2] W. Traupel, *Thermische Turbomaschinen (Thermal Turbo-Machinery), First Vol,* Springer-Verl. ag, 1977.
- [3] J. D. Denton, "The 1993 IGTI Scholar Lecture: Loss Mechanisms in Turbomachines," *Journal of Turbomachinery*, vol. 115, no. 4, p. 621, 1 10 1993.
- [4] P. J. Walker, "Blade lean in axial turbines: model turbine measurements and simulation by a novel numerical method.," 1987.
- [5] J. D. Denton and L. Xu, "The exploitation of three-dimensional flow in turbomachinery design," *Proceedings of the Institution of Mechanical Engineers, Part C: Journal of Mechanical Engineering Science*, vol. 213, no. 2, pp. 125-137, 1998.
- [6] M. E. Deich, A. E. Zaryankin, G. A. Fillipov and M. F. Zatsepin, "Method of increasing the efficiency of turbine stages with short blades," *Teploenergetika*, vol. 2, pp. 240-254, 1960.
- [7] M. Dejc and B. Trojanovskij, Untersuchung und Berechnug axialer Turbinstufen, Berlin: VEB Verlag Technik, 1973.
- [8] S. Havakechian and R. Greim, "Aerodynamic design of 50 per cent reaction steam turbines," *Proceedings of the Institution of Mechanical Engineers, Part C: Journal of Mechanical Engineering Science*, vol. 213, no. 1, pp. 1-25, 28 1 1999.
- [9] T. Germain, M. Nagel and R. D. Baier, "Visualisation and Quantification of Secondary Flows: Application to Turbine Bladings with 3D-Endwalls," in *Paper ISAIF8-0098, Proc. of the 8th Int. Symposium on Experimental and Computational Aerothermodynamics of Internal Flows, Lyon,* 2007.
- [10] R. Corral and F. Gisbert, "Profiled End Wall Design Using an Adjoint Navier–Stokes Solver," *Journal of Turbomachinery*, vol. 130, no. 2, p. 021011, 2008.
- [11] B. R. Haller, "VKI Lecture Series on "Secondary and Tip Clearance Flows in Axial Turbines"," *Full 3D turbine blade design*, pp. 10-13, 1997.
- [12] J. D. Coull and H. P. Hodson, "Predicting the profile loss of high-lift low pressure turbines," *Journal of Turbomachinery*, vol. 134, no. 2, p. 21002, 2012.
- [13] J. D. Coull, R. L. Thomas and H. P. Hodson, "Velocity distributions for low pressure turbines," *Journal of Turbomachinery*, vol. 132, no. 4, p. 41006, 2010.
- [14] T. Zoric, I. Popovic, S. A. Sjolander, T. Praisner and E. Grover, "Comparative Investigation of Three Highly Loaded LP Turbine Airfoils: Part I Measured Profile and Secondary Losses at Design Incidence," in *ASME Turbo Expo 2007: Power for Land, Sea, and Air*, 2007.
- [15] A. Huang, "Loss mechanisms in turbine tip clearance flows," 2011.
- [16] S. M. Goobie, S. H. Moustapha and S. A. Sjolander, "An Experimental Investigation of the Effect of Incidence on the Two-Dimensional Performance of an Axial Turbine Cascade," in *Proceedings, Ninth International Symposium on Air Breathing Engines*, 1989.
- [17] T. L. Chu, "Effects of Mach Number and Flow Incidence on Aerodynamic Losses of Steam Turbine Blades," Virginia Tech, 1999.



- [18] M. W. Benner, S. A. Sjolander and S. H. Moustapha, "Influence of Leading-Edge Geometry on Profile Losses in Turbines at Off-Design Incidence: Experimental Results and an Improved Correlation," *Journal of Turbomachinery*, vol. 119, no. 2, p. 193, 1997.
- [19] S. H. Moustapha, S. C. Kacker and B. Tremblay, "An improved incidence losses prediction method for turbine airfoils," *Journal of Turbomachinery*, vol. 112, no. 2, pp. 267-276, 1990.
- [20] T. Korakianitis and P. Papagiannidis, "Surface-curvature-distribution effects on turbine-cascade performance," in *ASME 1992 International Gas Turbine and Aeroengine Congress and Exposition*, 1992.
- [21] T. Korakianitis, "Prescribed-curvature-distribution airfoils for the preliminary geometric design of axial-turbomachinery cascades," *Journal of turbomachinery*, vol. 115, no. 2, pp. 325-333, 1993.
- [22] D. G. Ainley and G. C. R. Mathieson, A method of performance estimation for axial-flow turbines, Citeseer, 1951.
- [23] A. G. Klebanov and B. I. Mamaev, "Optimal pitch for a turbine blade cascade," *Thermal Engineering*, vol. 16, no. 10, p. 79, 1969.
- [24] O. Zweifel, "The spacing of turbo-machine blading, especially with large angular deflection," *Brown Boveri Rev.*, vol. 32, no. 12, pp. 436-444, 1945.
- [25] S. C. Kacker and U. Okapuu, "A Mean Line Prediction Method for Axial Flow Turbine Efficiency," *Journal of Engineering for Power*, vol. 104, p. 111, 1 1982.
- [26] E. Dejc, G. A. Filipov and L. Y. Lazarev, *Atlas of Axial Turbine Blade Characteristics*, Machinostroenie, Moscow, 1965.
- [27] R. D. Stieger, "The effect of wakes on separating boundary layers in low pressure turbines," 2002.
- [28] M. J. Atkins, "Secondary losses and end-wall profiling in a turbine cascade," *IMechE Paper C255*, vol. 87, 1987.
- [29] A. W. H. Morris and R. G. Hoare, "Secondary loss measurements in a cascade of turbine blades with meridional wall profiling," in *American Society of Mechanical Engineers, Winter Annual Meeting, Houston, Tex,* 1975.
- [30] J. I. Cofer, "Advances in Steam Path Technology," *Journal of Engineering for Gas Turbines and Power*, vol. 118, no. 2, p. 337, 1996.
- [31] A. Duden, I. Raab and L. Fottner, "Controlling the secondary flow in a turbine cascade by 3D airfoil design and endwall contouring," in *ASME 1998 International Gas Turbine and Aeroengine Congress and Exhibition*, 1998.
- [32] M. F. El-Dosoky, A. Rona and J. P. Gostelow, "An Analytical Model for Over-Shroud Leakage Losses in a Shrouded Turbine Stage," in *Volume 6: Turbo Expo* 2007, *Parts A and B*, 2007.
- [33] C. H. Sieverding and V. K. I. for Fluid Dynamics, Secondary flows and endwall boundary layers in axial turbomachines: May 7-11, 1984, Von Karman Institute for Fluid Dynamics, 1984.
- [34] B. Rosic and L. Xu, "Blade Lean and Shroud Leakage Flows in Low Aspect Ratio Turbines," *Journal of Turbomachinery*, vol. 134, no. 3, p. 31003, 2012.
- [35] K. N. Kumar and M. Govardhan, "Secondary Flow Loss Reduction in a Turbine Cascade with a Linearly Varied Height Streamwise Endwall Fence," *International Journal of Rotating Machinery*, vol. 2011, 2011.



- [36] J. Hourmouziadis and N. Hübner, "3-D Design of Turbine Airfoils," in *Volume 1: Aircraft Engine; Marine; Turbomachinery; Microturbines and Small Turbomachinery*, 1985.
- [37] S. Yoon, T. Vandeputte, H. Mistry, J. Ong and A. Stein, "Loss Audit of a Turbine Stage," *Journal of Turbomachinery*, vol. 138, no. 5, p. 51004, 1 2016.
- [38] P. J. Walker and J. A. Hesketh, "Design of low-reaction steam turbine blades," *Proceedings of the Institution of Mechanical Engineers, Part C: Journal of Mechanical Engineering Science*, vol. 213, no. 2, pp. 157-171, 1998.
- [39] M. K. Varpe, "Endwall contouring in a low speed axial flow compressor cascade.," 2015.
- [40] L. Qi, Z. Zou, P. Wang, T. Cao and H. Liu, "Control of secondary flow loss in turbine cascade by streamwise vortex," *Computers & Fluids*, vol. 54, pp. 45-55, 2012.
- [41] A. Nowi and B. R. Haller, "Developments in Steam Turbine Efficiency," *VGB KRAFTWERKSTECHNIK-ENGLISH EDITION-*, vol. 77, pp. 499-503, 1997.
- [42] K. N. Kumar and M. Govardhan, "Numerical study of effect of streamwise end wall fences on secondary flow losses in two dimensional turbine rotor cascade," *Engineering Applications of Computational Fluid Mechanics*, vol. 4, no. 4, pp. 580-592, 2010.
- [43] T. KAWAI, S. SHINOKI and T. ADACHI, "Visualization Study of Three-Dimensional Flows in a Turbine Cascade Endwall Region," *JSME international journal. Ser. 2, Fluids engineering, heat transfer, power, combustion, thermophysical properties*, vol. 33, no. 2, pp. 256-264, 1990.
- [44] T. KAWAI, T. ADACHI and K. AKASHITA, "Structure and Decay of Secondary Flow in the Downstream of a Cascade," *Bulletin of JSME*, vol. 28, no. 242, pp. 1642-1650, 1985.
- [45] T. KAWAI, S. SHINOKI and T. ADACHI, "Secondary Flow Control and Loss Reduction in a Turbine Cascade Using Endwall Fences," *JSME international journal. Ser. 2, Fluids engineering, heat transfer, power, combustion, thermophysical properties*, vol. 32, no. 3, pp. 375-387, 1989.
- [46] T. KAWAI, T. ADACHI and S. SHINOKI, "Improvement in Turbine Blade Aerodynamic Force in the Tip Region," *JSME international journal. Ser. 2, Fluids engineering, heat transfer, power, combustion, thermophysical properties,* vol. 33, no. 3, pp. 517-524, 1990.
- [47] T. Kawai, "Effect of Combined Boundary Layer Fences on Turbine Secondary Flow and Losses.," *JSME International Journal Series B*, vol. 37, no. 2, pp. 377-384, 1994.
- [48] H. Kawagishi and S. Kawasaki, "The effect of nozzle lean on turbine efficiency," *ASME Paper*, vol. 13, no. H00652, pp. 63-69, 1991.
- [49] D. Japikse, N. Baines and others, Introduction to turbomachinery, 1994, p. 377.
- [50] U. Hoffstadt, "Boxberg achieves world record for efficiency," *Modern power systems*, no. OCT, pp. 21-23, 2001.
- [51] F. Haselbach, "Axial Flow High Pressure Turbine Design," *Aero Engine Design-From State of the Art Turbofans Towards Innovative Architectures (Proceedings of VKI Lecture Series* 2008-03), von Karman Institute, Brussels, Belgium, 2008.
- [52] S. Harrison, "The Influence of Blade Lean on Turbine Losses," *Journal of Turbomachinery*, vol. 114, no. 1, p. 184, 1992.



- [53] M. Govardhan, A. Rajender and J. P. Umang, "Effect of streamwise fences on secondary flows and losses in a two-dimensional turbine rotor cascade," *Journal of Thermal Science*, vol. 15, no. 4, pp. 296-305, 12 2006.
- [54] T. E. Dorman, H. Welna and R. W. Lindlauf, "The Application of Controlled-Vortex Aerodynamics to Advanced Axial Flow Turbines," *Journal of Engineering for Power*, vol. 90, p. 245, 1968.
- [55] D. Denton J, "Axial turbine aerodynamic design".



10 Publications

- 1. Deshpande S., Thern M. and Genrup M., "Reduction in secondary losses in turbine cascade using contoured boundary layer fence", Proceedings of ASME Gas Turbine India Conference 2014: GTINDIA2014, December 15 17, 2014, New Delhi, India
- Deshpande S., Thern M. and Genrup M., "Vortexing Methods To Reduce Secondary Losses In A Low-Reaction Industrial Turbine Vane", Proceedings of ASME Turbo Expo 2015: Turbine Technical Conference and Exposition, GT2015, June 15 – 19, 2015, Montréal, Canada
- 3. Deshpande S., Thern M. and Genrup M., "Influence of Compound Lean on an Industrial Steam Turbine stage", Proceedings of ASME Gas Turbine India Conference 2015: GTINDIA2015, December 2 3, 2015, Hyderabad, India
- Deshpande S., "Improved Steam Turbine Design for Optimum Efficiency and Reduced Cost of Ownership", Thesis for the Degree of Licentiate (T-Lic), Lund University, 2015, ISRN LUTMDN/TMHP-15/7095-SE, ISSN 0282-1990
- 5. Deshpande S., Thern M. and Genrup M., "Efficiency Improvements in an Industrial steam turbine stage Part I", Proceedings of ASME Turbo Expo 2016: Turbine Technical Conference and Exposition, GT2016, June 13 17, 2016, Seoul, South Korea
- Deshpande S., Thern M. and Genrup M., "Efficiency Improvements in an Industrial steam turbine stage – Part II", Proceedings of ASME Turbo Expo 2016: Turbine Technical Conference and Exposition, GT2016, June 13 – 17, 2016, Seoul, South Korea
- 7. Deshpande S., "Improved Steam Turbine Design for Optimum Efficiency and Reduced Cost of Ownership", Thesis for the Degree of Doctor of Philosophy (PhD), Lund University, 2017, ISBN 978-91-7753-227-9
- 8. Deshpande S., Pradeep A. M., Thern M. and Genrup M., "Effect of Spanwise Variation of Chord on the Performance of a Turbine Cascade", Proceedings of ASME Turbo Expo 2017: Turbine Technical Conference and Exposition, GT2016, June 26 30, 2017, Charlotte, NC, USA



11 Appendices

11.1 SECONDARY LOSS

The work and reasoning related to secondary loss and aspect ratio (and row turning) can be explained by studying the empirical loss model by Traupel [2]. The Traupel loss model clearly correlates the secondary loss as a function of pitch over height (s/l) which simply is the of s/c over the aspect ratio.

Row efficiency:

$$\eta = 1 - \sum_{i=1}^{n} \zeta_i$$

The secondary loss is calculated as:

$$\zeta_{rest} = \frac{\zeta_P}{\zeta_{P,0}} \cdot F \cdot \frac{s}{l}$$
 $\frac{s/c}{AR} = \frac{s/c}{l/c} = \frac{s}{l}$

I.e. low secondary loss if:

- Small pitch (s or s/c)
- Tall blade (I or AR)
- Low turning $(\Delta \alpha, \Delta \beta)$
- · High acceleration (thin B.L.)

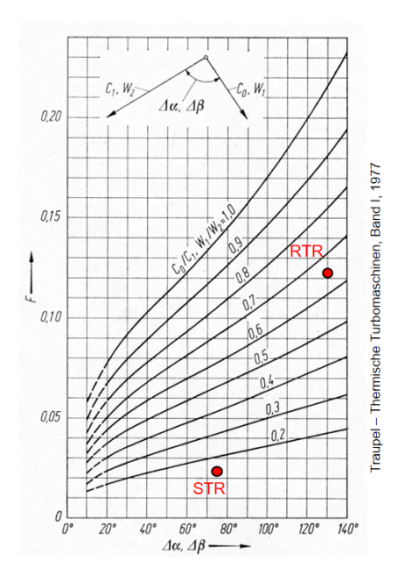


Figure 11-1 Traupel secondary loss model

The secondary loss in the Traupel model is shows in the figure above and the loss is proportional to the s/l value and the F-parameter. The latter is an empirical function of the row turning and acceleration.



11.2 **FINANCIAL REPORT**

0	
	Energimyndigheten

Skicka handlingarna till Energimyndigheten Box 310 631 04 Eskilstuna

1(2)

Ekonomisk slutredovisning (ESR)

39281-1 Projektnummer 2014-003190 Diarienummer Förbättrad design av ångturbiner för optimal verkningsgrad Projekttitel och reducerad livscykelkostnad

Ange total projektkostnad enligt kostnadsplanen i beslutet samt totalt upparbetade kostnader i projektet

	Total projektkostnad enligt beslut (kr)	Totalt upparbetade kostnader (kr)
Lönekostnader	6 647 010	5 142 444
Köpta tjänster		0
Utrustning		0
Material		24 992
Laboratoriekostnad		0
Resor		75 980
Övriga kostnader		0
Indirekta kostnader*	590 490	884 644
Summa	7 237 500	6 128 060

Observera! Bifoga handlingar som styrker behörigheten att underteckna den ekonomiska slutredovisningen, t.ex. registreringsbevis från bolagsverket och eventuell fullmakt.

Avviker något kostnadsslag med mer än ± 10 % jämfört med kostnadsplanen i beslutet?

ia (fyll i nedan)

Skillnader mellan upparbetade kostnader och projektkostnad enligt beslutet måste förklaras om de överstiger med mer än 10 procent för varje kostnadsslag. Vid större förändringar krävs Energimyndighetens

Hela projektets pengar har inte använts eftersom doktoranden valde att forcera disputationsdatum pga. anställning i industrin. Detta har dock inte påverkat projektets innehåll förutom viss tidsutdräkt.

Post avseende resor är väsentligen konferenser men även mätkampanj i Indien (hösten -16). Denna var inte med i ursprungsplaneringen utan visade sig nödvändig under projektets gång.

Kostnad för materiel avser licenskostnad för ett program som visade sig nödvändigt för utförandet av projektet.

Att indirekta kostnader är högre i utfallet är pga. att under pågående projekt (2014-2017) har vi haft olika OH% procent på institutionen vilket gör det svårt att beräkna i budgeten.

	1/ 1
Datum och firmatecknares namnteckning (prefekt motsv.) Ouvud Anderson	Projektledares namnteckning
Namnförtydligande	Namnförtydligande
Öivind Andersson	Magnus Genrup

Box 310 • 631 04 Eskilstuna • Besöksadress Kungsgatan 43 Telefon 016-544 20 00 • Telefax 016-544 20 99 registrator@energimyndigheten.se www.energimyndigheten.se Org.nr 202100-5000



^{*}endast för universitet och högskola

Improved Steam Turbine Design for Optimum Efficiency and Reduced Cost

The rationale for pursuing the project KME-707 is to lower the cost of ownership for the users but as natural result increasing the generation of climate-neutral electricity by increased efficiency.

The results show that there is potential for improvement and that the amount of renewable electricity can be increased. The work has been focused on stage #11 and #16 in a SST-900 turbine and stage #2 in a SST-700 module. The former is an IP/LP module with tall stages whilst the latter is a HP module with short stages. For the tall stage, the work has been directed towards the profile- and end-wall losses and for the short stage mainly the end-wall loss.

The results show, for example, that the stage #16 profile loss can be reduced by 0.74 percent and that the secondary losses is reduced by the suggested means. The analysis shows that the reduction in secondary losses are high on the order of 30 percent (expressed as secondary kinetic energy - SKE).

Energiforsk is the Swedish Energy Research Centre – an industrially owned body dedicated to meeting the common energy challenges faced by industries, authorities and society. Our vision is to be hub of Swedish energy research and our mission is to make the world of energy smarter. www.energiforsk.se

